ABSTRACT

Title of Dissertation:	NEXT GENERATION HEAT PUMP SYSTEM EVALUATION METHODOLOGIES
	Hanlong Wan, Doctor of Philosophy, 2021
Dissertation directed by:	Minta Martin Professor Reinhard Radermacher, Department of Mechanical Engineering

Energy consumption of heat pump (HP) systems plays a significant role in the global residential building energy sector. The conventional HP system evaluation method focused on the energy efficiency during a given time scale (e.g., hourly, seasonally, or annually). Nevertheless, these evaluation methods or test metrics are unable to fully reflect the thermodynamic characteristics of the system (e.g., the start-up process). In addition, previous researchers typically conducted HP field tests no longer than one year period. Only limited studies conducted the system performance tests over multiple years. Furthermore, the climate is changing faster than previously predicted beyond the irreversible and catastrophic tipping point. HP systems are the main contributor to global warming due to the increased demands but also can be a part of the solution by replacing fossil fuel burning heating systems. A holistic evaluation of the HP system's global warming impact during its life cycle needs to account for the direct greenhouse gas (GHG) emissions from the

refrigerant leakage, indirect GHG emissions from the power consumption and embodied equipment emissions. This dissertation leverages machine learning, deep learning, data digging, and Life Cycle Climate Performance (LCCP) approaches to develop next generation HP system evaluation methodologies with three thrusts: 1) *field test data analysis*, 2) *data-driven modeling*, and 3) e*nhanced life cycle climate performance (En-LCCP) analysis*. This study made following observations: First, time-average performance metrics can save time in extensive data calculation, while quasi-steady-state performance metrics can elucidate some details of the studied system. Second, deep-learning-based algorithms have higher accuracy than conventional modeling approaches and can be used to analyze the system's dynamic performance. However, the complicated structure of the networks, numerous parameters needing optimization, and longer training time are the main challenges for these methods. Third, this dissertation improved current environmental impact evaluation method considering ambient conditions variation, local grid source structure, and next-generation low-GWP refrigerants, which led the LCCP results closer to reality and provided alternative methods for determining LCCP input parameters with limited-data cases. Future work could be studying the uncertainty within the deep learning networks and finding a general process for modeling settings. People may also develop a multi-objective optimization model for HP system design while considering both the LCCP and cost.

NEXT GENERATION HEAT PUMP SYSTEM EVALUATION METHODOLOGIES

by

Hanlong Wan

Dissertation submitted to the Faculty of the Graduate School of the
University of Maryland, College Park, in partial fulfillment
of the requirements for the degree of
Doctor of Philosophy
2021

Advisory Committee:
Professor Reinhard K. Radermacher, Chair
Professor Peter Sunderland, Dean's Representative
Research Professor Yunho Hwang
Professor Nikhil Chopra
Professor Jelena Srebric
Professor Bao Yang

Preface

This dissertation begins from a field test conducted in a campus office building. I took over the experimental work of a Variable Refrigerant Flow (VRF) system from my colleague, Lei Gao, on August 22nd, 2017. L.G. Electronics sponsored this project. I never imagined that the VRF field evaluation works had been conducted for six years, and it would be the topic of my Ph.D. thesis at that time. As the test was conducted, the Data Acquisition System generated a large amount of data with different dimensions. I started to find appropriate methods to deal with the large data, the results of which were developed as chapter 2 in this dissertation. At the end of the year 2017, the visiting scholar, Dr. Wen Su, recommended me a paper about Neural Network's application in Organic Rankin Cycle. This work inspired me to apply a machine-learning-based algorithm in Heat Pump (HP) system data analysis. I took a machine learning class in Fall 2018 and started using deep learning to improve the HP system models. This was the starting point of chapter 3. In Fall 2019, I began to conduct Life Cycle Climate Performance (LCCP) analysis for different HP systems like Unitary Heat Pumps, Heat Pump Variable Refrigerant Flow (HPVRF) systems, etc., with my co-advisor Prof. Hwang and improved current enhanced LCCP evaluation approach for HP systems with Dr. Andersen from the Institute for Governance & Sustainable Development. The result became chapter 4 of this dissertation.

Everyone who had monitored the data from a building or conducted field tests for a HP system might have the same question: "How to make use of a large number of measured

data?" In this dissertation, I tried to use data digging tools, machine-learning-based algorithms, data visualization methods, and LCCP to answer this question. Previous HP system evaluations always focus on several energy efficiency metrics. In my opinion, this simple "scoring" approach would not be enough for future HP systems. A good evaluation methodology should be an all-around process including cost, energy efficiency, thermodynamic performance, environmental impacts, thermal comfort, etc. In addition, as future HP systems became more complicated and sampling time became smaller (data revolution became higher), the time consumed by the calculation functions and model training would also become longer. Thus, instead of only pursuing veracity, there would be a trade-off between accuracy and computational cost. Time-saving is a significant factor for data analysis and model selection in the dissertation.

I hope you enjoy your reading.

Hanlong Wan

University of Maryland, College Park

May 17th, 2021

Acknowledgements

It would not have been possible to complete this dissertation without the assistance of the kind people whose names may not be enumerated. Nevertheless, I would like to express my deep appreciation and indebtedness, particularly here.

First, I would like to give a sincere thanks to my advisor, Prof. Reinhard Radermacher, for his constant guidance as well as for providing me with a very stimulating research atmosphere. My deep gratitude also goes to my co-advisor, Prof. Yunho Hwang, who expertly guided me through my graduate education and who shared the excitement of all the research outcomes. I am very grateful to my committee members: Prof. Peter Sunderland, Prof. Nikhil Chopra, Prof. Jelena Srebric, and Prof. Bao Yang, for their service and advice to improve this thesis.

I would like to acknowledge the support and cooperation of all my colleagues in the CEEE. I am extremely thankful to Dr. Tao Cao for his insightful comments on my works and thesis. I wish to thank Mr. Jan Muehlbauer, who gave me a lot of help in the laboratory experiments and field tests. I would thank Dr. Jiazhen Ling and Dr. Vikrant Aute for their help and insightful advice in modeling, machine learning, and data analysis. I also want to thank Ms. Mary Baugher for her kindly help with the administrative work. Many thanks to Dr. Yiyuan Qiao, Dr. Zhenning Li, Dr. Ransisi Huang, Dr. David Catalini, Lei Gao, Zhenyuan Mei, Nehemiah Emaikwu, Dongyu Chen, Ellery Klein, Joseph Baker, Cheng-Yi Lee, Jangho Yang, Janel Niska, James Tancabel, and Gyeong Sung Kim for the enlightening discussions. Special thanks go

to the visiting scholars Dr. Wen Su, Dr. Qi Chen, and Dr. Jingye Yang for their inspiring advice on my works.

I gratefully acknowledge the support of the Air Solution R&D Laboratory at LG Electronics Inc. I would like to thank Dr. Sanghong Lee, Dr. Heunghee Bae, and Dr. Brain Yoon for their guidance on the system controls, test facilities, and software installation. Thanks also extend to Dr. Saikee Oh, Dr. Sedong Chang, Dr. Simon Jin, and Dr. Seokhoon Jang for their support on my project and paper publications. I would also like to thank Dr. Stephen Oliver Andersen from the Institute for Governance & Sustainable Development for his help on Life Cycle Climate Performance evaluation method improvement.

Most importantly, I am extremely grateful to my parents for their love, prayers, caring, and sacrifices for educating and preparing me for my future. I express my thanks to my grandparents for their valuable prayers. Without their encouragement, this dissertation would not have been possible.

Table of Contents

List of Tables

List of Figures

List of Abbreviations

20-c	20-coefficient correlation model
A	area, system matrix
a	correlation factor, the most dominating poles
AC	air conditioning
AD	average relative deviation [%]
ADP	atmospheric degradation product
Adp. GWP	GWP of atmospheric degradation product [kg CO_2e/kg]
AEC	annual energy consumption [kWh]
AHU	air handling unit
ALR	annual leakage rate [%/yr]
AMY	actual meteorological year
ANN	artificial neuron network
APF	annual performance factor
A_r	flow area [m^2]
b	bias, normalized matrix, correlation factor, control gain
B	input parameter matrix
BR	bypass ratio [%]
C	covariance matrix, regression parameter, system matrix, coefficient, charge of refrigerant [kg]
c	centralized matrix
CapFT	capacity modification function of temperature
CD	condition including temperature, pressure, and quality

C_f	mass flow coefficient
CFD	computational fluid dynamics
CNN	convolution neural network
CO_2e	carbon-dioxide equivalent emission
COP	coefficient of performance
Cp	specific heat [$J \cdot kg^{-1} \cdot K^{-1}$]
CSPF	cooling seasonal performance factor
D	orifice diameter [m]
d_c	needle diameter [m]
DOAS	dedicated outdoor air system
DPF	daily performance factor [-]
E	eigenvalue, carbon emissions [kg CO_2e]
ECC	embodied carbon-dioxide coefficient [kg CO_2e/kg]
EEV	electronic expansion valve
eff	efficient-based model
EIA	energy information administration
EF	emission factor [kg CO_2e/kWh]
EOL	end of life refrigerant leakage [%]
EPA	Environmental Protection Agency
ERV	energy recovery ventilation
F	frequency [Hz]
f	friction factor [-]

FDD	fault detection and diagnosis
FL	fault level
g	transfer function
G	heat capacity [W/K]
GEEF	grid electricity emission factor (carbon intensity) [kg CO_2e/kWh]
GHG	green house gas
GREEN-MAC-LCCP©	**g**lobal **r**efrigerants **e**nergy and **en**vironmental – **m**obile **a**ir **c**onditioning – **l**ife **c**ycle **c**limate **p**erformance
GSHP	ground source heat pump
GWP	global warming potential
H	position of the needle [m]
HE	heat exchanger
HFC	hydrofluorocarbon
HFO	hydrofluoroolefin
HP	heat pump
HR	heat recovery
HSPF	heating seasonal performance factor
HVAC	heating, ventilation, and air conditioning
I	identity matrix
IAQ	indoor air quality
IIR	International Institute of Refrigeration
ISD	integrated surface database
IU	indoor unit

K	controller
k	specific heat ratio [-]
L	average life [years]
LCA	life cycle assessment
LCCP	life cycle climate performance
$\dot{m}$	mass flow rate [kg/s]
m	mass of unit [kg]
M	correlation factor
MAC	mobile air conditioner
MCHX	microchannel heat exchanger
MEAC	multi evaporator air conditioning
MM	CO_2 produced per unit of material [kg CO_2e/kg]
MPC	model predictive control
mr	mass of recycled material [kg]
MRE	mean relative error [%]
MSE	mean square error [%]
N	number of data points
n	polytropic exponent
NIST	National Institute of Standards and Technology
NN	neural network
NOAA	National Oceanic and Atmospheric Administration
NTU	number of transfer units

OAD	outdoor air dehumidifier
OAP	outdoor air processing
OU	outdoor unit
P	pressure [kPa]
PAC	packaged air conditioner
PCA	principle component analysis
PCM	phase change material
Pw	power [W]
q	refrigerant quality [-]
$\dot{Q}$	capacity [W]
QSS	Quasi-Steady State
RCD	reverse cycle defrosting
RCL	refrigerant charge level
RD	relative deviation
RE	relative error
RF	random forest
RFD	refrigerant disposal emission [kg CO_2e/kg]
RFM	refrigerant manufacturing emission [kg CO_2e/kg]
RH	relative humidity [%]
RM	CO_2 produced per recycled material [kg CO_2e/kg]
RME	relative mean error
RMSE	root mean square error

RPM	revolutions per minute
s	complex frequency [Hz]
SCHX	subcooling heat exchanger
SCOP	seasonal coefficient of performance
SD	standard deviation
SEER	seasonal energy efficiency ratio [-]
SVM	super vector machine
SVR	support vector regression
T	temperature [°C]
TEV	thermostatic expansion valve
TEWI	total equivalent warming impact
THIC	temperature humidity independent control
TMY	typical meteorological year
U	overall conductance [W/(m·K)], uncertainty [-]
UAC	unitary air conditioner
UHI	urban heat island
UMCP	University of Maryland, College Park
V	volume [m^3], eigenvector
v	indoor thermal load [W]
VCC	vapor compression cycle
VI HP	vapor injection heat pump
VRCS	virtual refrigerant charge sensor

VRF	variable refrigerant flow
VRV	variable refrigerant volume
w	dimensionless weight factor in the neural network [-]
W	power [W]
X	EEV opening degree [%]

Greek symbols

π	dimensionless parameter group
μ	dynamic viscosity [kg m^{-1} s^{-1}]
α	needle angle [°]
ε	tolerance [-]
η	efficiency [-]
ξ	relaxing factor [-]
ρ	density [kg·m^{-3}]
σ	surface tension [N m^{-1}]
α	electric expansion valve opening degree [%]
ν	specific volume [m^3/kg]
ω	compressor frequency [Hz]
η	efficiency [-]
ε	effectiveness [-]
ρ	density [kg·m^{-3}]
Δ	difference [-]

ø	frictional two-phase multiplier

Subscripts

a	ambient, air
c	critical, condensing
comp	compressor
d	discharge
db	dry bulb temperature
dis	discharge
e	experiment, evaporating, evaporator’s two-phase region
EEV	electronic expansion valve
eq	equivalent
f	saturated liquid
g	saturated vapor
i	inlet
ind	indoor
l	liquid
max	maximum
meas	measured
min	minimum
out	outlet
outd	outdoor

pred	predicted
r	room, refrigerant
rate	rating condition
sh	superheat
sub	subcooling
suc	suction
th	throat
tot	total
wb	wet bulb temperature

1. Introduction

Air conditioning (AC) systems and heat pump (HP) systems are widely used to adjust the temperature and humidity of an occupied space to improve the users' thermal comfort or provide a unique environment. Not only in residential and commercial buildings but also in the industry and transportation, AC and HP systems play a significant role in providing a healthy and comfortable indoor environment for our daily life. For brevity, AC systems are referred to as HP systems operating in cooling mode in this dissertation. This dissertation mainly focuses on residential HP systems, while some mobile HP systems are also covered. The first section introduces the background knowledge and motivation of HP systems measurement. Then, the literature review results are summarized and discussed. Finally, three objectives of this dissertation are described.

1.1. Background

1.1.1. Energy Consumption and Carbon Emission of Heat Pump Systems

People spend 80% of their time in buildings (Brodrick, 2002). The global energy consumption from both residential and commercial buildings has steadily increased, reaching figures between 20% and 40% in developed countries (Pérez-Lombard et al., 2008). Among building services, the growth in Heating, Ventilation, and Air Conditioning (HVAC) system energy use is particularly significant as it is responsible for 50% of building consumption and 20% of total consumption in the U.S. (Pérez-Lombard et al., 2008). The rapidly growing energy consumption raised concerns over energy supply difficulties, exhaustion of energy resources, and severe environmental

impacts, like ozone layer depletion, global warming, and climate change (Pérez-Lombard et al., 2008). The climate is changing faster than predicted, with self-reinforcing feedback loops in the climate system that pushes the planet past beyond irreversible and catastrophic tipping point (The Climate Reality Project, 2020). HP systems are one of the main contributors to global warming (Yang et al., 2021) and part of the solution at the same time. The challenge is to drastically increase energy efficiency even as electric supply shifts from fossil fuel to renewable energies like wind, solar and hydroelectric power, and shift from using high global warming potential (GWP) refrigerants to lower ones even as leak rates are minimized and refrigerants are fully recovered at the end of (product) life (EOL).

1.1.2. Vapor Compression Cycle

Although heat-driven HP systems such as absorption cycle (Herold and Radermacher, 1989) and adsorption cycle (Suzuki and Suzuki, 1990) were developed in the 1900s, nearly all HP systems installed nowadays use the vapor compression cycle (VCC) for cooling and heating, in which the refrigerant undergoes phase changes and heat transfer. The VCC uses a circulating refrigerant as its working fluid, which absorbs heat from the space to be cooled and subsequently rejects that heat elsewhere. Figure 1-1 depicts a typical, single-stage VCC system. All such systems have four components: a compressor, a condenser, an expansion valve (also called a throttle valve or metering device), and an evaporator. Circulating refrigerant enters the compressor as a superheated vapor and is compressed to a higher pressure, resulting in a higher temperature as well. The hot, compressed vapor is then cooled and condensed with

either cooling water or ambient air at lower temperatures. This is where the circulating refrigerant rejects heat from the system, and the rejected heat is carried away by either the water or the air (whichever may be the case). This dissertation discusses VCC-based HP systems.

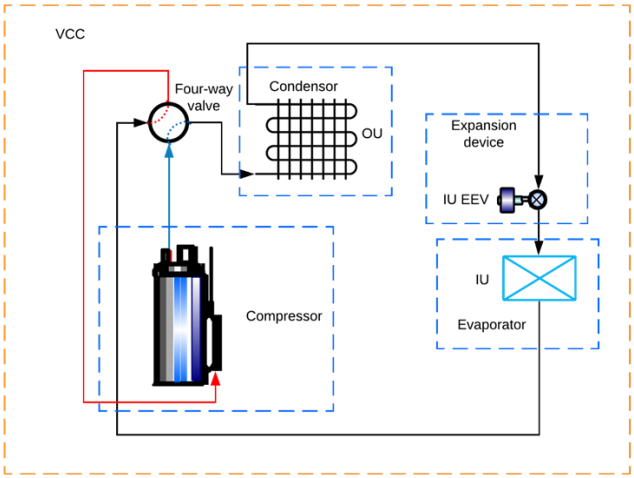

Figure 1-1 Schematic of Typical Vapor Compression Heat Pump Cycle

1.1.3. Heat Pump Systems Category

General residential HP systems can be classified as duct and ductless systems. Ductless systems are widely used in commercial buildings and apartments (Kovler et al., 2002). Duct systems can provide ventilation function (Okochi and Yao, 2016). Compared with duct systems like Fan Coil systems, ductless systems have lower installation costs and are more convenient for maintenance (Lin et al., 2015a). This dissertation uses three typical HP systems include the Single-split Heat Pump (SHP) systems, Unitary Heat Pump (UHP) systems, and Variable Refrigerant Flow (VRF) systems (Multi-split Heat Pump systems) as case studies.

Unitary Heat Pump Systems

Based on Air-Conditioning, Heating, and Refrigeration Institute (AHRI) definition, UHP systems refer to one or more factory-made assemblies and distribute the conditioned air directly to the space (AHRI, 2017). When such equipment is provided in more than one assembly, the separated assemblies shall be designed to be used together. Roof Top Unit (RTU), Window HP, and Packaged Through the wall Heat Pump (PTHP) Unit are common UHP systems in residential buildings. Figure 1-2 shows a typical PTHP system. Due to the all-in-one design, UHP systems are economically efficient for manufacture, installation, and maintenance.

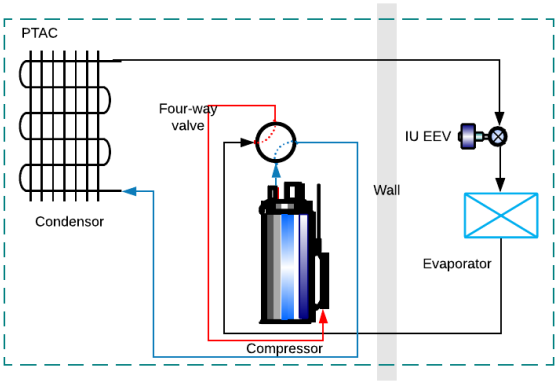

Figure 1-2 Schematic of Typical PTHP System

Split Heat Pump Systems

Split Heat Pump (SHP) systems are another type of commonly seen HP system. SHP systems have Indoor Units (IDU) and Outdoor Units (ODU), as shown in Figure 1-3. The strength of Split HP systems is flexibility. First, sub-units could be easily added to SHP systems to provide extra function, like Heat Recovery Units (HRU) (Li and Wu,

2010). Second, SHP systems are able to provide better control than UHP systems (Kim et al., 2016a).

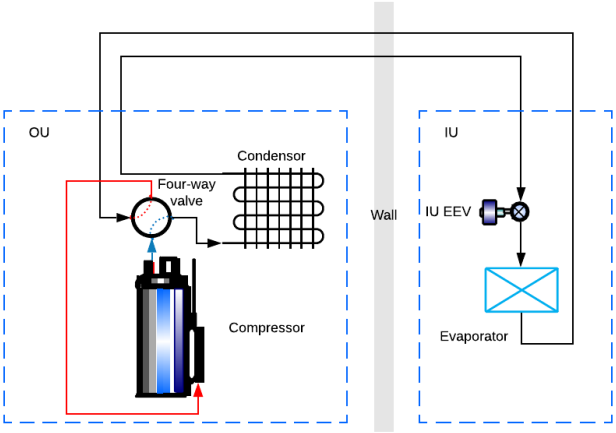

Figure 1-3 Schematic of Typical Split Heat Pump System

Variable Refrigerant Flow Systems

The term variable refrigerant volume (VRV) system was first introduced in 1982 and is also known as VRF system nowadays (Thornton and Wagner, 2012). Since the 1980s, VRF systems have been widely used in Japan: 50% of midsize office buildings (up to 6,500 m^2) and 33% of large commercial buildings (more than 6,500 m^2) (Goetzler, 2007). VRF systems were introduced to the U.S. around 2002 and are widely used in commercial and office buildings (Kwon et al., 2014). Figure 1-4 shows a schematic of a simplified VRF system. It typically consists of a variable speed compressor, one ODU, and multiple IDUs. The mass flow rate of each IDU is controlled by the electronic expansion valve (EEV). This simple VRF system is also called the Heat Pump VRF (HPVRF) system (Kwon et al., 2014). HPVRF systems can only provide heating or cooling at one time. By adding a so-called HRU, the Heat Recovery VRF (HRVRF) system can provide heating and cooling simultaneously (Joo

et al., 2011; Kang et al., 2009). VRF systems have many advantages (Kwon et al., 2014). First, the system is flexible to operate as each IDU can be controlled independently. In particular, the system with a variable speed compressor can easily match its cooling capacity to thermal loads at different indoor and ambient conditions. The VRF system is energy efficient as it does not lose too much energy through ductwork like conventional ducted UHP systems. Moreover, the HRVRF system can even provide heating and cooling to different IUs at the same time, which is especially useful in energy saving in shoulder seasons (Joo et al., 2011; Kang et al., 2009). Coefficient of Performance (COP), the most commonly used energy efficiency factor defined by output capacity over input power, could be 146.5% higher under HR mode than under cooling-only mode (Joo et al., 2011).

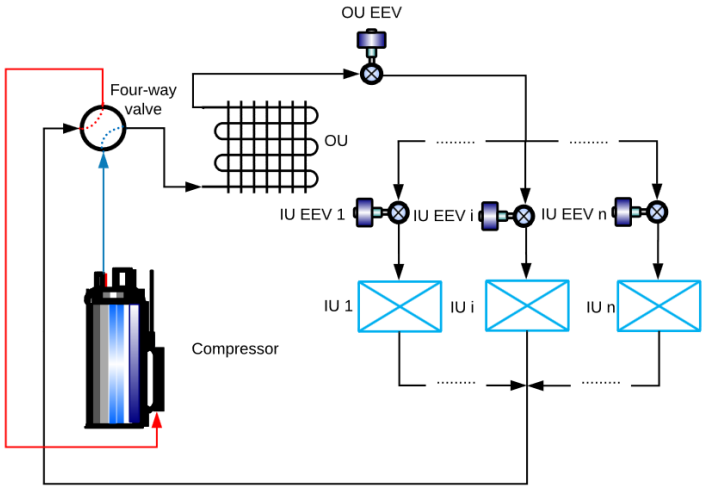

Figure 1-4 Schematic of Typical HPVRF System

1.1.4. Heat Pump Systems Evaluation

HP systems contribute a lot to the total energy consumption and carbon emissions of buildings. Thus, how to evaluate the energy efficiency and environmental impact of HP systems become a significant problem. A reasonable and efficient evaluation

standard could not only provide guidelines for customers but also contribute to energy saving and reduction of environmental damage. Figure 1-5 shows the invention and evolution process of HP systems evaluation metrics.

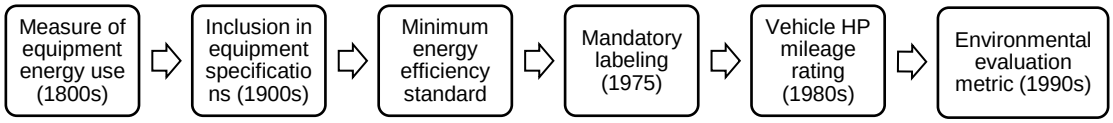

Figure 1-5 Invention and Evolution of HP Systems Evaluation

The most widely used test metric now is the Coefficient of Performance (COP). COP could be defined by the eq. (1):

$$COP = \frac{Cooling\ or\ Heating\ Capacity}{Power\ Consumption} \quad (1)$$

The drawback of COP is that it could only be used to represent the steady-state performance. COP is not sufficient to evaluate the transient performance of the HP systems. Thus, numerous test metrics were proposed, and different regions have different standards.

Wu et al. (2019) summarized the most commonly used energy efficiency metrics, as shown in Table 1-1. Seasonal Energy Efficiency Rate (SEER), Heating Seasonal Performance Factor (HSPF), Annual Performance Factor (APF), Cooling Seasonal

Performance Factor (CSPF), and Seasonal COP (SCOP) are different energy efficiency metrics. Engaging readers could read the reference (Wu et al., 2019).

Table 1-1 Energy Efficiency Metrics

Standard Category	Test method standard	Performance calculation method standard	Energy efficiency standard	Energy efficiency metrics
U.S.	AHRI 210/240:2017	AHRI 210/240:2017	Energy Star, DOE	SEER, HSPF, APF
China	GB/T 7725:2004	GB/T 7725:2004	GB 21455:2013(VRFACs)	SEER, HSPF, APF
Japan	JUSC 9612:2013, JRA 4048:2006, JISB 8615	JISC 9612:2013, JRA 4046	JRA 4046	CSPF, HSPF, APF
EU	EN 14511:2011	EN 14825:2012	EU No 206:2012, EU No 626:2011	SEER, SCOP
Australia	AS/NZS 3823.1.1, AS/NZS 3823.1.2	AS/NZS 3823.2:2013	AZ/NZS 3823.2:2013	AEER, ACOP, SRI
ISO	ISO 5151:2017	ISO 163581:2013, ISO 16368-2:2013	ISO 13612-2:2014	CSPF, HSPF, APF, TAPF

1.1.5. Summary

HP systems are widely used in residential and commercial buildings. Evaluating the performance of HP systems can help to cut energy consumption and carbon emissions. This dissertation uses VCC-based ductless HP systems as examples to explore the evaluation methods for any HP system.

1.2. Motivations

Conventional approaches to evaluating the performance of HP systems are through experiments and models. Nowadays, the traditional evaluation methods can not satisfy the new requirements. On the one hand, besides laboratory tests, people also show

interest in field tests. Moreover, as novel algorithms developed, simulation models were involved as well. Both approaches can generate a large amount of data. Managing and utilizing the data are becoming challenges. In addition, methodology to evaluate environmental performance quantitatively, especially for low-GWP refrigerants, is significant since it can be used as the target function to optimize the HP systems design.

1.2.1. Field Test and Data Analysis Methods Need

Experimental evaluation includes laboratory tests and field tests. Field testing is a practical and effective way to study the performance of HP systems. While HP systems showed high performance in the laboratory, the COP in field tests was reported to be as low as 1.74 (Zhang et al., 2019). The core of the COP calculation was the measurement of the cooling or heating capacities. According to the literature, mainly two methods exist: testing from the air side (Won et al., 2009) or testing from the refrigerant side (Kwon et al., 2012). Nevertheless, both have challenges. From the air side, the most crucial step is to measure the air flow rate. However, the non-uniformity of air velocity could obstruct achieving an accurate air flow rate. On the other hand, from the refrigerant side, measuring the refrigerant mass flow rate needs cutting the refrigerant pipe. Besides, precision mass flow meters, like Coriolis type mass flow meters, are required. Thus, more field test of ductless systems is needed, and an efficient field test method is also needed.

Modeling tools are another way to study HVAC systems, specifically complicated ductless systems (Qiao et al., 2017). However, some difficulties exist for using these

tools to analyze ductless systems. First, previous modeling tools required physical parameters from manufacturers, while some parameters were hard to achieve. Using the Electric Expansion Valve (EEV) as an example, manufacturers always only tested the valves with air flow, not refrigerant flow, for lower testing costs (Wan et al., 2019). Furthermore, previous modeling tools most require the system to be in a steady-state. However, in the field test, the ductless system seldom achieves a steady-state. Also, traditional modeling tools took a long time to get convergence and were difficult to debug. The software is also unfriendly to inexperienced users.

In the past, two separate groups of experienced engineers did the field test and modeling work. The communications were severe. Gaps between the test and simulation always existed. The process would be much simplified if people could develop a model directly from the field test data and use the model to help analyze field tests. The main challenges include the high uncertainty of the field test data, the large number of data dimensions, and the complexity of using the data. This study answers the following questions: what is the difference between the data in the lab and data from the field test?; what kind of method should I use to build the mode?; and what is the difference between the methods?

A large number of data is involved in the HP systems. These parameters include temperature, pressure, compressor frequency, the EEV opening pulse, humidity, etc. If I set the sampling time of the test to be 2 seconds, a VRF system for seven indoor units could generate 20 GB size data per year. The speed is 2.5 KB/s, which is similar to the

speed of a modem. The data of each component of the HP system could be stored in a table. Data tables of all the sub-components of a system can form a tablespace. In a building or house, all the system tablespaces can assemble a database. Such a database contains plenty of data. The challenge is digging important information from the database, storing the data, and utilizing the data.

1.2.2. Models Selection Methods Need

Simulation of HVHP systems is a popular topic nowadays, and VCC calculation is at the core of these software or programs (Aynur et al., 2009; Jiang et al., 2014; Okochi and Yao, 2016). The software is based on VCC models, which include empirical models and component-based models (Shao et al., 2012). Some researchers built their own model by the tools like Energy Plus (Crawley et al., 2000), TRANSYS (Wolf, 1994), Modelica (Fritzson and Engelson, 1998), EES (Klein and Alvarado, 2002), and MATLAB (Higham and Higham, 2016). Others developed software with a friendly user interface like CYCLE_D-HX by NIST (Domanski et al., 2018), Vapcyc by CEEE (Richardson et al., 2004), and CoolPack by DTU (Jakobsen, 1999).

1.2.3. Environmental Impact Evaluation Methods Need

HP systems' environmental impact is under people's concern due to recent severe climate change and global warming issues. A holistic evaluation of the HP system's environmental impact during its life cycle requires the translation of Green House Gas (GHG) emissions from the direct refrigerant leakage, indirect fuel consumptions, and the embodied equipment emissions (Andersen et al., 2018). Institute of International

Refrigeration (IIR) developed the Life Cycle Climate Performance (LCCP) evaluation, which adopted the rigorous approach to identifying and quantifying the direct and indirect environmental impact over a stated life cycle (IIR, 2017).

Andersen et al. (2018) summarized the calculation process of LCCP based on IIR's guidelines. LCCP is usually calculated in kgCO_2e, consisting of direct and indirect emissions, as shown in eq. 2:

$$LCCP = E_{direct} + E_{indirect} \quad (2)$$

Direct emissions (E_{direct}) are the emissions caused by:

$$E_{direct} = E_{leak} + E_{service} + E_{accid} + E_{EOL} \quad (3)$$

where E_{leak} is the total carbon dioxide equivalent emissions due to annual refrigerant leakage from the system over its operating lifetime (kg CO_2e), $E_{service}$ is the total carbon dioxide equivalent emissions due to refrigerant release during servicing events, over the operating lifetime of the system (kg CO_2e), E_{accid} is the total carbon dioxide equivalent emissions due to refrigerant release caused by accidents (kg CO_2e), and E_{EOL} is the total carbon dioxide equivalent emissions due to refrigerant release at the End Of Life (EOL) of the system (kg CO_2e).

Indirect emissions ($E_{indirect}$) include emissions from energy consumption, manufacturing of materials, manufacturing of refrigerant, and disposal of the unit (or recycling):

$$E_{indirect} = E_{energy} + E_{sys,man} + E_{sys,EOL} + E_{ref,man} + E_{ref,EOL} \quad (4)$$

where E_{energy} is the emission associated with the generation of electricity used to power the refrigeration system over its operating lifetime (kg CO_2e), $E_{sys,man}$ is the emissions associated with the energy to manufacture the refrigeration system (kg CO_2e), $E_{sys,EOL}$ is the emission associated with the energy to dispose of the refrigeration system components at the end-of-life of the system (kg CO_2e), $E_{ref,man}$ is the emission associated with the energy to manufacture the refrigerant (kg CO_2e), and $E_{ref,EOL}$ is the emission associated with the energy to dispose of the refrigerant at the end-of-life of the system (kg CO_2e).

Some literature also translated LCCP into three parts: direct GHG emissions, indirect fossil fuel GHG emissions, and emissions embodied in equipment. The fossil fuel GHG emissions are the E_{energy} if the energy used is all from fossil fuel. The embodied emissions include materials, manufacturing, transportation, installation, service, and recycling at the EOL, and this part is the rest of the parts in the eq. 5. Thus, this categorization is the same as eq. 6 (Andersen et al., 2018).

1.2.4. Summary

Labotorary tests and field tests were reported to have different results. The method used for laboratory tests is not applicable for field tests. First, a steady-state is hard to achieve in field tests. Second, field tests require long-time monitoring and a large number of measuring instruments, which are different from laboratory tests. Thus, field tests and new field test methodologies are needed for future HP evaluations. Modeling is another

tool to analyze HP systems. Conventionally, component-based white-box models were used. However, as new machine-learning and deep-learning algorithms develop, black box and grey box models gradually grasp people's interests. Plus, both AI-based modeling and field test experiments involve a large amount of data. Therefore, novel simulation models and data analysis software are needed for novel HP systems. Last but not least, global warming has been becoming a big issue for HP system design and application. Environmental impact evaluation, including life cycle carbon emission, is needed for future HP system selection.

1.3. Literature Review

Due to the need for field tests, simulation models, data analysis approaches, and environmental evaluation, the related literatures are reviewed in this section.

1.3.1. Field Tests and Experimental Works

SHP and UHP Systems

Due to the simple design, SHP and UHP systems typically show similar performances in field tests and laboratory tests. Most experimental studies for UHP systems focus on novel system design like using Vapor Injection cycle. Bourne et al. (2008) proposed a packaged rooftop unit (RTU) that provides heating, ventilation, and air conditioning solutions to buildings. Their work presents new RTU designs that include evaporative cooling of both ventilation air and a condensing refrigerant as well as other features to improve RTU efficiency significantly. Wohlert (2013) proposed a system comprising plural RTUs having a centralized refrigeration unit along with a method for retrofitting

existing independent HVAC units into the proposed system. Kennett et al. (2016) evaluated an extended-duct air delivery system in tall spaces by RTUs.

VRF Systems

Aynur (2010) and Lin et al. (2015) did a complete literature review about VRF system's experiment works before 2014. Three kinds of experimental studies have been conducted since 2014. First, researchers used measured data to validate their models, most of which were developed in EnergyPlus. I already discussed these papers above (Hong et al., 2016a; Jiang et al., 2014; Raustad et al., 2013). Second, some scholars developed new control systems, like temperature and humidity independent control systems, and used experimental methods to evaluate the performance. I also reviewed these works in the system configuration section. Third, some researchers used field tests to conduct a parametric study of the VRF system. I discuss these studies in detail in chronological order as follows:

Yun et al. (2016) conducted a series of experiments in the multi-calorimeter consisting of one outdoor unit chamber and two indoor unit chambers as part of their work to develop a load responsive control of the evaporating temperature in a VRF system under cooling operations. The results indicate that increasing the evaporating temperature can reduce the energy consumption of the system by up to 35%. Yu et al. (2016) compared the cooling performances of the VRF system and the VAV system in office buildings. The climate and operating hours data from their field measurements indicate that the cooling energy consumed by VRF systems was up to 70% lower than

that consumed by VAV systems. Xin et al. (2017) focused on the oil-return aspect. The sound velocity method was used to measure the oil concentration in the VRF system. The author mentioned that it was practical to use this method and the relative deviation between this method and the sampling method was 2.6%. The oil discharge ratio increased linearly with the increase of compressor speed. The oil separator had a limited separation efficiency. Guo et al. (2017) proposed a virtual variable-speed compressor power sensor for the VRF system. The author conducted a set of experiments to collect data to test the sensor under different refrigerant charge levels. Khatri and Joshi (2017) compared an inverted-based VRF HP performance with a constant speed unitary HP by using field performance testing. It was found that the VRF system had energy saving only on part-load conditions. Minimum savings were observed when the outdoor temperature was equal to the rated outdoor temperature, while maximum savings were observed when the outdoor temperature was nearly equal to the indoor set temperature. Özahi et al. (2017) compared the thermodynamic and economic performance of an air handling unit (AHU) and a VRF system in public buildings. Park et al. (2017) conducted a field test in an office building and compared the results with a simulation result by EnergyPlus. Three system configurations were used in this study: the VRF system without ventilation, the VRF system with energy recovery ventilation (ERV), and the VRF system with DOAS. According to their experimental results, the yearly energy use per unit area of the VRF system without ventilation was 213.6 $kWh \cdot m^{-2}$. The VRF system with ERV and the VRF with DOAS were 16.8% and 26%, respectively, higher than the VRF system without ventilation. Saab and Ali (2017) studied the performance of the VRF system under various

conditions in hot and humid climates. Their results show that the COP of the cooling cycle and the type of refrigerant used as working fluid were highly dependent on the evaporator and condenser pressures. They also mentioned that evaluating the effect of each parameter on the COP of the system could contribute to energy saving. Zhang et al. (2017) studied the operating performance of digital variable multiple HP systems, which was one type of VRF system. The results indicate that the variable refrigerant volume characteristics and excellent part-load performance were helpful for energy saving. Under the defrosting condition, the IU, which contributes the most to defrosting, was the one nearest to the OU, and its corresponding indoor thermal environment was adversely affected. Tu et al. (2017) used experiments to study the subcooling degree's effect on the performance of the VRF system. The results show that the reasonable adjustment of the subcooling EEV opening could improve the COP, increase the subcooling degree, and ensure the safe discharge superheat degree. They also discussed how to control the subcooling by EEV.

Table 1-2 shows a summary of the experiment works conducted since 2014. Observations from this survey are as follows: first, since 2017, a significant number of VRF system experiment papers have been published; second, nearly all of them were conducted in the Asia region; third, most of them focused on the cooling mode only.

Table 1-2 Experiment Studies Overview

Author	Year	Mode	Location	Building type	Research Target	Time
Jiang et al.	2014	Cooling, Heating	Shanghai, CN	Office room	Indoor air temperature, energy consumption, COP	2 months
Lin et al.	2014	Cooling, Heating	College Park, US	Office room	COP	1 year
Meng et al.	2015	Cooling	Shanghai, CH	n/a	COP, PLR	n/a
Kim et al.	2015	Heating	Busan, KR	Test chamber	COP, heating capacity	n/a
Yun et al.	2016	Cooling	Yongin Si, KR	Test chamber	Energy consumption, exhaust air temperature	n/a
Yu et al.	2016	Cooling	Beijing, CN	Office room	COP, energy consumption	1 year
Xin et al.	2017	Cooling	Qingdao, CN	n/a	Oil return	n/a
Guo et al.	2017	Cooling, Heating	Wuhan, CN	Test chamber	Energy consumption, exhaust air temperature	n/a
Khatri et al.	2017	Cooling	New Delhi, IN	Brick wall building	Energy consumption, outdoor air temperature	1 month
Ozahi et al.	2017	Cooling	Turkey, TR	Public building	Cost, energy consumption	1 year
Kani-Sanchez et al.	2017	Cooling, Heating	Ontario, CA	Office room	Energy consumption	1 year
Park et al.	2017	Cooling, Heating	Seoul, KR	Office room	Energy consumption, COP, ventilation	1 year
Saab and Ali	2017	Cooling	Abu Dhabi, AE	Office room	COP, energy consumption	1 year
Zhao et al.	2017	Cooling	Shanghai, CN	Office room, residential house	Indoor air temperature, stability	1 year
Zhang et al.	2017	Heating	Nanjing, CN	Laboratory	COP, PLR, defrost, energy consumption	n/a
Tu et al.	2017	Cooling, Heating	Ningbo, CN	Laboratory	COP, subcooling, superheat	n/a
Qian et al.	2020	Cooling, Heating	14 cities in China	Office, Residential, Public building	COP	1 year

A possible reason could be that in Southeast Asia (hot and humid conditions), the cooling demand is more significant than the heating demand. Fourth, most of the papers focused on the COP and energy consumption of the VRF system. Limited studies tackled other topics, like defrosting performance and the stability of the system. Thus, future research work could include more various environmental conditions around the world. Also, more studies on the effects of design parameters on the system performance are needed to be carried out. Finally, for the field test works, all the studies only conducted tests in one year. No one compares the performance of the same system in different years. Except for Qian et al. (2021), no study studied large data analysis for field tests.

1.3.2. Modeling Methods for HP Systems

Researchers built computer models as a bias for simulations to develop data utilized for HP system design, analysis, or comparison. Models were developed to describe the systems.

HP models can be categorized as steady-state or transient models. The steady-state is defined as for all parameters of a system or process, the partial derivative to time is zero (Lecompte et al., 2018a). The unsteady-state is also called the transient state or the dynamic state. Besides steady-state or transient models, HP models could also be categorized as black-box models or gray-box models. The HP modeling could be categorized as shown in Figure 1-6.

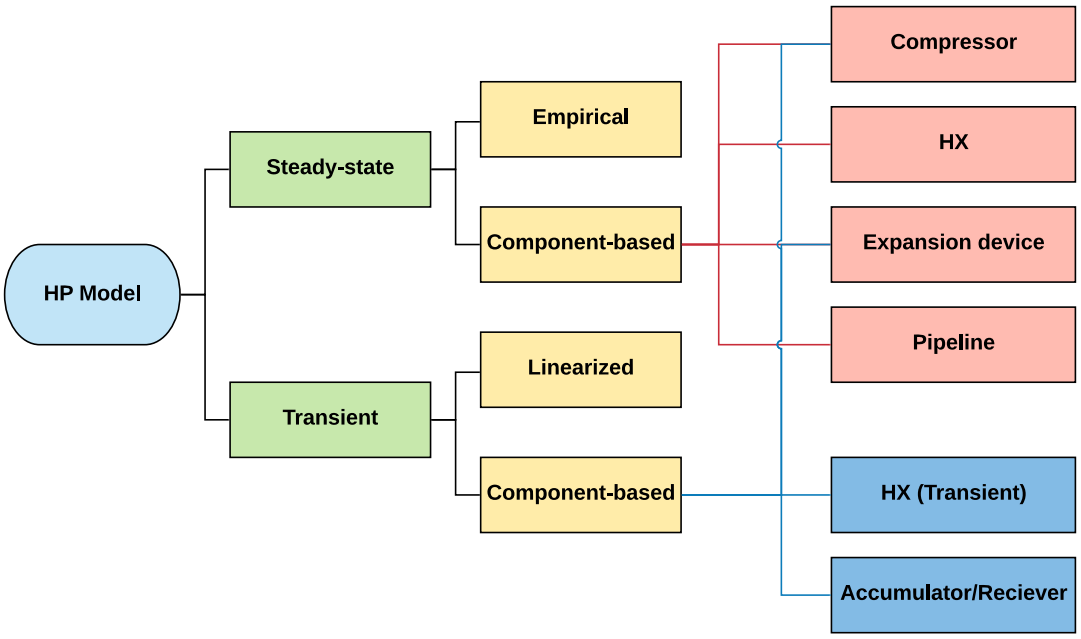

Figure 1-6 HP Modeling Category

Developing a transient model is more complicated than the steady-state model due to time derivative terms. The transient models were typically published in control design journals. In this part, some transient models are reviewed, and the control logics of the HP system are further discussed later. As for the transient models, state-space representation, which is a mathematical model of the physical system, is commonly used (Rovelli and Smolin, 1990). Two kinds of models exist, known as black-box models and gray-box models. In the black-box model, linearization is employed to simplify the models. In the grey-box model, some researchers considered the system in detail and built a complete component-based model.

Steady-state Empirical Model

The most commonly used empirical model is the one used in EnergyPlus 7.2 (Crawley et al., 2000). Polynomial equations are used to predict the parameters, like capacity, as shown below (Hong et al., 2014).

$$Q_{tot,ind} = Q_{rate,ind} \cdot CapFT_{ind} \tag{7}$$

$$\begin{aligned} CapFT_{ind} = {} & a_1 + a_2 T_{wb,ind} + a_3 T_{wb,ind}^2 + a_4 T_{db,outd} \\ & + a_5 T_{db,outd}^2 + a_6 T_{wb,ind} T_{db,outd} \end{aligned} \tag{8}$$

Eq. (7) is used to calculate the actual output of each IU by the capacity in the rated condition. The correction factor can be computed by eq. (8), which incorporates the modifiers correlated with average room wet bulb temperature and outdoor dry bulb temperature. This model is called the "system-curve-based model" or "SysCurve." As shown by the equations, the system is described by several curves. EnergyPlus is an open-source simulation engine for building performance analysis. According to Lin's research (Lin et al., 2015b), most of the steady-state modeling studies (Hong et al., 2014; Li and Wu, 2010; Liu and Hong, 2010; Raustad et al., 2013; Shen et al., 2013; Shen and Rice, 2012) were based on EnergyPlus and started with a hard-coded module due to the reason that early version of EnergyPlus was unable to support an HP system. EnergyPlus is a popular tool in HP system simulation, and some studies (Hong et al., 2016a; Kim et al., 2016b; Wang, 2014) are introduced in detail in the simulation section. As the new version of EnergyPlus (version 9.0) was released, other models, such as the physics-based model, also known as "FluidTCtrl," were developed to be able to describe the system dynamics (Hong et al., 2016a).

Recently, the Artificial Neural Network (ANN)-based model is a hot topic. ANN, also called Shallow Neural Network (SNN), or just Neural Network (NN), is a kind of black-box data-driven model, which was typically used to predict energy consumptions. Kang et al. (2018) proposed an ANN model using weather data including outside temperature, relative humidity, solar radiation, cloudiness, wind speed, and rainfall events as input data to predict the energy consumption. The mean square error (MSE) of their work is 10.3%. Chung et al. (2017a) used ambient temperature, outside humidity, cooling load, saturated temperature, condensate temperature, and condense pressure as input neurons to predict energy consumptions. ANN, which is one kind of machine learning methods, is a powerful method with low error and can be used as a substitute for traditional empirical methods in most cases. Since this method is also widely used in subcomponent modeling, control design, and FDD, I use a separate chapter to discuss this topic.

Steady-state Component-based Model

Some researchers used component-based models for the HP system (Cheung and Braun, 2014; Sun et al., 2017). These models consist of compressor models, condenser models, evaporator models, EEV models, pipeline models, and accumulator models. Various algorithms were adopted to connect the component models.

a. Compressor Model

For the simulation of VCC systems, the compressor models fell into three categories: 1) map-based models, 2) efficiency-based models, and 3) distributed parameter models (Zhao et al., 2009; Qiao et al., 2010). The most commonly used model for the HP system was the efficiency-based model (Cheung and Braun, 2014; Sun et al., 2017).

Several research groups also studied the efficiency-based model (Jähnig et al., 2000; Li, 2013a). Jähnig's model is listed here:

$$\dot{m} = \left\{1 - C_{comp,1}\left[\left(\frac{P_{dis}}{P_{suc}}\right)^{1/k} - 1\right]\right\} \cdot \frac{V \cdot RPM}{\nu_{suc} \cdot 60} \tag{9}$$

$$W \cdot \eta_{comp} = \dot{m} \cdot \frac{k}{k-1} \cdot \frac{P_{dis}}{P_{suc}} \cdot \nu_{suc}\left[\left(\frac{P_{dis}}{P_{suc}}\right)^{\frac{k-1}{k}} - 1\right] \tag{10}$$

$$\eta_{comp} = C_{comp,2} + C_{comp,3}\exp\left(C_{comp,4}P_{suc}\right) \tag{11}$$

where k is the specific heat ratio. $C_{comp,1}$, $C_{comp,2}$, $C_{comp,3}$, and $C_{comp,4}$ are regression parameters that are obtained from experimental data. Cheung and Braun (2014a) used this model. They also made a polytropic compression assumption, as shown in eq. (12).

$$P_{suc}\nu_{suc}^{n} = P_{dis}\nu_{dis}^{n} \tag{12}$$

where n is the polytropic exponent and can be calculated from experimental data by eq. (13).

$$n = \frac{1}{N}\sum_{i=1}^{N}\frac{\ln\left(P_{suc,i}/P_{dis,i}\right)}{\ln\left(\nu_{suc,i}/\nu_{dis,i}\right)} \tag{13}$$

Then the model can be solved by minimizing the objective functions in eq. (14) and eq.(15).

$$J = \sum_{i=1}^{N}\left(\frac{\dot{m}_{pred,i} - \dot{m}_{meas,i}}{\dot{m}_{meas,i}}\right)^2 \tag{14}$$

$$J = \sum_{i=1}^{N}\left(\frac{\dot{W}_{pred,i} - \dot{W}_{meas,i}}{\dot{W}_{meas,i}}\right)^2 \tag{15}$$

The accumulator is a device that stores liquid refrigerant before the compressor while maintaining the refrigerant close to the vapor state at its outlet (Cheung and Braun, 2014). Some authors merged it with the compressor (Sun et al., 2017). Others

considered it separately (Cheung and Braun, 2014). The accumulator was generally modeled as a liquid-vapor separator, which discharged vapor only. This also implied that pressure and enthalpy remained unchanged across the accumulator, and the inlet quality of the accumulator should be greater or equal to one (Cheung and Braun, 2014).

b. Heat Exchanger Model

Heat exchanger models could be classified into four groups: 1) lumped parameter models, 2) zone model or moving boundary model, 3) distributed parameter models or finite volume models, and 4) tube-by-tube models (Qiao et al., 2010). Cheung and Braun (2014b) used a lumped parameter model, which is the simplest one. The heat exchanger was treated as a single control volume. The so-called NTU-effectiveness (NTU-ε) method (Bergman et al., 2011) was adopted without providing details of the model. Sun et al. (2017) used a four-section lumped model developed by Ge and Cropper (2005). They also used the NTU-ε method to carry out the calculation of heat transfer. The heat balance is provided by eq. (16).

$$\dot{Q} = \dot{m}_a Cp_a\left(T_{a,in} - T_{a,out}\right) = \varepsilon(G)_{min}\left(T_{r,in} - T_{r,out}\right) \tag{16}$$

where the effectiveness "ε" can be calculated by eq. (17).

$$\varepsilon = \begin{cases} 1 - \exp\left[\dfrac{NTU^{0.22}}{(G)_{min}/(G)_{max}}\left(\exp\left(-(G)_{min}/(G)_{max}\right) \cdot NTU^{0.78}\right) - 1\right] & \textit{single-phase region} \\ 1 - \exp(-NTU) & \textit{two-phase region} \end{cases} \tag{17}$$

The inlet refrigerant parameters of each section are from the outlet parameters of the section above directly except for the superheated region. For steady-state modeling, researchers generally use a lumped parameter model for heat exchanger modeling. The

simplified model is enough to describe the steady-state. However, for the transient state, the case is different, which is further discussed later.

c. EEV Model

The EEV model is typically described by the mass flow rate equation, as shown in eq. (18) (Wile, 1935):

$$\dot{m} = C_{EEV} A \sqrt{2\rho_{in}(P_{in} - P_{out})} \tag{18}$$

where A, ρ_{in}, P_{in}, and P_{out} are the flow area of the EEV, the inlet density of the refrigerant, the inlet pressure, and outlet pressure, respectively. C_{EEV} is the EEV correlation factor (Wan et al., 2018). Different authors used different forms of correlations to estimate the C_{EEV}. Three kinds of EEV correlations existed: 1) power-law correlation (Chen et al., 2009a, 2017a; Park et al., 2007a; Tian et al., 2015a; Ye et al., 2007a; Zhang et al., 2006a; Zhifang et al., 2008a); 2) polynomial correlation (Li, 2013a); and 3) Neural Network (NN) correlation (Cao et al., 2016a; Tian et al., 2015a; Wan et al., 2019). The most common correlation adopted in the HP model was the power-law correlation.

d. Pipeline Model

The pressure drop across the pipeline was typically evaluated by a simple correlation (Müller-Steinhagen and Heck, 1986), as shown in eq. (19) for single-phase flow and eq. (20) for multi-phase flow:

$$\Delta P = (fL\rho u^2)/2D \tag{19}$$

$$\Delta P = \emptyset(fL\rho u^2)/2D \tag{20}$$

where f is the frictional coefficient, u is the flow velocity, D is the diameter, and ∅ is the frictional two-phase multiplier, L is the length of the pipe, and ρ is the density of the fluid.

e. System Configuration

Most studies relied on a fixed system configuration. Park et al. (2001) and Shah et al. (2004) studied two IUs' models. Wu et al. (2005a) and Lin and Yeh (2007) conducted three IUs' models. Very limited scholars focused on models for arbitrary system configuration. Shao et al. (2012) developed a dynamic model for an arbitrary configured refrigeration cycle, which would be further discussed later. Sun et al. (2017) carried out a steady-state model for arbitrary system configuration based on Shao's research. They used a matrix to save the arbitrary system configuration and solved the model by graph theory. Interested readers can read the references for detail.

f. Iteration Algorithm

Though different authors used a slightly different iteration algorithm in their models due to different component models, the basic process was similar. Most researchers used the same order from the compressor model to the accumulator model. As mentioned above, Sun et al. used a graph-theory-based generation method of computation sequences to trace the calculation order of components and pipeline. Thus, their solver was different from the traditional one. A tailor-made refrigerant mass-induced iteration algorithm was developed to solve the internal coupled component models.

Transient Linearized Model

Perhaps due to confidential policy, most transient model-related papers just mentioned the dynamics of their model generally. Only one research group gave the details of their model. Lin and Yeh (2007) used the following approach, as shown in eq. (21) to describe the dynamics of the HP system.

$$\begin{bmatrix} \delta T_{sh} \\ \delta T_e \end{bmatrix} = \begin{bmatrix} \frac{b_{11}}{s+a_1} & \frac{b_{12}}{s+a_1} \\ \frac{b_{21}}{s+a_2} & \frac{b_{22}}{s+a_2} \end{bmatrix} \begin{bmatrix} \delta\omega \\ \delta\alpha \end{bmatrix} \tag{21}$$

This model could describe each IU of the HP system. This model was expressed in Laplace transform form. a_1 and a_2 represent the most dominating poles for each indoor unit. T_{sh} and T_e are superheat and evaporate temperature, respectively. b are the control gains. δ is used to show the model is based on linearization, so inputs (compressor frequency ω and target IU EEV opening degree α) and outputs are all in the perturbed form. The parameters (a and b) are identified from the experiments.

Transient Component-based Model

Shao et al. (2012) built mathematical component models of the HP system and integrated them with the framework of the two-phase fluid network. They also mentioned that the models used for the transient state of the compressor and EEV model were the same as that of the steady-state model.

a. Heat Exchanger Model

Shao et al. (2012) adapted the moving boundary method. The evaporator has two refrigerant regions, i.e., two-phase and superheated regions. The condenser has three refrigerant regions, i.e., superheated vapor, two-phase, and subcooled liquid regions.

The non-linear state-space matrix representations of the evaporator were given by Shao et al. The axial conduction in the unidirectional pipe can be neglected as compared to the heat transfer through the condenser surface. They used mass balance equations, energy balance equations, and temperature relationships to set up the model. Interesting readers can check more details from references.

b. Accumulator and Receiver Model

Since the accumulator volume is typically small, its effect is generally considered to be negligible by some researchers (Sun et al., 2017). However, the lumped parameter model was widely used when the accumulator was modeled. The following model was adopted by Shao et al. (2012). They applied the mass and energy balances in their model. The equations of the accumulator are shown in eqs. (22) and (23). The receiver model can be expressed in a similar way, which is not be repeated here.

$$V_{acc}\frac{d\rho_{acc}}{dt} = \dot{m}_{in,acc} - \dot{m}_{out,acc} \tag{22}$$

$$V_{acc}\left(\frac{d(\rho_{acc}h_{acc})}{dt} - \frac{dP_{acc}}{dt}\right) = \dot{m}_{in,acc}h_{in,acc} - \dot{m}_{out,acc}h_{out,acc} + \alpha_{acc}A_{acc}(T_{a,acc} - T_{r,acc}) \tag{23}$$

Summary

The steady-state HP system model has been well studied. The component-based steady-state model is mature. Future work of this part could be exploring new refrigerants, like flammable refrigerants. Furthermore, complicated structured HP systems, like the system with HRU or subcooling heat exchanger, need further study. A lot of empirical steady-state models exist. However, these methods require big data sets and are unexplainable.

Nearly all of the previous works of the dynamic models were component-based. The methods used to describe each subcomponent were also similar. Nevertheless, the component-based method has some flaws. First, the current dynamic HP model lacks in accuracy. Second, such model utilization requires a high level of knowledge. When some error existed, the model would be hard to converge. Third, different researchers used different platforms. Evaluating and comparing different models brought challenges. Future work could be made to develop some user-friendly dynamic tools. A model that can detect its faults and provides the users some suggestions might be a good appraoch. Scholars rarely mentioned empirical dynamic models. Future research may also be done in this area since the characteristics of the knowledge-based method could fill in the gap of the traditional methods.

1.3.3. Data Analysis and Current Applications

Researchers already proposed a framework for HP systems control, as shown in Figure 1-7. As I mentioned above, data analysis is a significant part of modeling, simulation, control, and FDD. Namely, three methods including statistics-based, machine learning-based, and physic-based exist as shown in Figure 1-8. Some readers might argue about the differences between statistical methods and machine learning methods. They are two different critters. Machine learning models aim at making the most accurate predictions, while statistical models are designed for inference among variables. They also have many other different characteristics. Engaging readers could read the famous

paper for reference (Breiman, 2001). Statistic methods are usually considered more interpretable than machine learning methods.

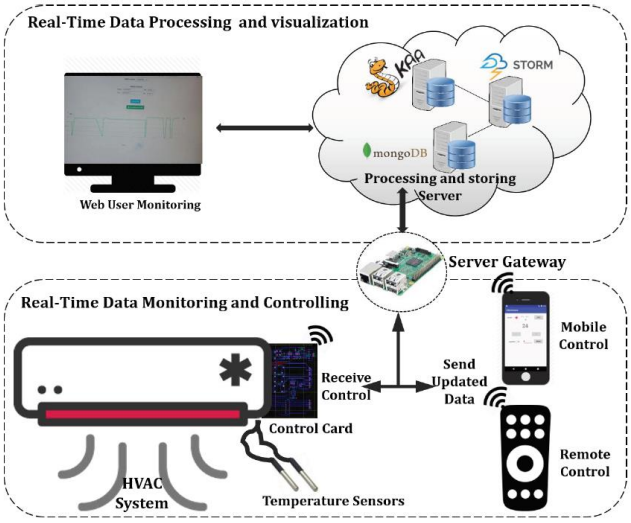

Figure 1-7 Existing Database Framework for HP Systems (Lachhab et al., 2018)

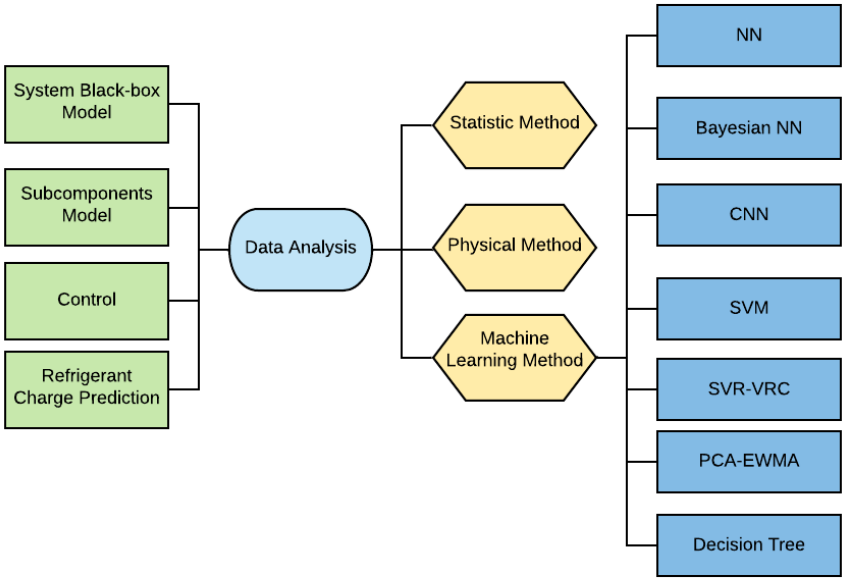

Figure 1-8 Data Analysis Framework

In the first place, I prefer physics-based models since they could be explained well and have decent accuracy. However, a physics-based model is usually hard to derive. A more general way is a semi-empirical method, which is also known as the grey-box method, as I mentioned in the modeling chapter. Take eq. 18, the EEV mass flow rate equation, as an example. The equation is based on fluid mechanics, but statistic methods still can obtain the EEV correlation factor (C_{EEV}) through the experiment. It is the most commonly used method in the past few years.

As for machine learning, it has become a hot topic recently due to its amazing accuracy for some proper cases. As shown in Figure 1-8, numerous algorithms exist. However, only NN was widely used in nearly every field, including modeling (Cao et al., 2016a; Tian et al., 2015a; Wan et al., 2019), control (Kang et al., 2018), and FDD (Nasrabadi, 2007). Other methods were only used in FDD. The reason might be the toolbox function of some commercial software like Matlab lowers the threshold to the field. Other algorithms do not have such an easy way until now. Since different researchers use different standards of these algorithms in different fields, it is hard to conclude which algorithm has the best performance in HP modeling. The different device capacities and the test conditions also brought difficulty in comparing their works. Thus, the future work of the HP system modeling study could be using different machine learning algorithms for the same system and developed a component-based model to evaluate the performance of these algorithms.

All the previous studies only focused on three months to one-year scale data as mentioned in Table 1-2. The system performance was seldom compared year by year. The reason could be that previous slow hardware and shorten data analysis techniques limited the scale of the database.

As the industry has been evolving to the 4.0 Industrial Revolution environment, including cyber-physical systems, artificial intelligence, cloud computing, and the internet of things (Yan et al., 2017), big data techniques have been utilized in the construction industry (Bilal et al., 2016), to building management (Dey et al., 2018), and now gradually to HP systems (Capozzoli et al., 2017; Lachhab et al., 2018; Li et al., 2020). The existing big data analytic method provides us a tool for dealing with a much larger scale database. Thus, how to apply these tools would become a problem for novel HP systems.

1.3.4. Life Cycle Climate Performance Analysis

The climate is changing faster further than predicted, with self-reinforcing feedback loops in the climate system that risk pushing the planet past irreversible and catastrophic tipping points (The Climate Reality Project, 2020). HP systems are both one of the main contributors to global warming (Yang et al., 2021) and can be part of the solution. The challenge is to drastically increase energy efficiency even as electric supply has been shifting from fossil fuels to renewable energies and simultaneously shift from high global warming potential (GWP) refrigerants even as leak rates are minimized and refrigerants are fully recovered at the end of (product) life (EOL).

Life Cycle Climate Performance (LCCP) has been invented and evolves in the past decades, as shown in Figure 1-9. Other environmental evaluation metrics exist for HP systems before the LCCP. Global warming potential (GWP), a famous ecological metric for refrigerants, only accounts for the direct emission from the refrigerant (Makhnatch and Khodabandeh, 2014). Total Equivalent Warming Impact (TEWI) is the summation of carbon-equivalent direct refrigerant and indirect power generation GHG emissions (Sand et al., 1997). At the same time, LCCP, which is more comprehensive, adds carbon-equivalent and embodied emissions. In turn, Life Cycle Assessment (LCA) involves a thorough inventory of the energy and materials that are required across the industry value chain of the product (Mota-Babiloni et al., 2020). LCA is widely used in other fields like building and aviation sectors other than HP systems (Bachmann et al., 2017; Vilches et al., 2017). Recently, some researchers came up with a new concept: Enhanced-LCCP (EL-LCCP) (Andersen et al., 2018), which considers local climate, heat islands, and local power supply characteristics.

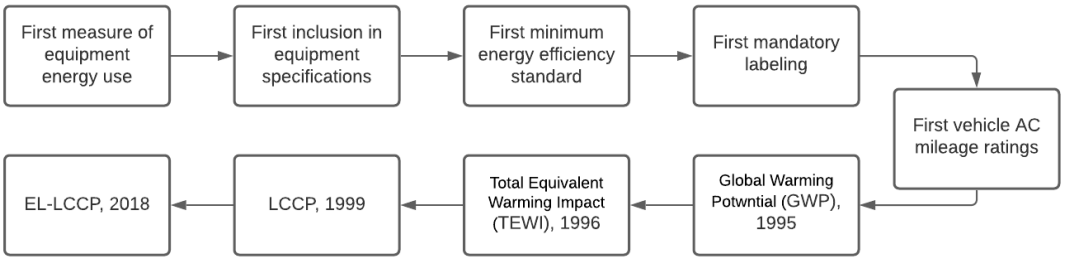

Figure 1-9 Invention and Evolution of LCCP

The LCCP has been used to evaluate the LCCPs of different HVAC systems in the past ten years, as shown in Table 1-3.

Table 1-3 Recent LCCP Evaluation Research

Author (year)	System	Refrigerant	Country
Horie et al. (2013)	1.3 kW HP	R-410A, R-32, R-1234yf	Japan
Zhang et al. (2014)	11 kW HP	R-410A, R134a, R-1234yf	U.S.
Li (2015)	13, 14 kW AC	R-410A, R-22	U.S.
Troch et al. (2016)	11 kW HP	R-410A	U.S.
Lee et al. (2016)	11 kW HP	R-410A, R-32, R-290, DR5, L41, D2Y60	U.S.
Choi et al. (2017)	11 kW VI HP	R-410A, R-32, R-290	Korea
Wu and Jiang (2018)	-	R-410A	China
Kim et al. (2018)	12.4 kW VI HP	R-410A	U.S.

Horie et al. (2010) assessed the LCCP of the residential heat pump in Japan. Zhang et al. (2011) developed an LCCP tool for a residential heat pump for four U.S. cities. Li (2015a) evaluated the LCCP of various Packaged Air Conditioners (PAC) involving micro-channel heat exchangers for typical U.S. cities. Troch et al. (2016) and Lee et al. (2016) conducted an LCCP evaluation for the same heat pump system in five U.S. cities. Choi et al. (2017) developed an LCCP model and evaluated it for South Korean weather conditions. Wu and Jiang (2017) developed an LCCP calculation software to analyze different climate zones in China. Kim et al. (2018) applied a Neural Network algorithm to predict the LCCP value using three different U.S. weather conditions. In most of the past LCCP works, the environmental impact of the system was not evaluated in different countries but rather evaluated in one country. Also, half of the literature only focused on R-410A. Almost none of them discussed the recently announced refrigerants like R-466A and R-452B. Besides weather conditions, other factors can affect the LCCP evaluation. First, the grid emission factors are different in different countries. The range could be from 0.1 to 1.0 kg CO_2e per kWh (Transparency, 2018). This difference can bring obvious gaps in indirect carbon

emission calculation. Second, the Embodied Carbon-dioxide Coefficients (ECCs) of the materials are different. They can bring discrepancies in calculating the carbon emission in the system's manufacturing phase. Previous studies did not consider all these differences at the same time.

The LCCP has some successful applications. In 2009 SAE International approved standard J2766-200902 "GREEN-MAC-LCCP" (SAE International, 2009), which was the basis for industry decision to shift from HFC-134a to HFO-1234yf rather than to other refrigerant candidates available at that time (Andersen et al., 2013). Horie et al. (2010) assessed a residential heat pump in Japan. Zhang et al. (2011) developed an LCCP tool for a residential heat pump for four U.S. cities. Li (2015a) evaluated various Packaged Air Conditioners (PAC) involving micro-channel heat exchangers for typical U.S. cities. Troch et al. (2016) and Lee et al. (2016) conducted an LCCP evaluation for the same heat pump system for five U.S. cities. Choi et al. (2017) developed an LCCP model and evaluated it for South Korean weather conditions. Wu and Jiang (2017) developed LCCP-calculation software to analyze different climate regions in China. Kim et al. (2018) applied a Neural Network algorithm to predict the LCCP value using three different U.S. weather conditions. A new application in replacing older refrigeration and HP with refrigerators using LCCP was reported (Aprea et al., 2016).

Studies related to HP system environmental impact have grown steadily over the last 20 years and have become a mainstream topic but not always using the comprehensive LCCP metric. Figure 1-10 shows the number of papers reported on ScienceDirect using

the keywords “life cycle” for “heat pump” or “air conditioning.” 1,508 papers mentioned LCA, while only 84 papers mentioned the LCCP concepts. Makhnatch et al. (2014) reviewed LCCP, TEWI, and GWP publications in 2014 but mainly focused on different calculations of carbon-equivalent refrigerant effect. Chau et al. (2015) and Sharma et al. (2011) reviewed LCA for buildings, but although the HP systems were mentioned in their work, they were not analyzed in detail.

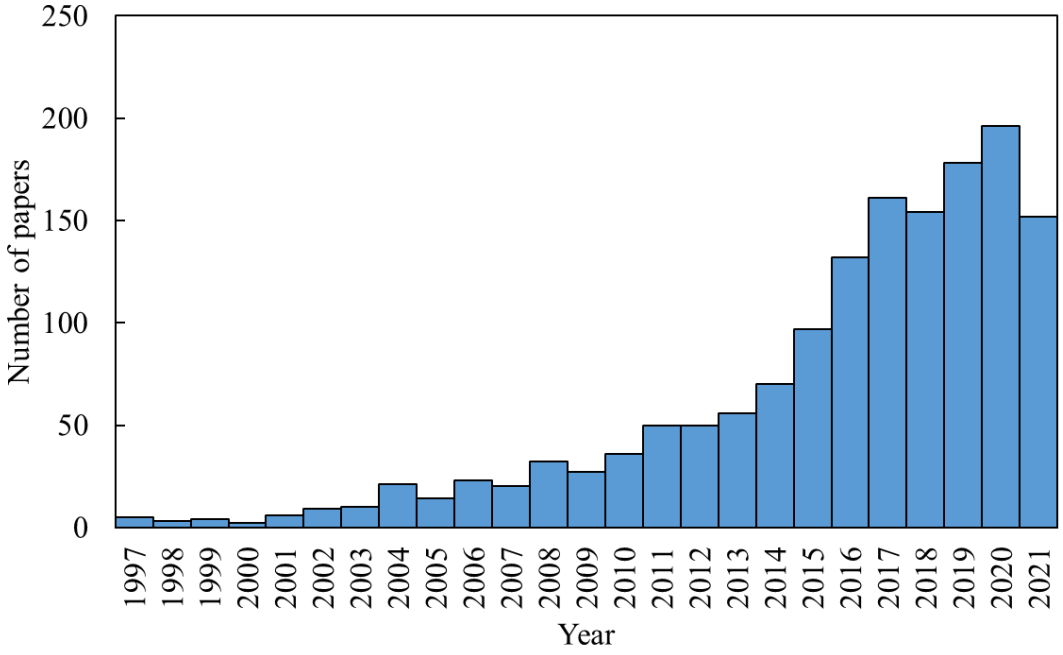

Figure 1-10 Histogram of Annual Environmental Impact Publications for HP systems (ScienceDirect, 2021)

This study presents the first survey of how different researchers estimate the direct, indirect, and embodied carbon-equivalent emission factors listed in IIR LCCP guidelines (IIR, 2017). In addition, my study could be considered as a supplement to the guideline. In the IIR LCCP guideline, the recommendation values were based on

North American regions, and some assumptions used in the guideline were not realistic enough. My review study analyzes how these assumptions were handled in the latest literature. For the current research gap, I provide my suggestions for future works.

Figure 1-11 shows the relationship between each sub-emission of LCCP. This study 1) discusses the refrigerant effects on LCCP calculations, 2) compares four different methods to predict the annual energy consumption of a given HP system, 3) adds the grid effect that is usually ignored by previous studies, and 4) summarizes a commonly used dataset for material embodied emissions. I then discuss current LCCP studies focusing on different impact factors, challenges, and purposes. Finally, I point out possible future work to enhance the framework and improve the LCCP studies.

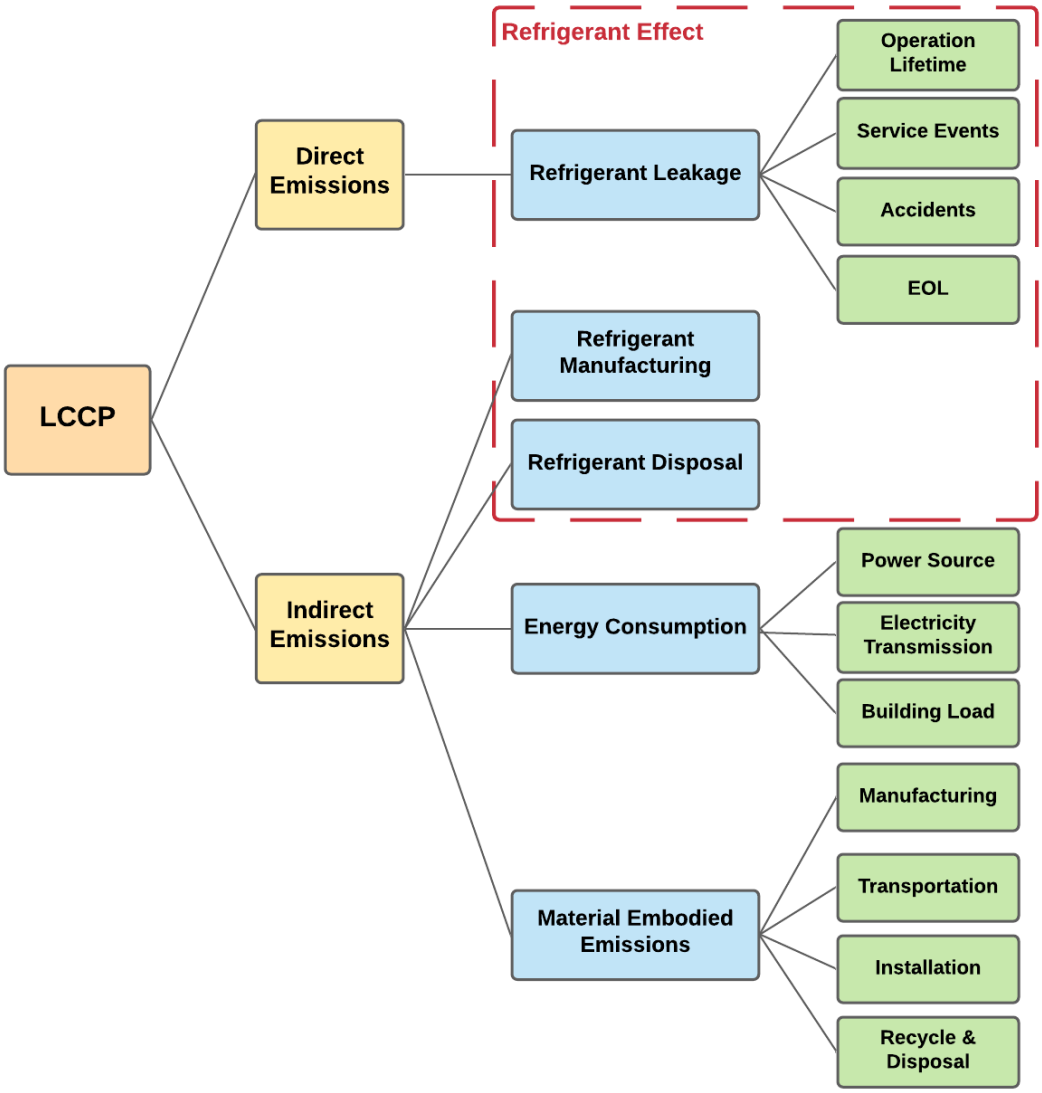

Figure 1-11 Elements of LCCP

1.3.5. Summary

Nearly all the researchers conducted field tests only in one city. Moreover, all the field tests were conducted in less than one year. Thus, the large data was seldom mentioned in the literature. Only Qian et al. (2021) reported data from multiple cities. However, they focused on "space," not "time." Though they had a large data set, the data was not collected from the same space. The systems in different climate regions were

compared, but the system's performance in the same place in different years was not reported.

"FlyData" summarized several challenges in large data (usually more than 10 Giga Byte) analysis ("The 6 Challenges of Big Data Integration | FlyData," 2021). First, a talent gap exists in large data. Several tools were developed to analyze large data, but handling these tools requires expertise. Second, getting data into a large data structure is difficult. The large data is usually saved in a different format from the normal data source. Loading the data into a large data platform also has a high cost. Third, the data sources are usually different, which means synchronizing across the sources is not easy. The data copies migrated from a wide range of sources at different rates, and schedules can rapidly evade the synchronization with the originating system. Fourth, extracting information from the data set requires knowledge.

For the HVAC system, I summarize several challenges based on our previous works and the literature. The data source would be a big challenge. I need to consider cross-platform data analysis and simulation. In addition, in the HVAC industry, our devices usually had limited Radom-Access Memory (RAM). This could bring an extremely long time in data analysis or breakdown of the program. Besides, previous researchers always focused on energy efficiency. How to find out other crucial information from the field test dataset is a problem.

1.4. Problem Statement

As the background information, the energy consumption of HP systems plays a significant role in the world residential building energy sector. The conventional HP system evaluation method focused on the energy efficiency of a given time scale (e.g., hourly, seasonally, or annually). From the literature review part, previous evaluation methods or test metrics were unable to reflect the thermodynamic characteristics of the system. In addition, previous researchers conducted HP tests within one year. Limited studies revealed the system performance in different years. Finally, as the climate is changing faster than predicted with self-reinforcing feedback loops in the climate system that risk pushing the planet past irreversible and catastrophic tipping points, HP systems are both main contributors to global warming and can be part of the solution. A holistic evaluation of the HP system's global warming impact during the life cycle needs to account for the direct refrigerant GHG emissions, indirect fossil fuel GHG emissions, and embodied equipment emissions. This dissertation proposes an experimental, emulational, and environmental (EEE) evaluation method for modern HP systems. National Institute of Standards and Technology (NIST) came up with HVAC Functional Inspection and Testing Guide (Kao, 1992), as shown in Figure 1-12. This dissertation mainly focuses on the data analysis part. The author leverages machine learning, deep learning, data digging, and LCCP approaches to develop next generation HP system evaluation methodologies with three thrusts: 1) *field test data analysis*, 2) *data-driven modeling*, and 3) *Enhanced Life Cycle Climate Performance* (En-LCCP). First, the dissertation compares time-average performance metrics with quasi-steady-state performance metrics in all time scales. Second, different machine

learning and deep learning algorithms are compared with physics-based and statistical methods. Third, the current environmental impact evaluation method is enhanced by considering ambient conditions variation, local grid source structure, and next-generation low GWP refrigerants.

The objectives of this dissertation are listed below:

- Develop a field test method and large-scale database for HP systems;
- Develop data-driven models for HP systems and sub-components;
- Improve current HP environmental evaluation method using more realistic criteria.

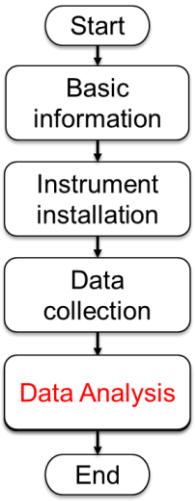

Figure 1-12 HP System Evaluation Process

2. Field Test, Database Development, and Data Analysis

Field tests are commonly used to test the energy efficiency of HP systems in buildings. They are considered as one of the most convincing ways to reflect the systems' performance in residential buildings. Current research and standards only focus on short-term field tests and average performance metrics. This chapter uses a HP-VRF system case study as an example to discuss the field test approach and data analysis.

2.1. Basic Information

I conducted field tests of a VRF system since August 2017 in an office building in MD, U.S. As shown in Figure 2-1, seven same indoor units were installed in five rooms. The users controlled the indoor units. The system had two HRUs and one Water Heating Unit (WHU). In the presented tests, the WHU was not used. Interested readers can use Lin et al. (2014) as a reference for WHU related tests.

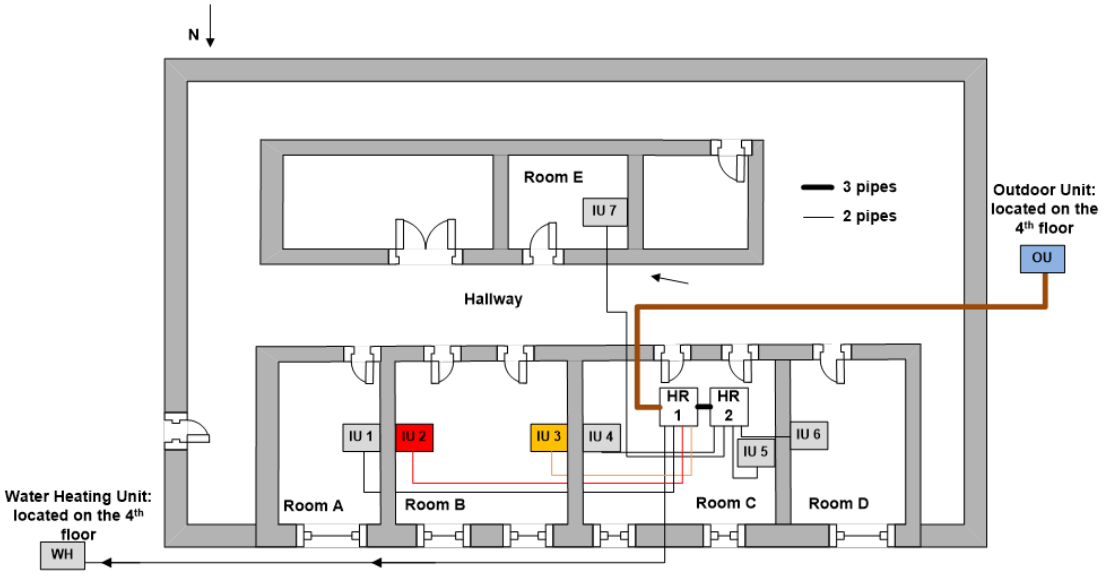

Figure 2-1 Room Layout (third floor)

Figure 2-2 describes the fourth-floor plan. The ODU of the system was installed on this floor, as well as the water tank and hydro kit of the WHU. For both room and ambient environments, I measured the temperature and humidity. Figure 2-3 shows the indoor and outdoor photos of the tested building.

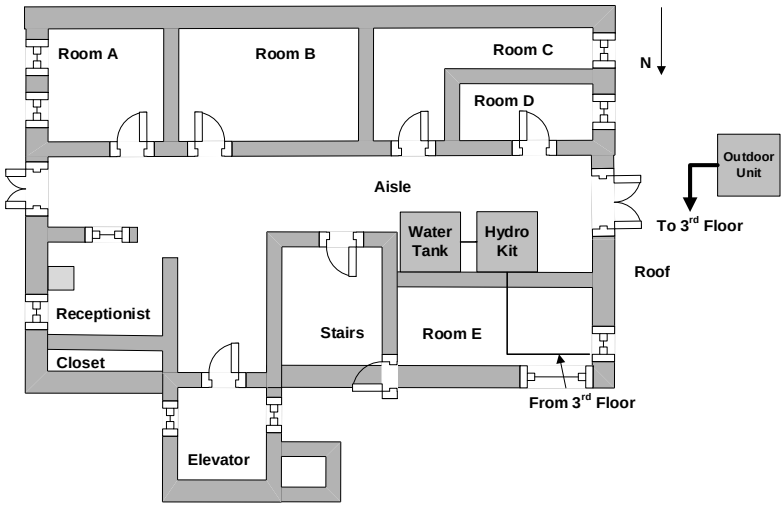

Figure 2-2 Room Layout (fourth floor)

Figure 2-3 Pictures of Indoor and Outdoor Units

The system diagram is given in Figure 2-4. This figure shows the system operation status when seven indoor units are in cooling mode, as an example. I measured the pressure, temperature, mass flow rate, and power consumption of the system. The sensors' positions are also shown in this figure. I used the DAQ system and made the measurement every two seconds, as shown in Figure 2-5. The thermocouples were calibrated as shown in Figure 2-6. The specifications of the measuring instruments are shown in Table 2-1. The tested system also had built-in sensors. The data like compressor frequency, fan speed, and EEV openings could be reached from the manufacture's software.

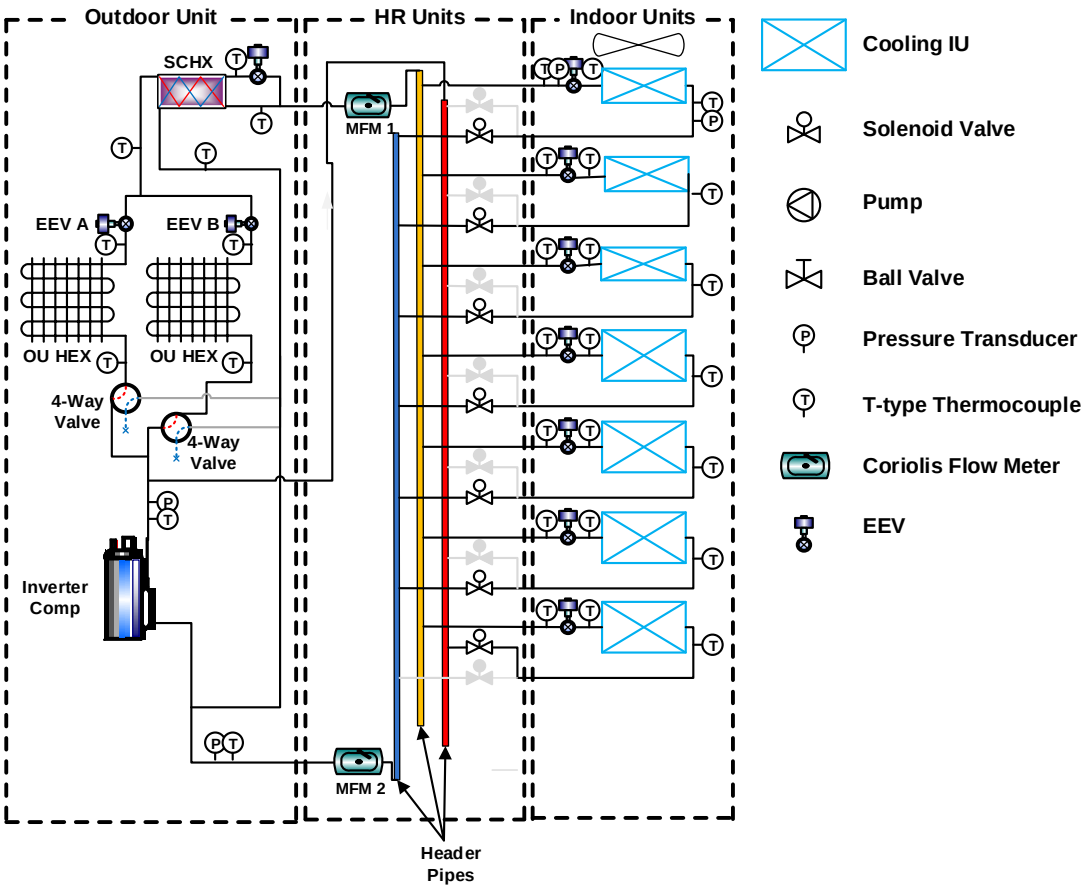

Figure 2-4 System Diagram

Table 2-1 Specifications of Measuring Instruments

Instrument	Type	Range	Accuracy
Thermocouple	T type	-200~350 °C	± 0.5 K
Pressure transducer (high pressure)	Capacitive	0~6,770 kPa	± 6.34 kPa
Pressure transducer (low pressure)	Capacitive	0~3,339 kPa	± 4.21 kPa
Mass flow meter	Coriolis	3~457.5 $g \cdot s^{-1}$	± 0.9 $g \cdot s^{-1}$
Wattmeter (Outdoor unit)	Electrostatic	0~40 kW	± 0.5% FS
Wattmeter (Indoor unit)	Electrostatic	0~4 kW	± 0.5% FS
RH sensor	Capacitive	0~100%	3%

(a)Sensors in ceiling b) Power sensors for ODU (c)Thermocouples in ODU

Figure 2-5 Sensors Installation

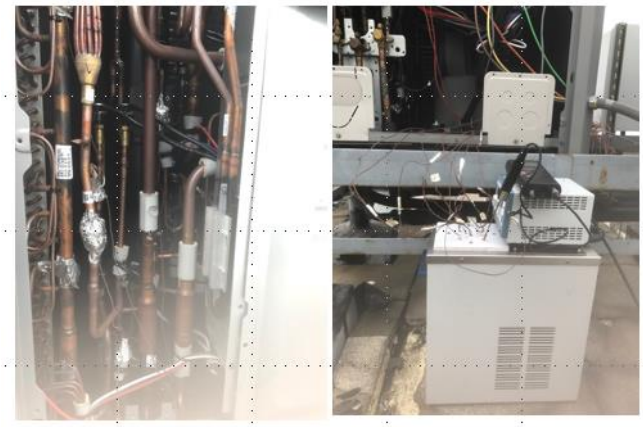

(a) Thermocouples (b) Water Bath

Figure 2-6 Sensors Calibration

2.2. Data Processing and Database Development

Figure 2-7 shows the process of analyzing the data. The crucial part is how to synchronize the data from the manufacture monitoring system and the data from the field test sensors. Besides, the data from the weather station can also be used for the data analysis. These data also need to be synchronized with the data from other sources. I handled the data with different platforms. Based on my experience, MATLAB is more user-friendly due to the "structure" and "mat" functions (or called data type). When MATLAB handles large data set (> 1 GB), the software automatically compresses and separates the data sheet. This can avoid the problem like exceeding the RAM limitation. If the user used EXCEL or Python to handle the data, the user may want to write the compress and separation process themselves.

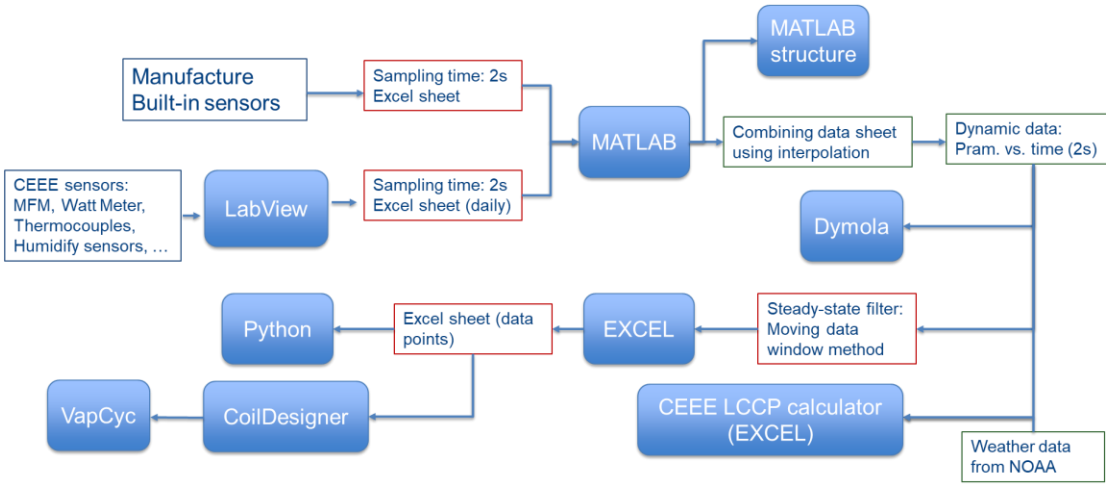

Figure 2-7 Data processing flow chart

I summarized the methods used in my previous publication (Wan et al., 2020). A lot of field test studies only focus on time-average power, part-load ratio, and COP using

statistical methods. The other methods were usually adopted by modeling or control researchers. In fact, in field tests, many parameters can also be focused and are able to affect the system performance, like peak pressure values, refrigerant charge levels, the time needed to reach setting IDU temperature, IDU humidity variation, etc.

Table 2-2 Datasheet Example

Time	Condensing Pressure [kPa]		Evaporating Pressure [kPa]		Mass flow rate [g·s^{-1}] (LabView)	ODU Power [kW] (LabView)
	LGMV	LabView	LGMV	LabView		
…						
'26-Dec-2019 08:53:29'	866	780	778	783	0.86	18.22
'26-Dec-2019 08:53:31'	890	796	742	718	0.97	28.48
'26-Dec-2019 08:53:33'	890	810	742	685	1.20	25.56
'26-Dec-2019 08:53:35'	947	842	669	614	1.44	26.21
'26-Dec-2019 08:53:37'	988	902	585	576	1.54	26.08
…						

A database for four-year field test data (2017-2021) was developed. The database is a two-dimension matrix or a table. The row is the time. The difference between two adjacent rows is 2 seconds, which is the sampling time. The table has 99 columns, which are the tested parameters like temperatures, pressures, mass flow rate, power consumption, etc.

Figure 2-8 shows an example of the data, which could be accessed from the database directly except COP. The COP here is the energy efficiency at each tested time point,

which could be calculated by eq. 24. The cooling capacity and heating capacity can be calculated by the enthalpy difference across the indoor units. The power consumption is the measured value.

$$COP_i = \frac{Cooling\ Capacity(t_i) + Heating\ Capacity(t_i)}{Power(t_i)} \tag{24}$$

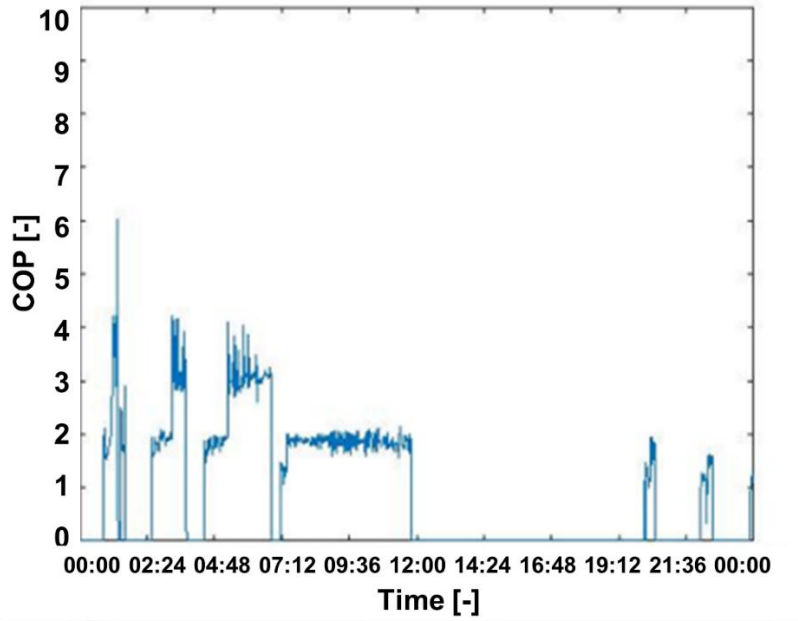

Figure 2-8 January 14th 2018 Data Example

2.3. Online Monitoring and Time-average Performance Metrics

For HP system measurement, people usually take an interest in energy efficiency. In chapter 2.2, the author gives an equation to calculate the COP at each measured time point, *t*. However, for a large dataset, it's impossible to calculate the COP for each measured time point since if the sampling time is short (e.g., 1 second or 2 seconds), the number of the measured time points can exceed billions easily. In order to describe the system's performance in a time period, previous researchers used time-average

performance metrics to evaluate the system performance. Daily Performance Factor (DPF) is a commonly used metric defined as follows:

$$DPF = \frac{\int_{t_0}^{t_1} \dot{Q}(t)dt}{\int_{t_0}^{t_1} P(t)dt} \tag{25}$$

$\dot{Q}$ is the total capacity at time t, while P is the total power at time t; t_0 is the start time in the day, while t_1 is the end time. Other similar metrics, like Annual Performance Factor (APF), Seasonal Performance Factor (SPF), etc., are summarized in the literature view part (chapter 1.3.1) and can be calculated using the same approach.

In practice, the integral is not easy to calculate. Researchers used an approximation form to estimate the DPF (Kwon et al., 2014):

$$DPF \approx \frac{\sum_{i=1}^{n} \dot{Q}_i \cdot \Delta t_i}{\sum_{i=1}^{n} P_i \cdot \Delta t_i} \tag{26}$$

The DPF of the VRF system field test is shown in Figure 2-9.

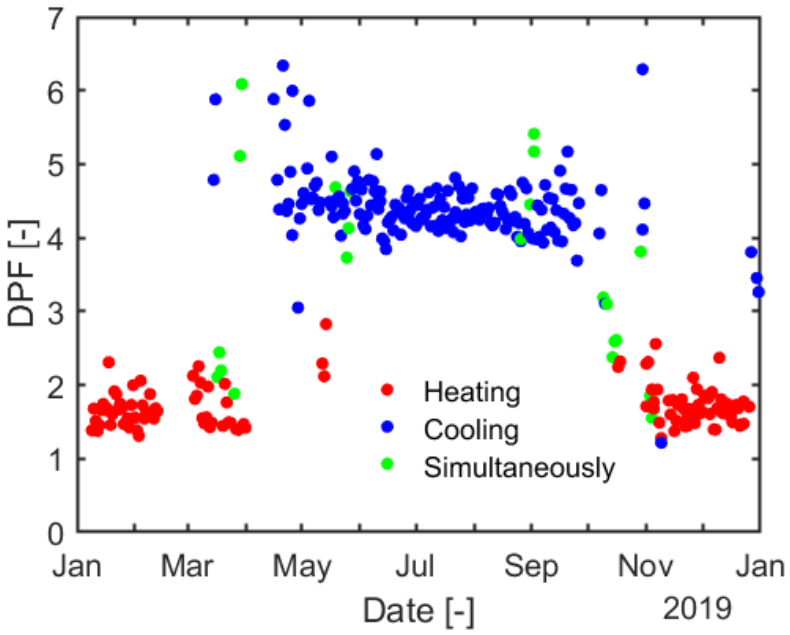

Figure 2-9 2019 DPF Evaluation

$$\dot{Q}_i = \left(h_{1,i} - h_{2,i}\right) \cdot m_i \tag{27}$$

$$h_i = h(P, T, \sigma) \tag{28}$$

The capacity could be calculated by enthalpy difference and mass flow rate as shown in eq. 27. The enthalpy is a function of pressure, temperature, and quality. For each time slot, the total capacity should be calculated by multiplying the differential time (Δt_i) to the instantaneous capacity. The true performance is to calculate the enthalpy at each time slot and then calculate the overall enthalpy difference. This could be explained by eq. 29.

$$\bar{Q}_i \cdot \Delta t_i = \sum_{j=1}^{n\to\infty} \left(h_{1,ij} - h_{2,ij}\right) \cdot m_{ij} \cdot \Delta t_{ij} \tag{29}$$

However, in practice, people usually used the average property (pressure, temperature) to calculate the enthalpy. This could be explained by eq. 30.

$$\bar{Q}_i \cdot \Delta t_i = \left(\bar{h}_{1,i} - \bar{h}_{2,i}\right) \cdot \bar{m}_i \cdot \Delta t_i \tag{30}$$

So, the question is that do the two methods give the same result? Mathematically, it's obvious that the two equations don't agree with each other. In this study, the author used the field test data to check whether, in engineering, this approach is acceptable.

In this dissertation, the difference of performance among two metrics is described by a metric, Mean Absolute Percentage Error (MAPE), which could be given by the following equation:

$$MAPE = \frac{1}{n}\sum_{i=1}^{n}\left|\frac{\boldsymbol{Y}_i - \widehat{\boldsymbol{Y}}_i}{\boldsymbol{Y}_i}\right| \times 100\% \tag{31}$$

In addition, the authors also set the error bound to be within ± 15% to check whether a metric could be used as a substitute for another metric. Figure 2-10 shows the results. The x-axis is the accumulative performance factor, which is the metric given by eq. 27

($\dot{Q}_i$) and is the true performance. The y-axis is the time-averaged property performance, which is the metric given by eq. 30 ($\bar{Q}_i$) and is the estimated performance.

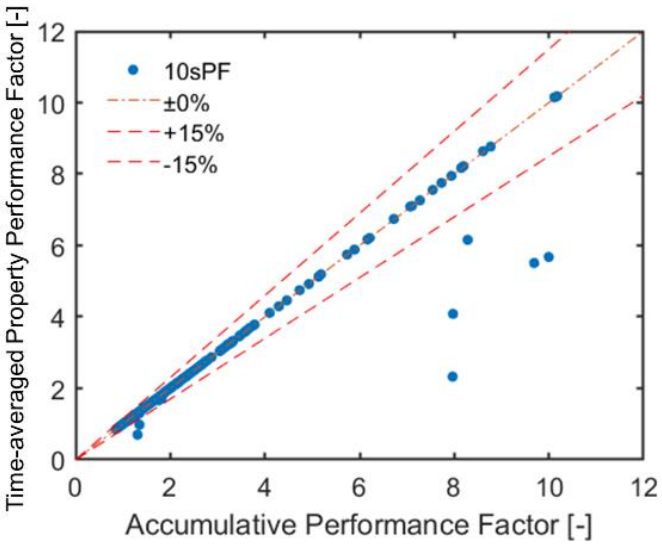

(a) 10-second Performance Factor (10sPF)
MAPE=0%; P=97%

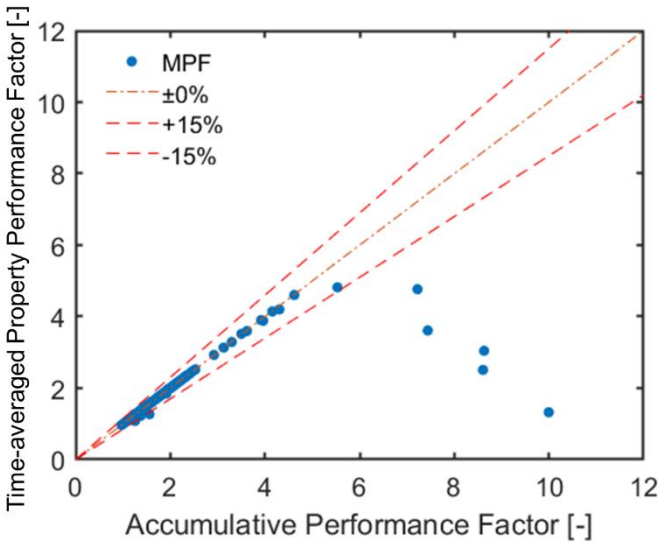

(b) Minutely Performance Factor (MPF)
MAPE=1%; P=95%

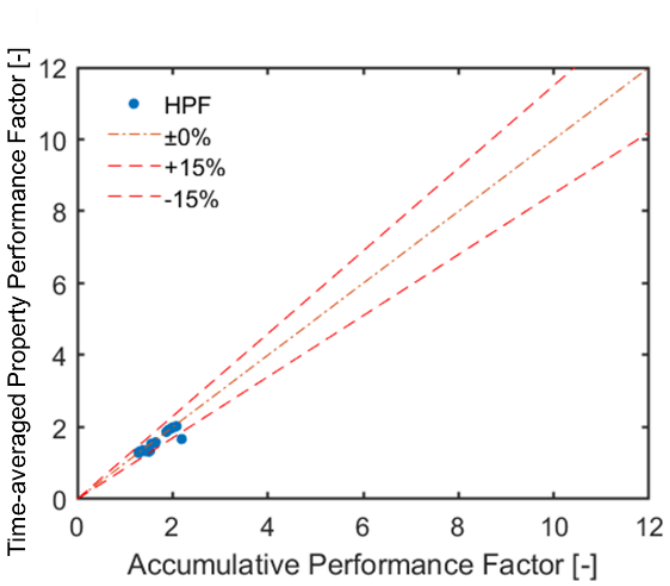

(c) Hourly Performance Factor (HPF)
MAPE=6%; P=69%

Figure 2-10 Comparison between the Accumulative Performance Factor and Average Performance Factor

As a result, Δt is very important for the accuracy of the estimation performance. When Δt equals 10 seconds, the overall error would be very close to 0%, and the possibility the error appears would also be very low, which means the average performance could be used as the substitute of the accumulative performance. The reason is that the slope of enthalpy is not continuous at the phase change point. I pick one point, which the estimation performance is far from the accumulative performance in the MPF figure, and check what was happened in this minute duration.

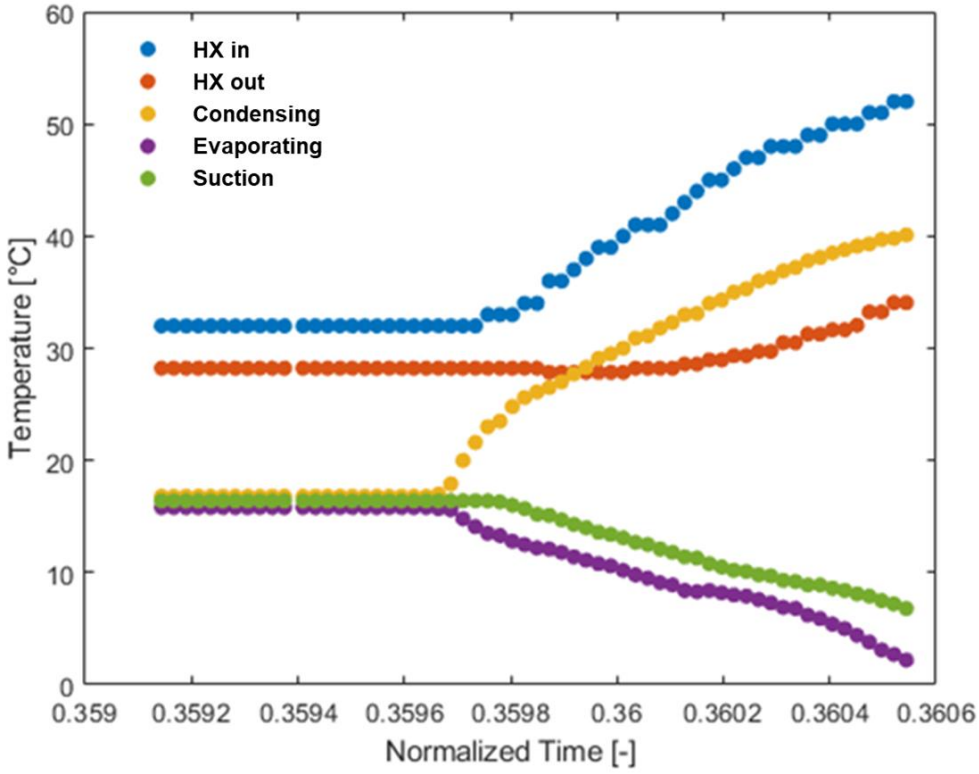

Figure 2-11 Temperature Change Example of the Misestimated Point

Figure 2-11 shows the inlet of the heat exchanger, the outlet temperature of the heat exchanger, the condensing temperature, the evaporating temperature, and the suction temperature of the misestimated point. The x-axis is the normalized time in one day (normalize 00:00-24:00 to 0-1). This example is in heating mode. In this one-minute duration, the outlet of the heat exchanger becomes the two-phase state. Thus, the enthalpy at the outlet of the heat exchanger is a piecewise function. Mathematics knowledge tells us that for a piecewise function $f(\bar{x}) \neq \overline{f(x)}$.

The reason to use the time average performance is that the enthalpy calculation takes a large time in the whole process to calculate the system efficiency.

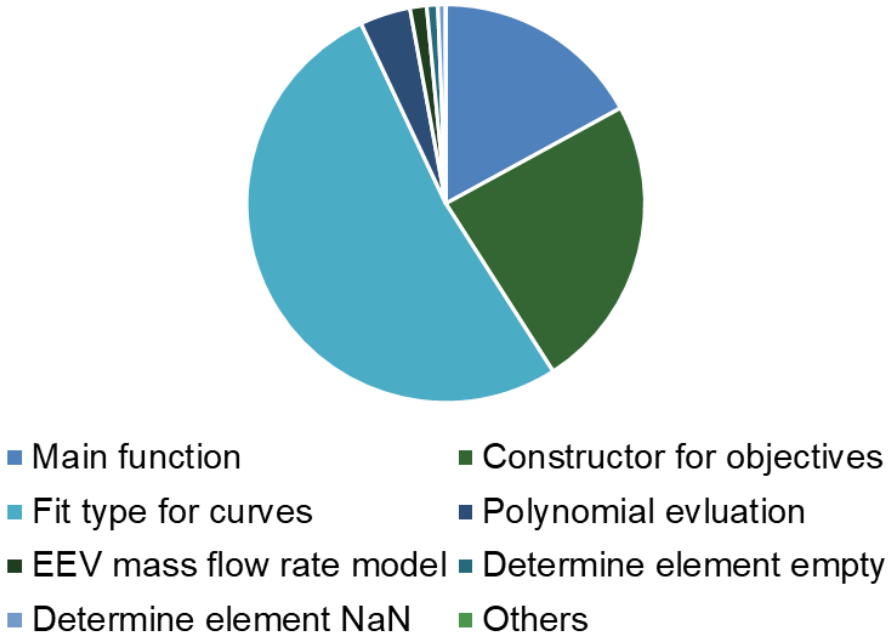

Figure 2-12 Time Consuming for Each Function to Calculate System Efficiency

Figure 2-12 shows the time consumed by each sub-function in the program to calculate the system efficiency. In this program, refrigerant properties were calculated and stored in tables by "REFPROP." Then polynomial interpolation was used for "lookup" tables. Thus, the light blue part in the figure called "Fit type for curves" (or selection of types of fitting equations) shows the time consumed to calculate the enthalpy. This part takes more than 50% of the total time. Thus, using time-average performance means that one can call the "lookup" function less, and this definitely leads to a time-saving result.

Determining Δt is important in the time-average performance calculation. The frequency that one side of the heat exchanger becomes the two-phase state needs to be considered since this is the reason that the error occurs. Obviously, the on-off ratio is a significant factor affecting the frequency that the heat exchanger outlet becomes the

two-phase state. The on-off ratio is affected by the system's load and maximum capacity. If the system's maximum capacity is larger than the building load, the frequency that the heat exchanger outlet becomes the two-phase state would be high. If the system capacity is lower than the building load, the system is kept operating, which means that the frequency would be low. In conclusion, for the case that the system maximum capacity is small but still larger than the building load, the time average performance method is not recommended to be used.

2.4. Quasi-steady State Performance

Another method, which can also screen out some data, is the Quasi-Steady State (QSS) performance method. In HP system field tests, the QSS data was seldom mentioned. However, the QSS performance usually reflected the performance of the system better than time-average performance metrics. The first challenge of QSS data analysis is searching for semi-steady-state or QSS data.

2.4.1. Steady-state and Filter

A great number of methods have been adapted to detect the steady-state of the systems. Some of them were shown in Table 2-3.

Table 2-3 Different Steady-state Detection Methods

Methodology	Author and Year	Demonstrated Application
F-test	Cao et al., 1995	Experimentally measured pH, temperature, and pressure
Standard deviation	Kim et al., 2008, 2017 Bejarano et al., 2016 Lecompte et al., 2018	Heat pump, Organic Rankine cycle (ORC), vapor compression refrigeration system
Linear regression	Holly et al., 1989 Bethea and Rhinehart, 1991 Wu et al., 2013	Acoustic emission monitoring, mass flow rate measurements
T-test	Narasimhan et al., 1987	Simulation
Bayesian inference	Wu et al., 2016	Cavitation Noise Power (CNP) signals
Slope and Second Derivative	Perez et al., 2018	Building Management System (BMS)
R-test	Bianchi et al., 2017	ORC

These methods can be divided into several groups. One is using the so-called moving data window. This method sets only one moving data window and monitors the standard deviation or does linear regression and compares the target value with a threshold value. If the value is below the threshold value, the status can be considered to be a steady-state.

Another group is setting two recently adjacent moving data windows. Some statistical values can be used to detect the steady-state. In these methods, Kim's method (Kim et al., 2008) is the most widely used method for vapor compression cycle.

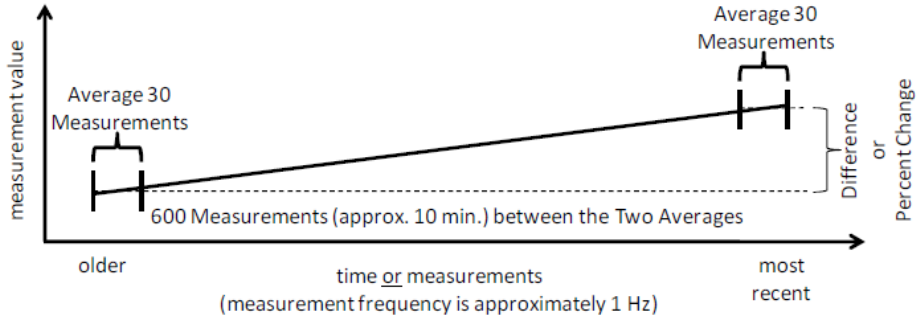

Figure 2-13 Kim's Method Explanation (Kim et al., 2008)

Figure 2-13 (Kim et al., 2008) shows that measurements are averaged, and the space between those averages is used to determine steady-state conditions. Table 2-4 shows the comparison criteria for each measurement for steady-state conditions.

Table 2-4 Kim's Method Criteria (Kim et al., 2008)

Measurement	QSS Criteria
Temperature	Difference < 0.5 K
Pressure	Change < 2%
Mass Flow	Change < 2%
Rotating Equipment Speed	Change < 2%

For the steady-state detection, three questions need to be answered. First, which method is the most proper one for HP systems? Second, which parameter is important? And third, which moving data window scale is proper?

I applied Kim's method in the VRF system case study. The test time was July 7th to July 18th, 2018. Table 2-5 shows the ratio between the STD and average value for four parameters in 30 seconds (four points were shown as examples). It could be found that the mass flow rate had the highest deviation. In other words, for VRF systems, we can assume that the QSS filter only needs to constrain the mass flow rate. The benefit is

time-saving. Considering that we need a label to check the system's on-off status, the compressor frequency was also used in the filter for QSS detection.

Table 2-5 Parameter Difference

No.	**Pressure 1**	**Pressure 2**	**Temperature 1**	**Temperature 2**	**MFR**
1	0.70%	1.33%	0.67%	0.48%	0.44%
2	0.60%	1.57%	0.70%	0.57%	1.89%
3	0.41%	1.22%	1.34%	0.50%	1.89%
4	0.34%	0.90%	1.35%	0.36%	1.81%

Thus, in this dissertation, the author used the following equations as the filter to detect QSS in an *M*-second time widow with *n* data points exist:

$$\begin{cases} STD(MFR) = \sqrt{\dfrac{1}{n-1}\sum_{i=1}^{n}(MFR_i - \overline{MFR})^2} \le Tr \\ F_i = \bar{F} \qquad\qquad i = 1,\ 2,\ \ldots,\ n \end{cases} \tag{32}$$

In the VRF system field test, the author used M=60, n=30, and Tr=1 $g \cdot s^{-1}$. The M value is from the literature (Qiu, 2018). The time for HP system charging is around one minute. The Tr value is set based on the uncertainty of the MFR meter used, which is 0.98 $g \cdot s^{-1}$. In fact, setting M and Tr also need to consider how many data points are expected to get.

The steady-state status of a typical day is shown in Figure 2-14. The mass flow rate shows the average measurements due to noise in the signal. The pressure was the original value. '1' means steady-state while '0' means not.

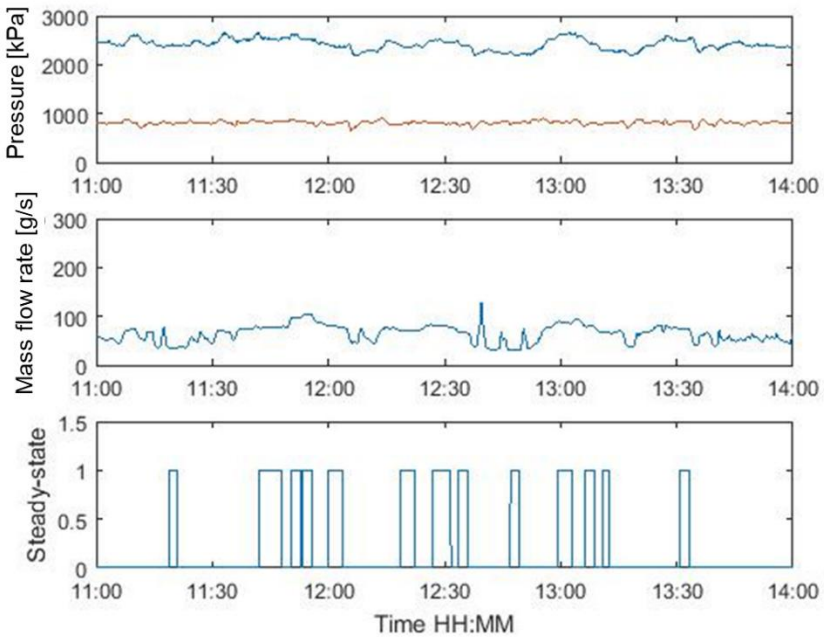

Figure 2-14 Steady-state Status Example

Studying the system's QSS performance can lead to several interesting results. Chapter 2.4.2, 2.4.3, and 2.4.4 show the power consumption in QSS, COP in QSS, and some information found from QSS performance, respectively.

2.4.2. Power Consumption in QSS

The QSS conditions in my study were set for the standard deviation of the total mass flow rate to be smaller than 5 $g \cdot s^{-1}$ in a ten-second time window while the compressor frequency and all the Electric Expansion Valve (EEV) opening degrees were kept unchanged. I finally secured 23,323 data points. I defined a one-digit number "M." The "M" value means the number of indoor units operating in cooling mode. As an example, "M=3" means that three cooling units operated. Table 2-6 shows the distribution of the "M" value of my database. The second column, count number, means the number of data points that "M" indoor units operate in cooling mode. I ignored the group with a

count number smaller than 100 (ignored “M” equaled “6” or “7”, which means the system was seldom operating with 6 or 7 indoor units in cooling mode).

Table 2-6 Tabulated Data

M Value	Count	Percentage
1	1,167	5.0%
2	6,182	26.5%
3	7,425	31.8%
4	3,191	13.7%
5	371	1.6%

The field test result of the power consumption is shown in Figure 2-15. Different rows indicate a different number of cooling units. For example, the first row means that there is only one cooling unit operating. As can be found in Figure 2-15, the slope of the data points increases with the number of cooling units (M). It is because the cooling load is increased with the ambient temperature. In this situation, the system control logic would apply a higher frequency of the compressor. Therefore, the power consumption of the compressor was increased with the compressor frequency. According to Figure 2-15, it is hard to conclude the energy efficiency of different cases. Thus, I conducted a machine learning-based model using the two data sets. The goal was to predict the power consumption under the same ambient and operating conditions.

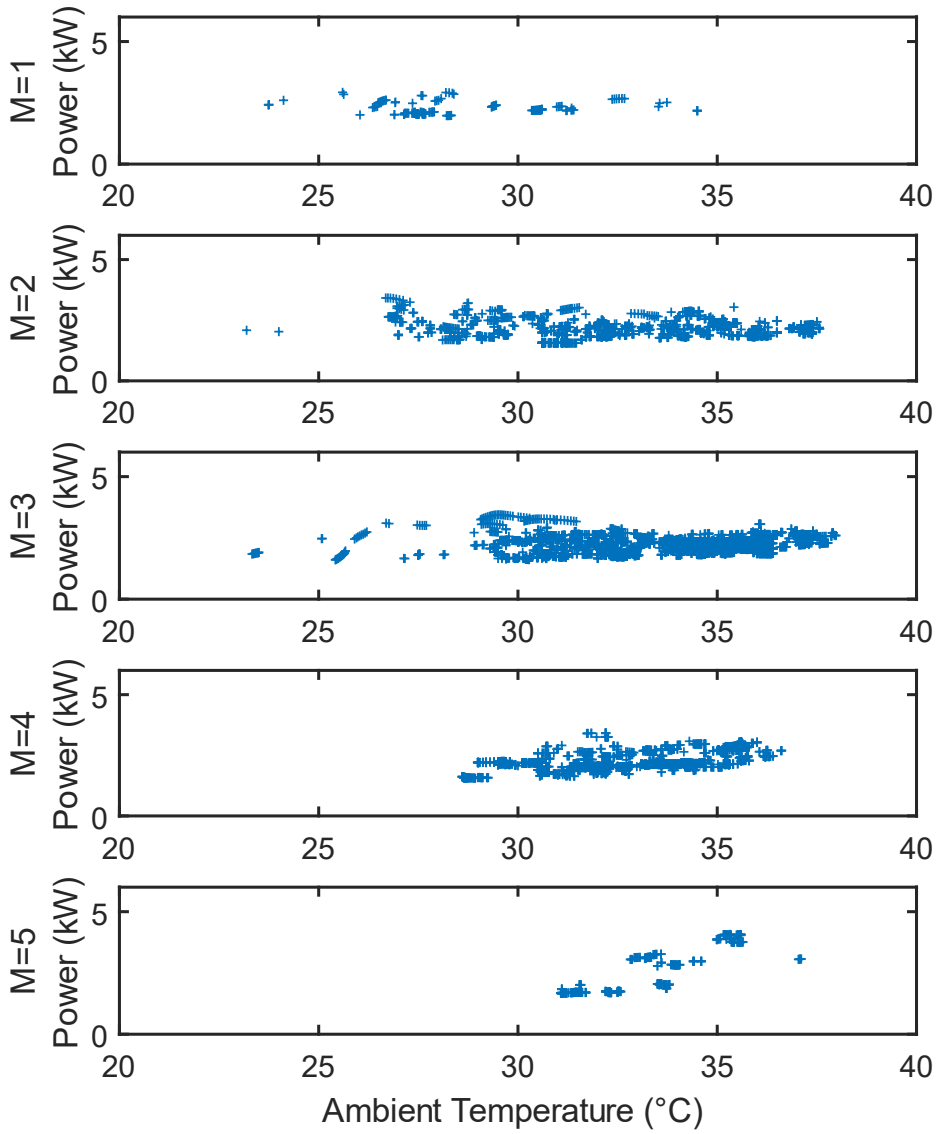

Figure 2-15 Power Consumption versus Ambient Temperature

2.4.3. Energy Efficiency Analysis in QSS

Figure 2-16 shows the Coefficient of Performance (COP). Similar to what Figure 2-15 shows, the trend of the COP is not apparent when M is small. When M equals 4 or 5, as the ambient temperature increases, the COP of the system decreases. The reason might be that when only 1 or 2 indoor units operated, the cooling load was not high

enough. Thus, the compressor was working under low frequency, which caused that the efficiency of the compressor was low due to a low inverter drive efficiency. This would make a complicated result for the COP. However, when the compressor frequency was high, the efficiency of the heat exchanger would be a significant factor. When ambient temperature decreases, the heat transfer efficiency of the outdoor unit heat exchanger increases and the COP of the system should also increase. In addition, lower ambient temperature also results in a lower pressure ratio, which results in higher compressor efficiency.

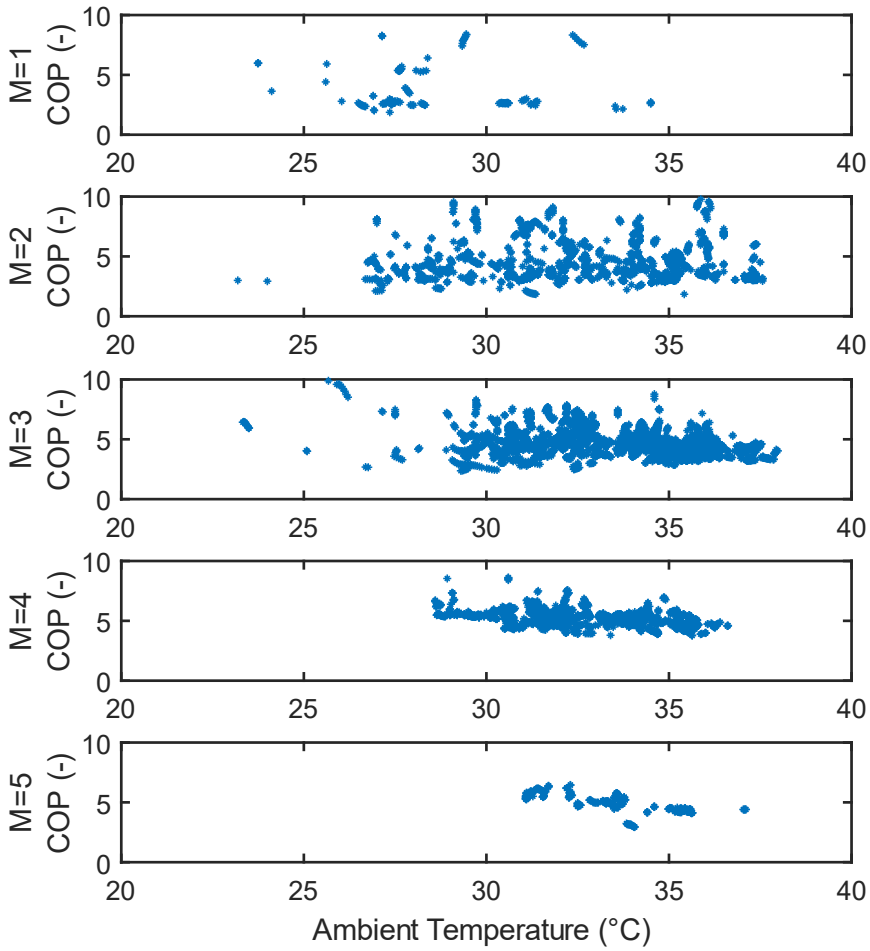

Figure 2-16 COP versus Ambient Temperature

2.4.4. Data Digging in QSS

QSS performance can show the relationship between different system parameters. Figure 2-17 shows the cross-relationship map for HP systems with different parameters, including cooling capacity, power consumption, ambient temperature, subcooling EEV opening degree, COP, and compressor frequency. All the parameters were normalized. From the figure, a linear relationship between cooling capacity, power consumption, and compressor frequency can be noticed easily.

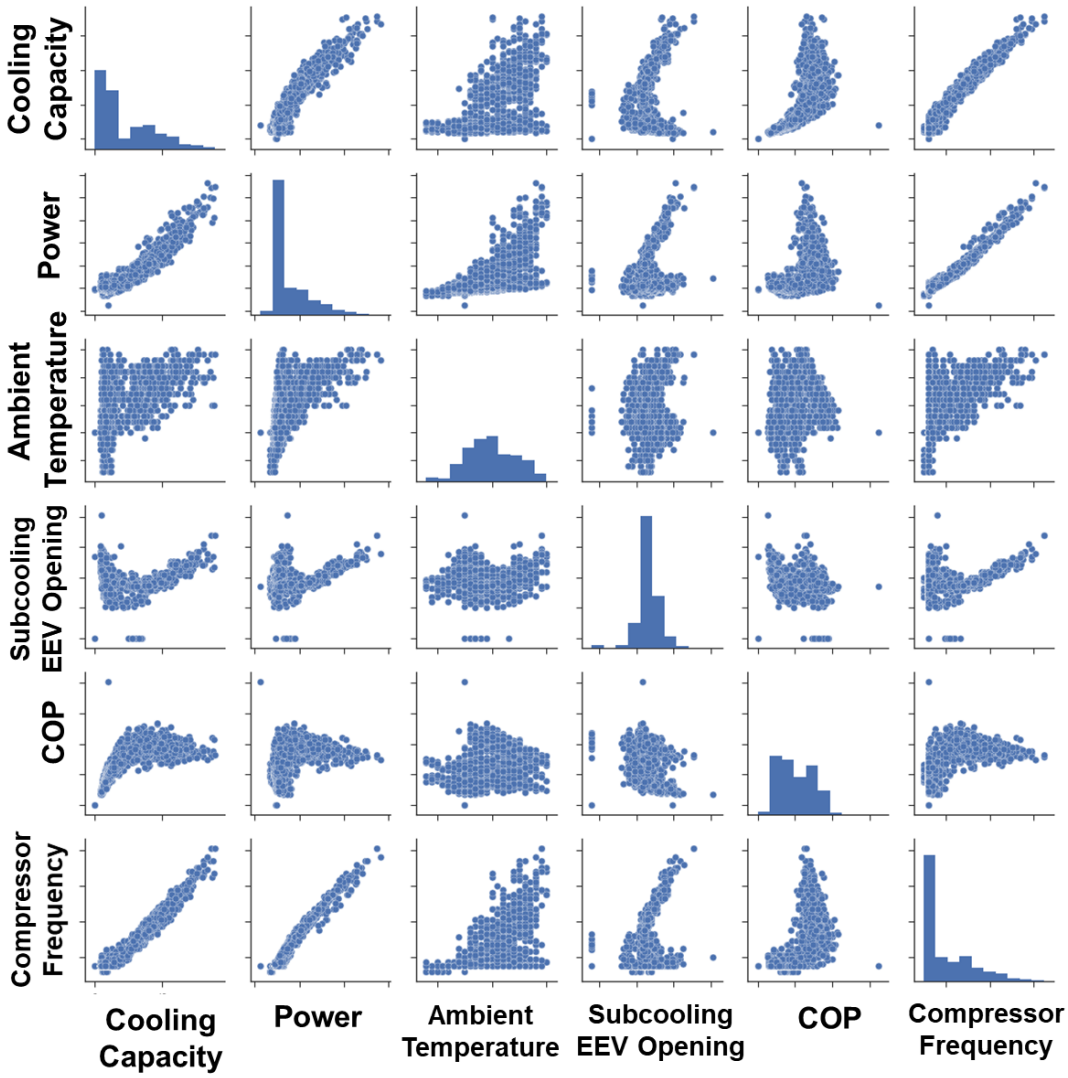

Figure 2-17 Cross-relationship Map for HP System

The relationship between the ambient temperature and COP is not obvious. I draw a figure for these parameters alone in Figure 2-18 for two different controls: “OFF” and “DSEC.” “OFF” mode didn’t consider changing of IDU capacity and fixed value of target refrigerant temperature, while “DSEC” mode can calculate the target value of system actuator, especially ODU and IDU fan RPM, to optimize COP of the system. Similar to Figure 2-16, the trend between the two parameters is not strong since some small M value points exist. The author applied a different method to screen out the information. If the data is screened out by only considering the compressor frequency larger than 30 Hz, Figure 2-19 shows the new trend. A nearly linear relationship can be found.

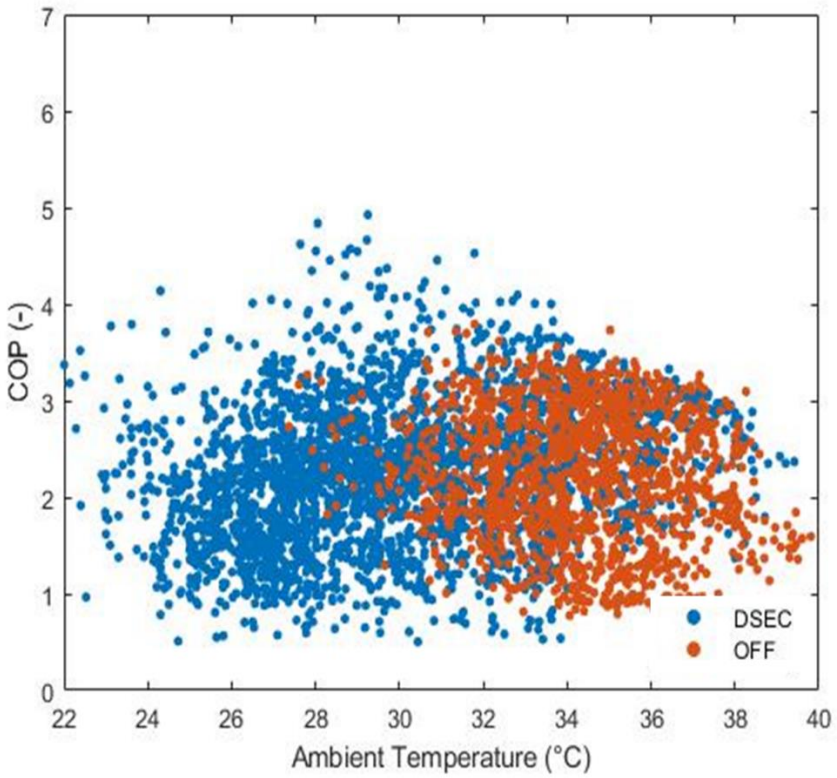

Figure 2-18 COPs for Two Controls for all Compressor Frequencies

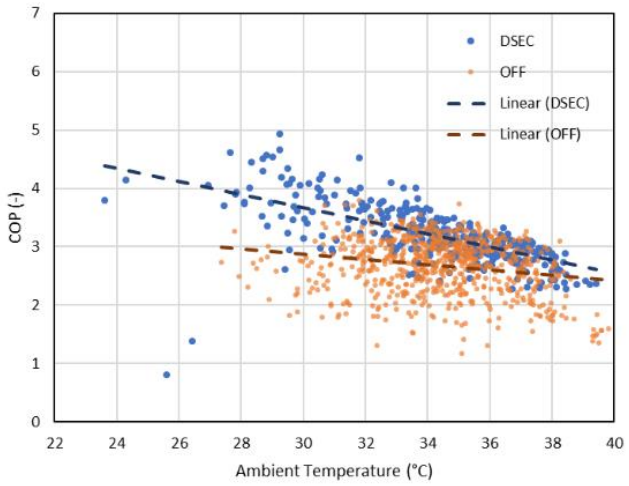

Figure 2-19 COPs for Two Controls (Compressor Frequency > 30 Hz)

In addition, from Figure 2-19, the difference between the two controls can also be found. The "DSEC" control has a better performance than the "OFF" control. The author used a similar method to study the relationship between power consumption and outdoor fan speed. The two modes can be differentiated clearly in Figure 2-20. More about labeling points with control modes are discussed in the next chapter.

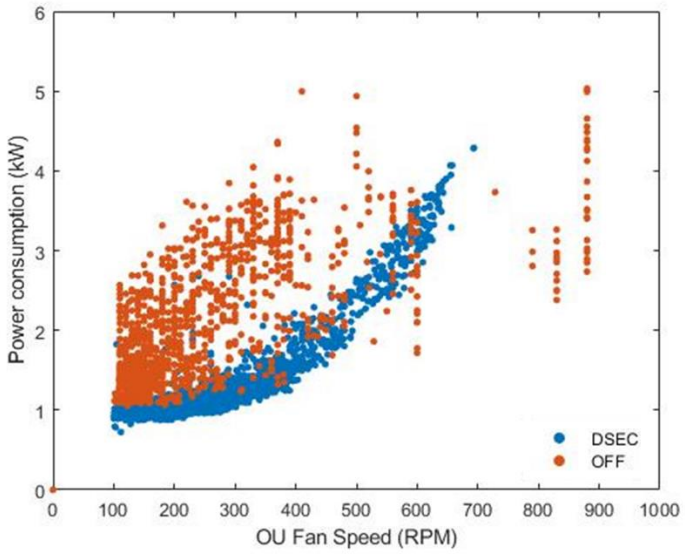

Figure 2-20 Comparing Power Consumption of Two Controls

2.5. Comparing Time-average Performance with QSS Performance

The next question is what the difference between the QSS performance metric and the time-average performance metric is. To further compare the two metrics, the author picked one typical day, January 11th, 2019. The QSS performance factor (QSS-COP) is compared with MPF and HPF. The moving window size is 60 s, and the threshold value is 1 $g \cdot s^{-1}$. The result is shown in Figure 2-21.

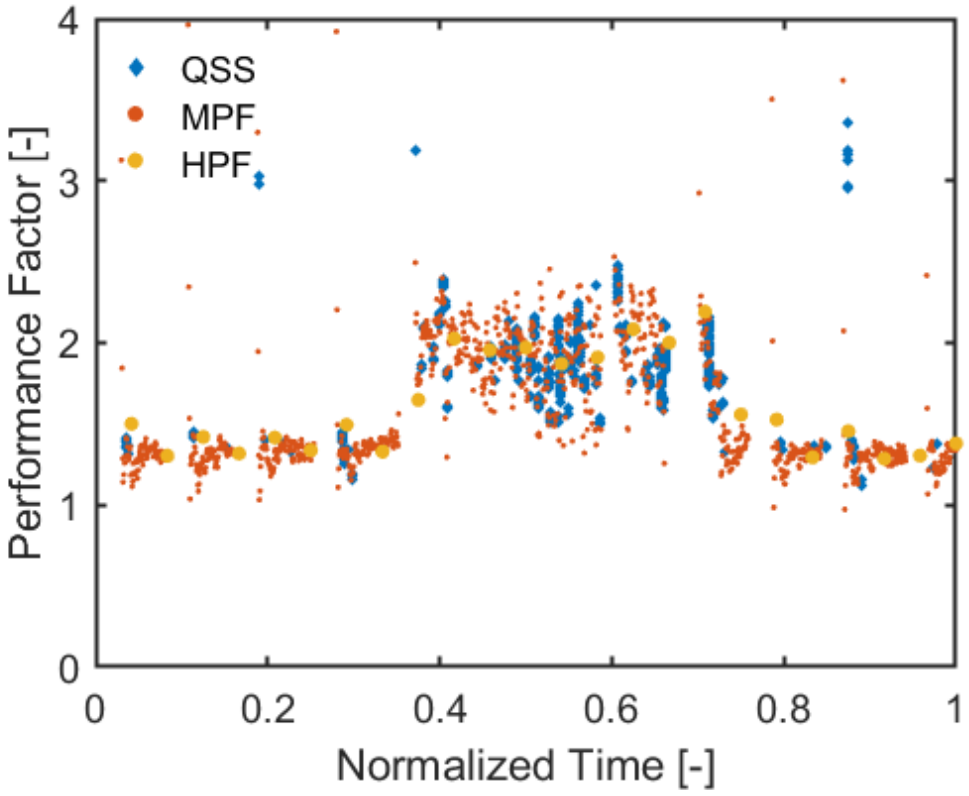

Figure 2-21 Performance Factor on January 11th, 2019

Except for limiting data points, the two methods show a close result. For the points in which the two methods have different results, the system is in either start-up or shut-down process and loses superheat or subcooling.

Table 2-7 Comparisons of Two Methods

	QSS performance	Time-average performance
Core parameters	Moving window size, Target function, Target thresholds	Δt
Pros	• Make sense on the P-h diagram • Reflect the highest performance of the system • Reflect the relationship between ambient conditions and system performance (like COP versus ambient temperature)	• Save time when Δt is large • Reflect the transient phase performance to some extent
Cons	• Cannot reflect the transient performance between on and off status • Does not get enough data if the system startup and shut down frequently	• Doesn't make sense thermodynamically • Provide limited information to improve system design

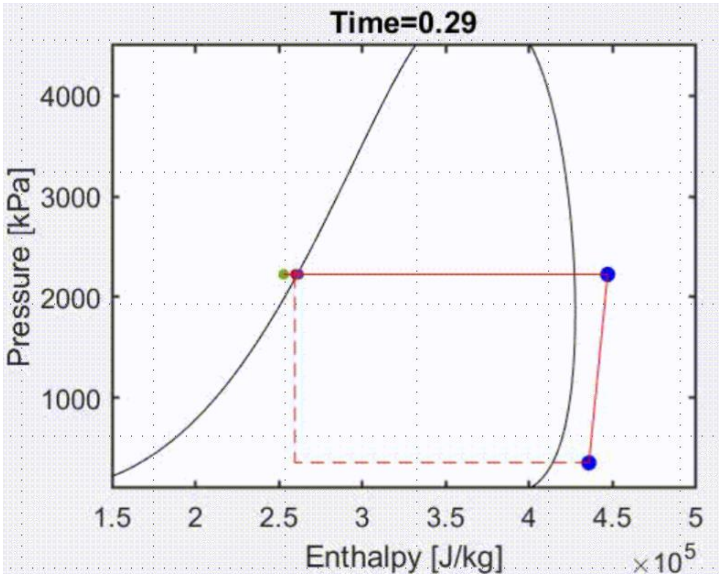

Figure 2-22 P-h Diagram Example of the System at 7:00 am January 11th, 2019

Table 2-7 shows the comparison of the two methods. The moving window size, target function, and target threshold are the most important parameters for QSS performance. Δt is the most significant parameter for time-average performance. The benefits of using the QSS metric include reflecting the heist performance of the system, reflecting

the relationship among different tested parameters, and making sense on the P-h diagram, as shown in Figure 2-22. In contrast, the benefits for using time-average performance are saving time when Δt is large and reflecting the transient phase performance to some extent.

2.6. Dynamic Performance in Field Test

Dynamic performance is the direct way to show the system performance and comparing two different controls. However, it's hard to find the system operating in the same condition under different control logics. Figure 2-23 shows the comparison of two control start-up processes.

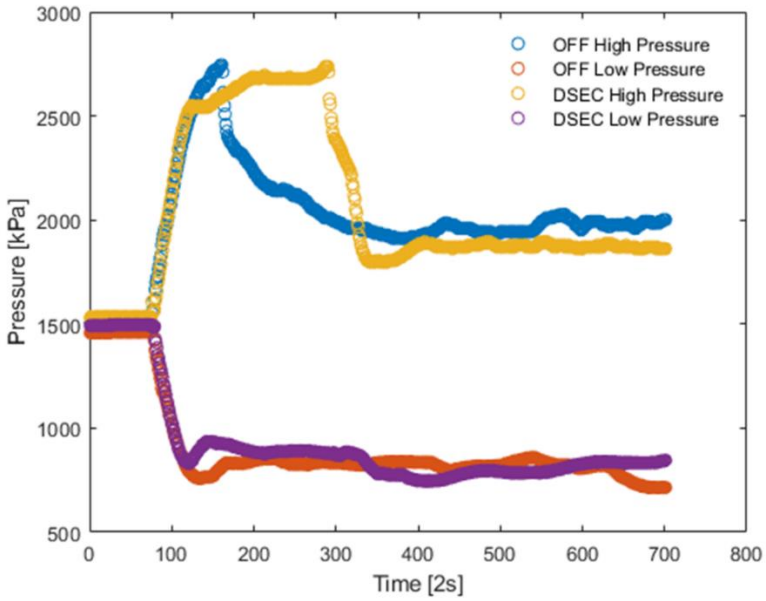

Figure 2-23 Pressure Variations during Start-up Process for Two Controls

The whole start-up process lasts nearly 15 minutes. The ambient conditions are shown in Figure 2-24. The ambient condition would not keep unchanged in 15 minutes. It can be found that for the "DSEC" mode, the ambient temperature has a 1.5 ℃ sharp

increase in the middle of the process. This caused the high-pressure value of the "DSEC" mode to keep increase by 200 seconds.

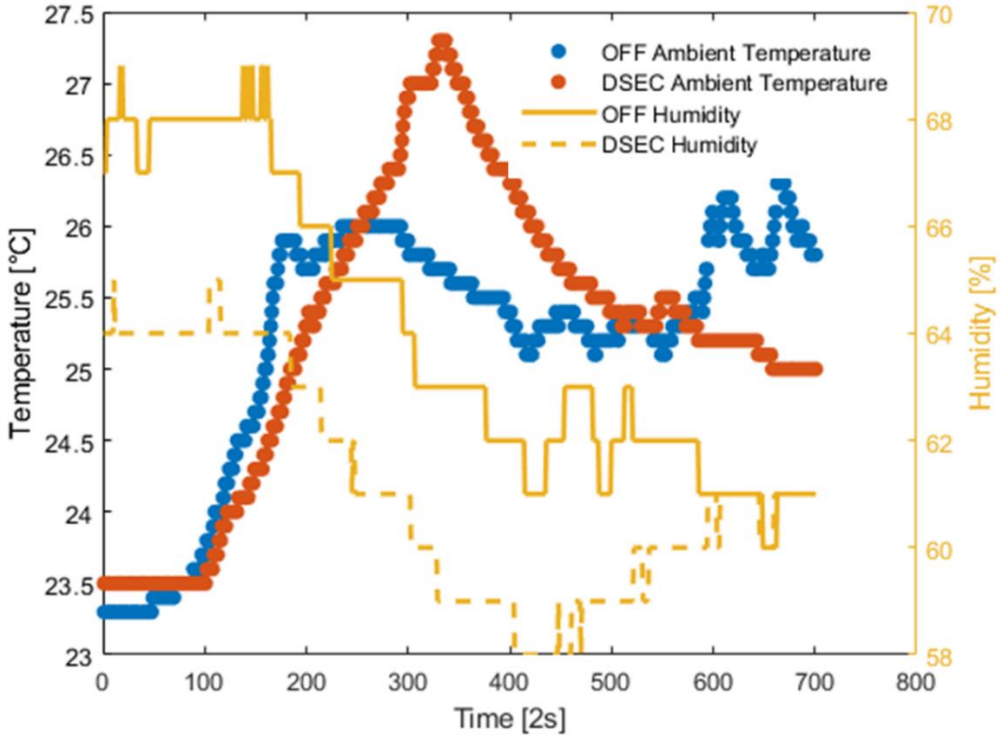

Figure 2-24 Ambient Conditions for Two Modes

Figure 2-25 shows the power and compressor frequency changes for the same time periods. For the "DSEC" mode, the compressor frequency keeps unchanged from time=110 to time=320. In contrast, the "OFF" mode keeps decreasing in this range. In order to compare the two modes in the same condition, a Neural-Network-based (NN-based) model was used to predict the performance. The time period in which the performances showed differences caused by the different ambient conditions were eliminated. The performance was predicted by the NN-based model using the same ambient condition.

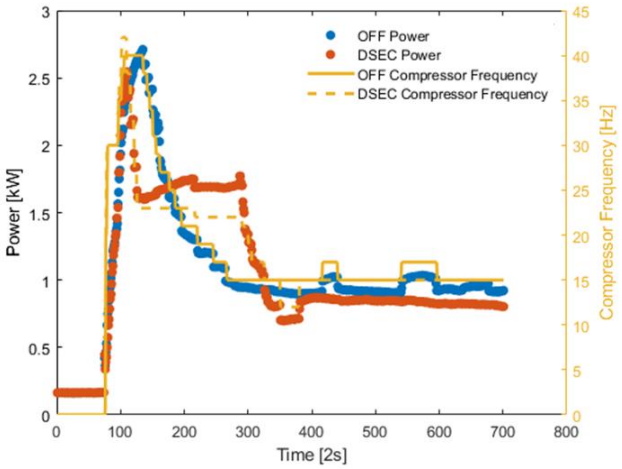

Figure 2-25 Power and Compressor Frequency for Two Modes

The results are shown in Figure 2-26. The input setting and ambient conditions are shown in Figure 2-27 and Figure 2-28, respectively. "A" is the baseline mode, which is the "OFF" mode. "B" is the "DSEC" mode, while "NB" ("New mode B") is the predicted mode for the "DSEC" mode. "A" using a lower outdoor fan speed than "NB" mode, which caused a better heat transfer performance of the outdoor heat exchanger. The high pressure for the "NB" mode is lower, and lower pressure is higher than those of "A" mode. These differences bring better performance for the "NB" mode than the "A" mode (which means "DSEC" mode is better than "OFF" mode) as a conclusion.

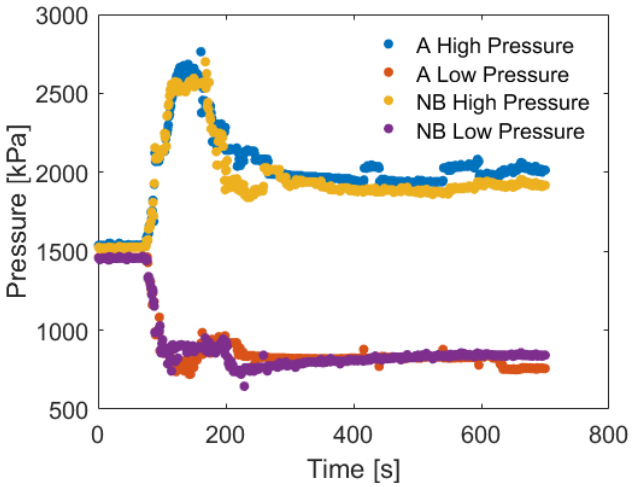

Figure 2-26 Predicted Pressure for Two modes

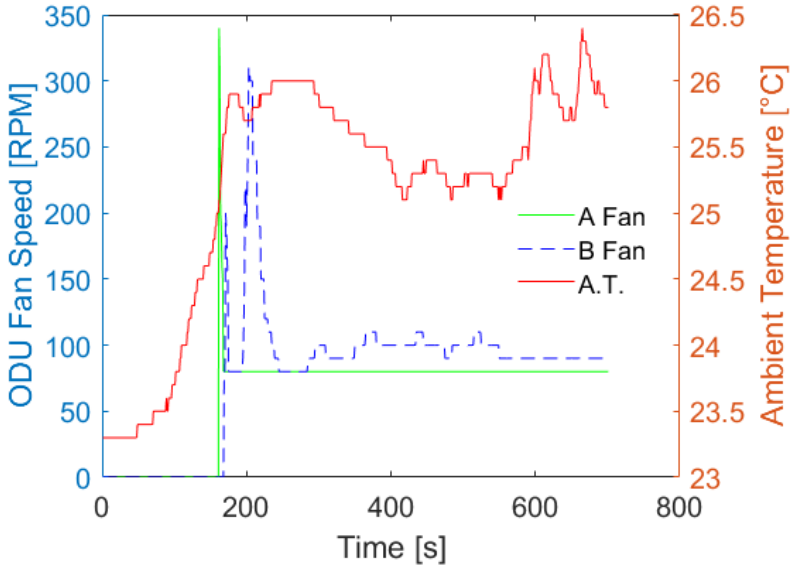

Figure 2-27 Outdoor Fan Speed and Ambient Temperature for Prediction

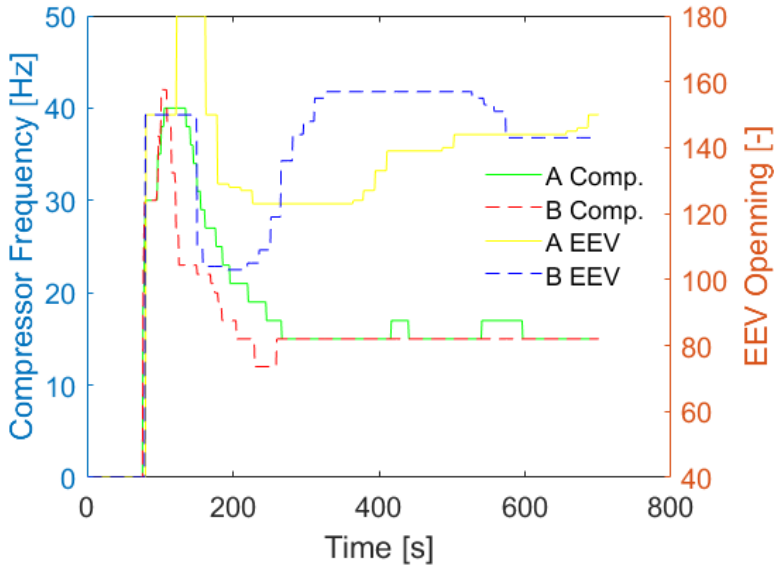

Figure 2-28 Compressor Frequency and EEV Opening Used for Prediction

2.7. Summary

In this chapter, a data analysis process for field tests is developed. Figure 2-29 shows the process suggested for HP system-tested data analysis. The first step is the direct metrics calculation, including part load ratio, usage ratio, cooling combination ratio,

operating unit ratio, etc. The next step is to decide whether the details could be ignored or not. If this study doesn't care about the system performance details, the time-average performance metrics are recommended to be used. If the study needs some details of the system, for example, the P-h diagram, then the QSS performance method is recommended to be used. The final decision to make is whether transient data needing analysis or not. If the transient performance needs to be studied, some modeling tools might be needed for prediction.

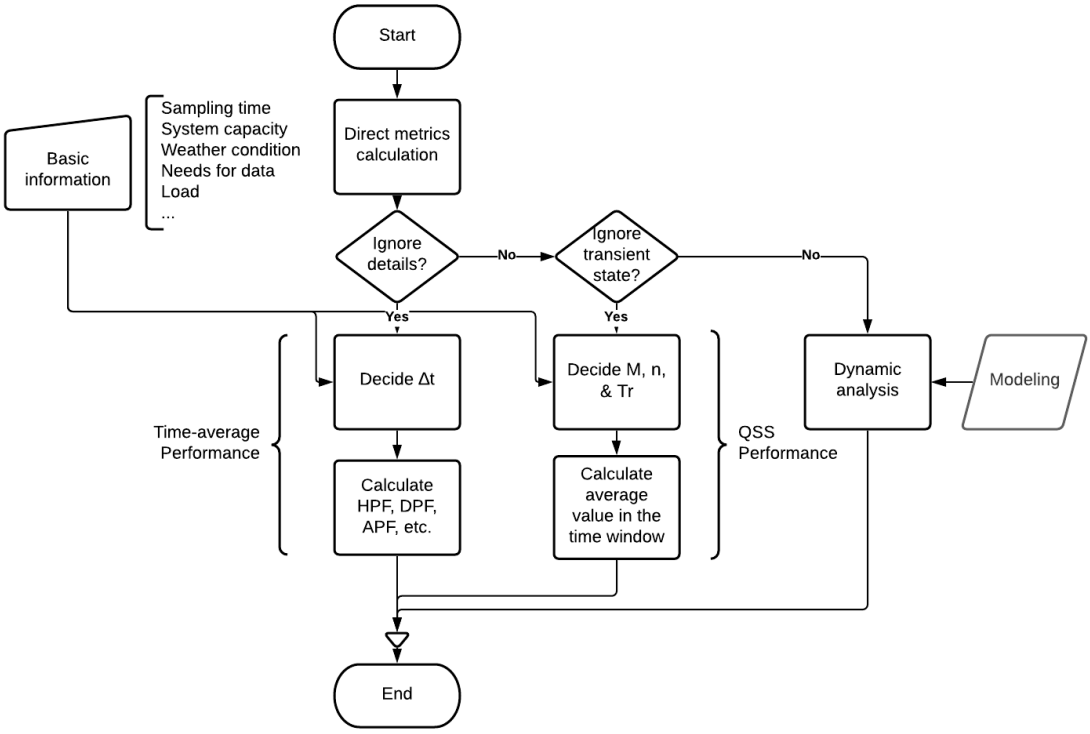

Figure 2-29 Flow Chart Suggested for the Data Analysis Process

In fact, choosing an appropriate method needs to consider a lot of factors. Goals (the purpose of the field test) and testing constraints (test facility, computer performance, etc.) also need to be considered.

3. Modeling from the Field Test Data

Modeling is an important tool for data analysis. The Shallow-Neural-Network-based model was used to predict the dynamic system performance presented in chapter 2.6. In this chapter, different modeling approaches, as shown in Figure 3-1, are compared when dealing with HP system data.

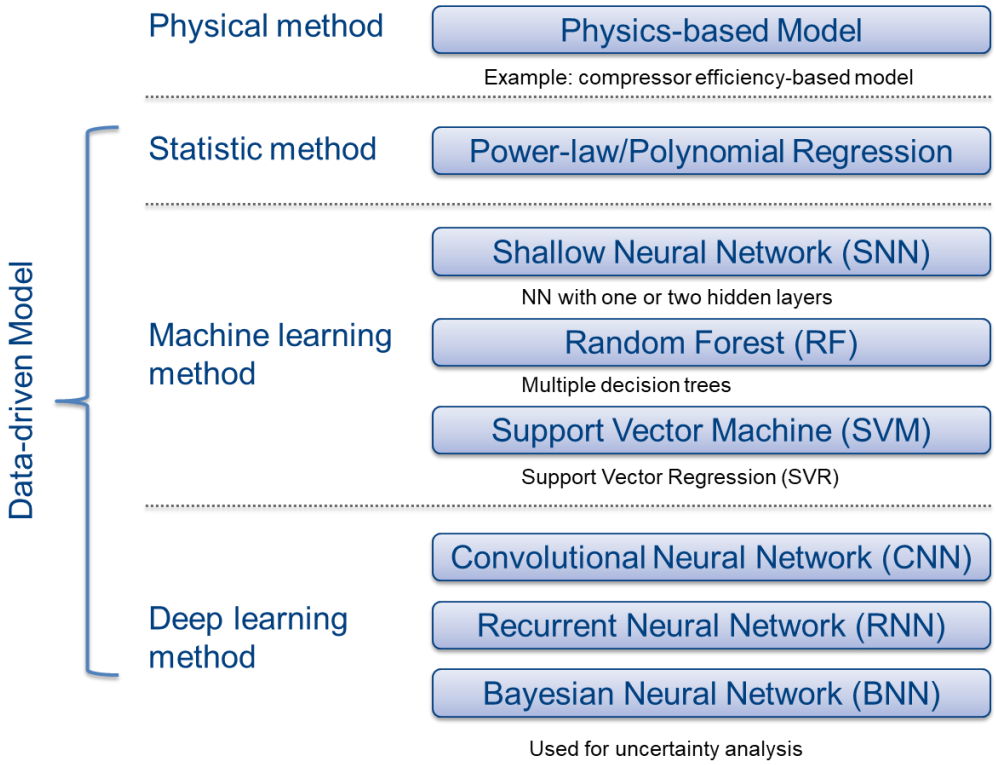

Figure 3-1 Modeling Approaches for HP System Data Analysis

3.1. System Modeling

3.1.1. Classification: Control Labeling

I want to study whether I can distinguish two controls by only using some previous test data. The reason is that identifying different controls in the datasheets from the field tests may not always be straightforward. First, I need to find the target value and the reference value for the classification. I did part of the work in Figure 2-20 using outdoor

fan speed and power consumption to compare two controls. However, no evidence shows whether power consumption and outdoor fan speed are independent parameters. Thus, I use linear Principal Component Analysis (PCA) to generate several new dimensions. PCA can be used to decrease the dimensions of the inputs and also make the dimensions in the new input matrix be independent of each other. The details of PCA are discussed in chapter 3.2.1. One important metric used to select a new dimension in PCA is the Percentage of Variance Explained (PVE).

$$PVE_i = \frac{\boldsymbol{\lambda}_i}{\sum_{j=1}^{5} \boldsymbol{\lambda}_j} \tag{33}$$

A larger PVE means that the dimension is more important in the new input matrix. Table 3-1 shows the PVE for the top five dimensions in the new input after PCA. The first three dimensions can explain 98.7% of the data. Thus, only the first three dimensions need to be considered in the classification.

Table 3-1 PVE for Different New Dimensions

Dimension	**PVE [%]**
1	68.95
2	18.69
3	11.18
4	0.92
5	0.24

The data can be drawn in the new 3-Dimension space, as shown in Figure 3-2. The two groups of data for the two control modes are at different sides in the new space.

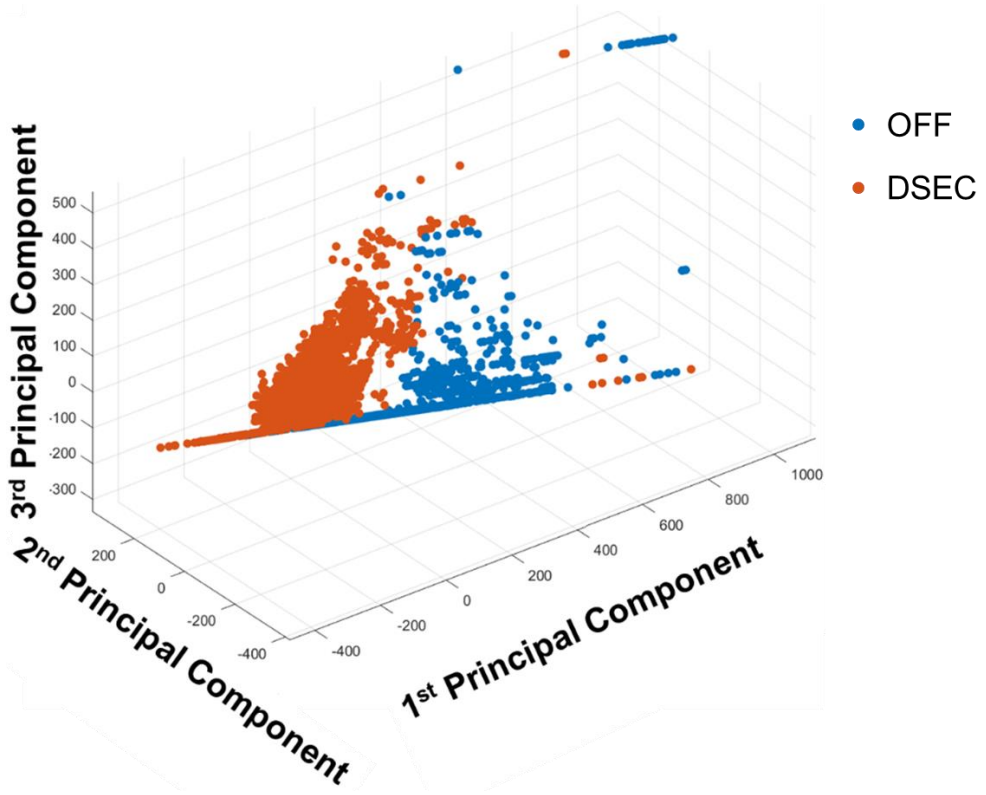

Figure 3-2 Classification of Two Controls

3.1.2. Regression: Power Consumption and Pressure Predictions

Power Consumption Prediction

In the field test, the ambient conditions were not controlled. It was challenging to make the system working under the same condition. Thus, modeling work was needed to simulate each working model of the system to compare their performance under the same conditions. In the model, SVR was applied. The SVR was a regression algorithm based on a classification algorithm called Support Vector Machine (SVM). The objective of the SVM algorithm is to find a hyperplane in a space that distinctly classifies the data points (Cortes and Vapnik, 1995). For the details of this algorithm, interested readers could read the reference (Li et al., 2016). In a simple two-dimension case, the algorithm was used to solve the following optimization problem:

$$Min(\frac{1}{2}\|w\|^2 + C\sum_{i=1}^{N}(\xi_i + \xi_i^*)) \quad (34)$$

subject to

$$y_i - wx_i - b \leq \varepsilon + \xi_i \quad (35)$$

$$wx_i + b - y_i \leq \varepsilon + \xi_i^* \quad (36)$$

$$\xi_i, \xi_i^* \geq 0 \quad (37)$$

where symbols “w” and “b” are weighting factor and bias, respectively. “C” and “ε” are two crucial parameters that would affect the performance of the algorithm. “x” and “y” are inputs and outputs. “ξ” is the deviation from the margin.

In this study, I conducted a parametric study to optimize the two parameters to build a robust and accurate model. I used Python to conduct this study. The ambient temperature range was from 20 °C to 40 °C.

Typically, the compressor map, which is developed under the steady-state operation at a given ambient condition, is used in VRF system models. However, in the field test, the steady-state condition is difficult to find, and the ambient temperature is not controlled so that the compressor map cannot be used. Therefore, I proposed machine learning-based modeling work, which only required hundreds of field test data points. For this, I conducted data-based modeling work to simulate the power consumption of the system based on the SVR algorithm. This model could be used as a substitution for the compressor map. However, before the modeling work, I needed to decide which input parameters should be used. I drew a so-called heatmap to see the effect of seven

possible parameters that might affect the outdoor unit power consumption. The parameters selected were outdoor power consumption, compressor frequency, condensing temperature, suction temperature, outdoor fan speed, evaporating temperature, and ambient temperature, respectively.

The heatmap, Figure 3-3, shows the covariance between each pair of these parameters. The covariance means the relation between the two parameters. The absolute value of the covariance equals one means the two parameters are the same, while if the covariance equals zero, the two parameters have no relationship. In Figure 3-3, I use the light color to show a positive relationship, while the dark color to show a negative relationship. I sort the parameters according to the absolute value of their covariance with the outdoor unit power consumption. The frequency of the compressor is the most significant factor which might affect power consumption. The ambient temperature is a minor factor compared with the compressor frequency. It is possible since a significant part of the outdoor unit power consumption is from the compressor.

The performance of the model is evaluated by Mean Squared Error (MSE), which is defined by the following equation:

$$MSE = \frac{1}{N}\sum_{i=1}^{N}\left(y_{train,i} - y_{pred,i}\right)^2 \quad (38)$$

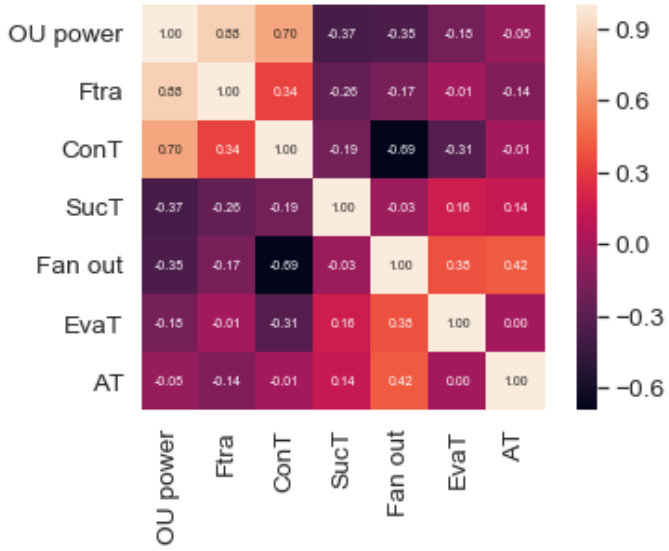

Figure 3-3 Covariance Heatmap

It was also known as the loss function in SVR modeling. I built SVR models based on the data sets. All the data were normalized before the modeling. I first used "C=1 and ε=0.08". The result validation was shown in Figure 3-4. The two dash lines in these figures represented a "±10%" deviation. The denormalized result is shown in Figure 3-4 (a). The measured value and the predicted value did not match very well before the parametric study. Then I continued to optimize the parameters, C and ε, in the model. I separated the data set into training and testing data set. The training data set has 60% data points, and the testing data set has 40% data points, respectively. The MSE, C, and ε listed here are dimensionless since all the parameters are normalized.

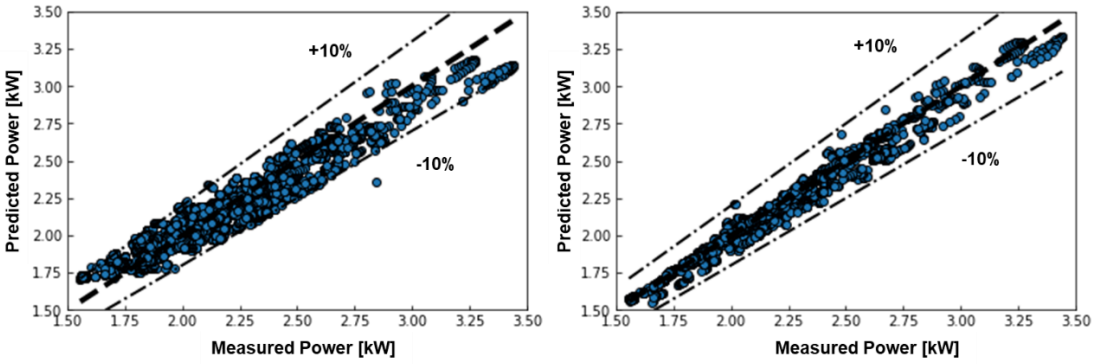

(a) Before Parametric Study (b) After Parametric Study

Figure 3-4 Model Validation

From Figure 3-5, I could see that for the training data set, C should be as large as possible, while for the testing data set, the MSE decreased first and then increased as C increased. Thus, C should not be too large. Furthermore, as Figure 3-5 (b) shows, ε should be as small as possible. In this case, ε should be small, and C should not be too large. I used "C=20 and ε=0". The mean relative error, which represented the average percentage error of the prediction of this case, was 7%.

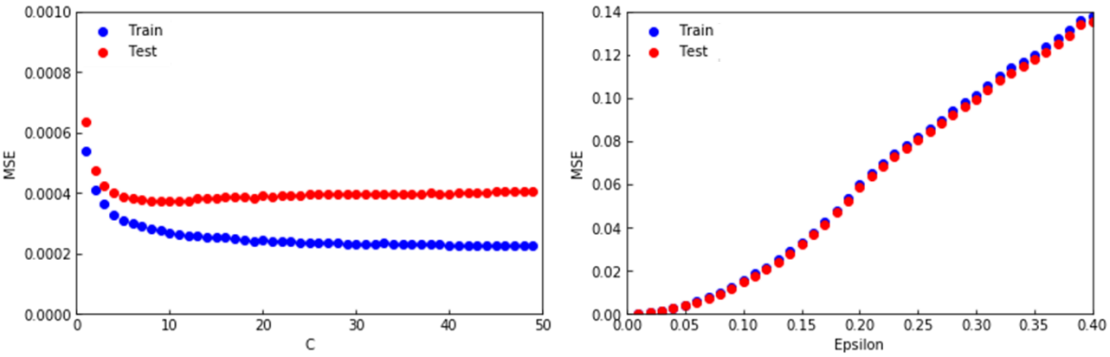

(a) Effect of C on MSE (b) Effect of Epsilon on MSE

Figure 3-5 Parametric Study

As mentioned above, I applied the three operating conditions for the model to predict power consumption. Table 3-2 shows the modeling results. The parameters in each column mean suction temperature, condensing temperature, evaporating temperature,

compressor frequency, outdoor fan speed, and outdoor power consumption, respectively. However, the conclusion could not be made without the uncertainty analysis.

Table 3-2 Modeling Results

SucT (°C)	ConT (°C)	EvaT (°C)	Comp. Frequency (Hz)	Fan out (RPM)	OU Power (kW)
9.8	45.3	4.5	30	200	2.02
10.2	42.4	6.3	40	200	2.39
12.4	45.4	8.7	50	200	3.18

I used the quantitative method introduced by Lecompte et al. (2018a) and Koçyigit and Bulgurcu (2015) to conduct an uncertainty analysis. The uncertainty on the variable y was calculated as a function of uncertainties U_{xi} on each measured variable xi, as shown in eq. (39).

$$U_y = \sqrt{\sum_i \left(\frac{\partial y}{\partial xi}\right)^2 {U_{xi}}^2} \tag{39}$$

The accuracy of the measurement equipment used is given in Table 2-1. Since the correlation obtained from the model is complicated, the value of the partial derivative was derived by numerical differentiation. The uncertainty of the modeling power consumption varied when the input values varied. Thus, I only gave the uncertainty of one point when the suction temperature was 10.2 °C, condensing temperature was 42.4 °C, the compressor frequency was 40 Hz, and the outdoor fan speed was 200 RPM, respectively. I applied a 1% variation to each input parameter, excluding compressor frequency and outdoor fan speed. The condensing temperature and evaporating temperature were calculated by the high pressure and low pressure. Thus, the instrument uncertainty was calculated based on the uncertainty of the pressure sensor.

Table 3-3 Uncertainty Analysis

	Instrument uncertainty (°C)	1% Deviation (°C)	OU Power deviation (-)	Uy (-)
SucT	0.5	0.1	0.01%	1.54e-06
ConT	0.1	0.4	0.71%	1.82e-05
EvaT	0.03	0.06	0.06%	6.99e-07
Uncertainty of the model (B type)				0.5%
Power meter uncertainty (A type)				0.5%
Total Uncertainty				0.7%

According to the calculation, the total uncertainty of power consumption should be 0.7%, as shown in Table 3-3. I could further find that the condensing temperature, which also meant the high pressure had the most critical impact on the outdoor power consumption when frequency and outdoor fan speed were fixed. This result was consistent with my result shown in the heatmap.

Pressure Prediction

In this part, I report one prediction work for the high pressure and low pressure only using the control metrics. The inputs for the model are the control parameters metrics on the time domain, including ODU fan speed, EEV openings, and compressor frequency. The initial status of the outputs was also required. A Neural Network (NN) method or Convolutional Neural Network (CNN) method can all be used. If the NN was used, the filter to reduce the input dimensions was needed to be designed separately. Figure 3-6 shows the result.

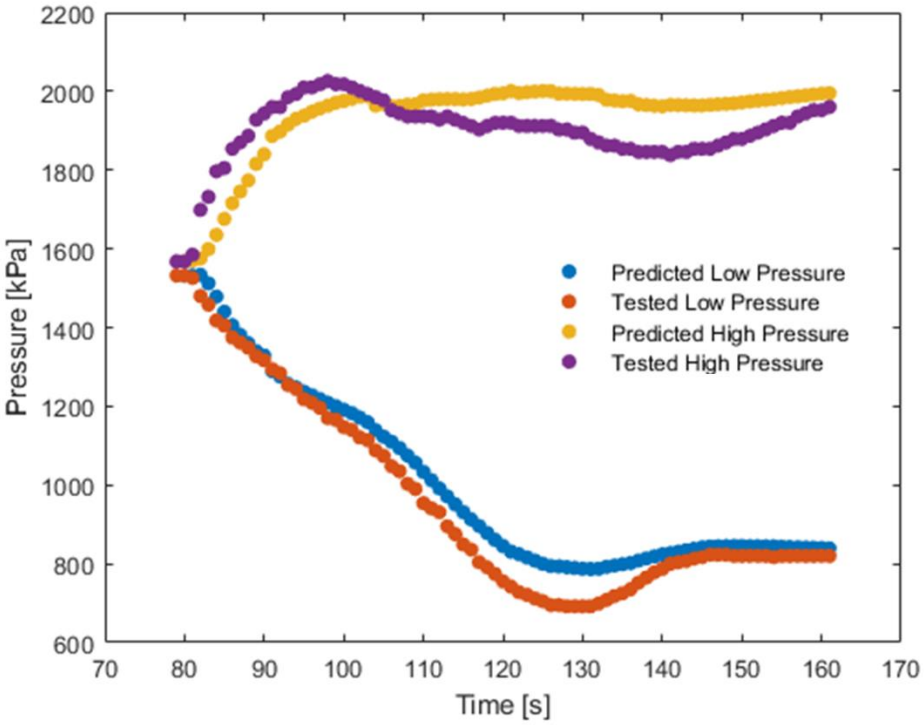

Figure 3-6 Pressure Validation

The benefit of the work is that I can predict the performance for different controls using the same ambient conditions. This can be helpful for us to compare different controls. A similar method can be used to predict other temperatures like the suction and discharge temperature of the compressors.

3.2. Subcomponent Modeling

3.2.1. EEV Model

Background

As for the HP system, the significance of controlling the EEV opening to regulate the part-load efficiency has been confirmed by some researchers (Choi and Kim, 2003; Wu et al., 2005b; Tu et al., 2011; Xiangguo et al., 2013; Yun et al., 2017). In order to know

the coefficient of performance (COP) of the cooling system, the accurate mass flow rate of each indoor unit is needed. However, most commercial HP systems don't measure it. Only for research purposes, one mass flow meter is typically installed for the total mass flow rate. Thus, finding the relationship between the opening degree of the EEV and the mass flow rate through the EEV is necessary. Eq. 40. first developed by Wile (1935), which is derived from Bernoulli Equation, it has been widely used to describe the characteristics of the EEV for single-phase flow.

$$\dot{m} = C_f A_r \sqrt{2\rho_i (p_i - p_o)} \tag{40}$$

where the parameters (ρ_i, p_i, and p_o) are the inlet density of the refrigerant, inlet pressure, and outlet pressure, respectively. The flow area (Ar) can be calculated by:

$$A_r = \frac{\pi d_c^2}{4} - \pi (H_c - H)^2 \tan^2 \alpha = \frac{\pi D^2}{4} \tag{41}$$

where the parameters (d_c, H_c, H, and α) are the geometric parameters shown in Figure 3-7. D is called 'orifice diameter' in some literature (Zhifang et al., 2008), which is used to describe the flow area.

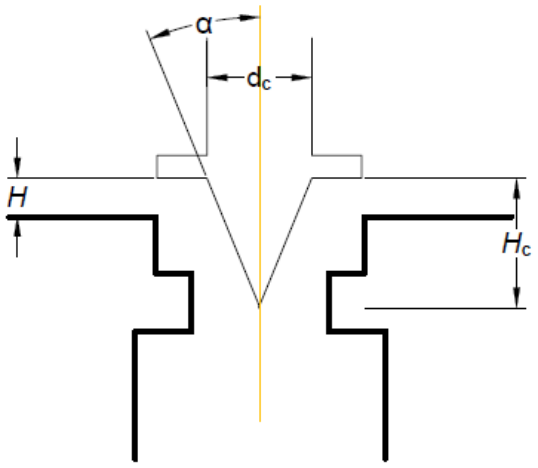

Figure 3-7 The Geometrical Structure of EEV

The coefficient (C_f) must be determined to predict the mass flow rate (Chen et al., 2017, 2018). Since the flow through the EEV is typically a multi-phase flow, C_f in eq. 40 can be affected by many factors, such as the pressure, geometry of the EEV, and the physical properties of the refrigerant. The most convenient and economical way is to request the data from the EEV manufacturer. Nevertheless, EEV manufacturer often only provides test data obtained by testing with air instead of refrigerant. Furthermore, due to the two-phase flow and complicated geometry, building a physical model to calculate C_f is difficult (Zhifang et al., 2008b). As an alternative method, an empirical correlation seems a reasonable way (Park et al., 2007b). However, some other correlations like polynomial correlation exist (Li, 2013; Chen et al., 2017, 2018). The power-law correlation method is the conventional and most popular method for the EEV correlation (Chen et al., 2009, 2017, 2018; Hou et al., 2014; Kim et al., 2010; Liang et al., 2009; Liu et al., 2016; Park et al., 2007; Shanwei et al., 2005; Ye et al., 2007; Zhang et al., 2006; Zhifang et al., 2008). This method is also recommended by the American Society of Heating, Refrigerating, and Air-Conditioning Engineers (ASHRAE) (Kavanaugh and Simplified, 2006). The core of this method is to develop a power-law correlation formula of the mass flow coefficient C_f by several dimensionless π groups as shown:

$$C_f = a_0 \prod_{i=1}^{n} \pi_i^{a_i} \tag{42}$$

where a_i (i=0, 1, …, n) are constants.

While the same π groups could have similar forms, they have the same physical meaning unnecessarily. The performance of this method varies depending on the

authors and refrigerants. Correlations were usually assessed by relative deviation (RD) as defined:

$$RD = \frac{\dot{m}_{pre} - \dot{m}_{exp}}{\dot{m}_{exp}} \tag{43}$$

This method is based on the assumption that all the dimensionless correlations obey the Buckingham π theorem (Sonin, 2001), but no study shows that the relationship should be power-law. Some researchers (Chen et al., 2017b) stated that the result was from Choi's work (2004). However, Choi's paper is for short tube orifices, and no study proves that this work can be used for EEV correlation. In another paper (Chen et al., 2018), the authors mentioned that the proposed correlations mentioned above could only be available when the orifice diameter is smaller than 1.4 mm and propose a new correlation that was more normalized.

Neural Network Method

Recently, the Artificial Neural Network (ANN) or NN, SNN method, developed by Warren and Walter (1943), is widely adopted to build a nonlinear correlation between inputs and outputs, especially in air conditioning and refrigerant fields (Deng et al., 2016; Yun et al., 2017; Liu et al., 2017; Jahani et al., 2018). The ANN structure consists of an input layer, several hidden layers (always one or two in practice), and an output layer. The input neurons can include as many parameters as possible. Nevertheless, to reduce the time of training, only a limited number of inputs are used. The input values (X_i) and output values (Y_k) are always normalized (x_i and y_k) by following equations to ensure the equivalence between the variables (Tian et al., 2015b).

$$x_i = 2\left(\frac{X_i - X_{i.min}}{X_{i,max} - X_{i.min}}\right) - 1 \tag{44}$$

$$y_k = 2\left(\frac{Y_k - Y_{k.min}}{Y_{k,max} - Y_{k.min}}\right) - 1 \quad (45)$$

If there's only one hidden layer, the process of the ANN can be given by:

$$y_k = g_{output}\left\{\sum_{j=1}^{n} w'_{jk} \times \left[g_{hidden}\left(\sum_{i=1}^{m} w_{ij}x_i + b_j\right)\right] + b'_k\right\} \quad (46)$$

The normalized input parameter x_i is multiplied by the weight factor w_{ij} and added by the bias bj to get a new value x'. The value x' can be used to get the value g_{hidden} (x') for each hidden neuron by the hidden layer transfer function g_{hidden}, which is called transfer function or activation function. Similarly, the value of the hidden layer can also be multiplied by another group of weight factors w'_{jk}, added up with another group of bias b'_k, and transferred by the output transfer function g_{output} to get the kth output parameter. Researchers always use the linear function as the output transfer function.

The next step of the ANN is the training process, which is repeated to obtain optimized groups of the weight factor w_{ij} and w'_{jk}, and bias b_j and b'_k for each neuron with a minimized deviation between the predicted data and the original data (e.g., measured data). Back Propagation (BP) is a popular method for the training process. Figure 3-8 illustrates the process of the BP algorithm.

The ANN has been used in various engineering fields due to its ability to solve physical problems in engineering applications without explicit mathematical equations (Tian et al., 2015b). In the field of HP system design, the ANN also works. For example, the ANN was used to determine the energy-efficient operation set-points of the HP cooling system (Chung et al., 2017b). As for EEV correlation, the ANN is a reasonable method

due to the complexity of the fluid dynamic process and many factors involved. Two research papers about using the ANN for EEV correlation have been published since 2015 (Cao et al., 2016; Tian et al., 2015). Cao's group used the Levenberg-Marquardt BP algorithm ('trainlm') in MATLAB for the ANN training (Cao et al., 2016). There was one hidden layer. They used four input parameters, which are the input pressure of the EEV, the output pressure of the EEV, the inlet subcooling temperature of the EEV, and the opening degree of the EEV. They chose the most popular Tan-sigmoid function (eq. 47) and the n^{th}-order polynomial function (eq. 48), which had been found quite accurate by some researchers (Deng et al., 2016; Su et al., 2017) as the hidden layer transfer functions. They used 'purelin' function, which is the linear function, as the output layer transfer function.

$$g_{hidden}(x) = \text{tansig}(x) = \frac{2}{1+e^{-2x}} - 1 \tag{47}$$

$$g_{hidden}(x) = x^n \tag{48}$$

Tian's group also used the Levenberg Marquardt BP algorithm (trainlm) as the gradient-based training algorithm. They also chose the Tan-sigmoid function and Log-sigmoid function for the transfer function of the hidden layer.

$$g_{hidden}(x) = \text{logsig}(x) = \frac{1}{1+e^{-x}} \tag{49}$$

They also used 'purelin' function as the output layer transfer function.

The dimensionless output is given by:

$$y = \pi_1 = \frac{\dot{m}}{(d_c^2\sqrt{\rho_i(p_i - p_o)})} \tag{50}$$

Tian also conducted the parametric study, in which one parameter was removed each time, and the ANN model was trained with the other seven parameters. As a result, they

found that π_6 was the most significant factor in the ANN sensitivity and accuracy because of the surface tension, which represented the metastable flow.

The ANN performance could be evaluated by several statistical coefficients. Though the two groups of authors used a different name, they used a similar standard for assessment. Mean Relative Error (MRE) used by Tian, also called the average relative deviation (AD) by Cao, was given in the following equation. The correlation of Tian's group resulted in MRE of 4 %, and that of Cao's group was 1 %.

$$MRE = AD = \frac{1}{n}\sum_{i=1}^{n}\frac{|y_{pre}-y_{exp}|}{y_{exp}} \tag{51}$$

Furthermore, Tian also used Root Mean Square Error (RMSE), which was given by eq. 52 for evaluation. According to their study, the ANN model showed the RMSE of 7.59 kg h^{-1}. In addition, Cao used another parameter, Standard Deviation (SD), in eq. 53, which was 2.7 % of their work to assess the performance.

$$RMSE = \sqrt{\frac{1}{n}\sum_{i=1}^{n}\left(y_{pre}-y_{exp}\right)^2} \tag{52}$$

$$SD = \sqrt{\frac{1}{n-1}\sum_{i=1}^{n}\left(\frac{y_{pre}-y_{exp}}{y_{exp}}-AD\right)^2} \tag{53}$$

In addition, the R-squared (R^2) statistic was also used by Tian. Their model had R^2 of 0.994.

In this study, I adopted MRE, RMSE, and R^2 to evaluate the correlations. The MRE, RMSE, and R^2 are all widely used to evaluate a model, but they are different. MRE is

a measure of deviation, while RMSE and R^2 are statistical measures of the variance. MRE and R^2 are relative measurements, while RMSE is an absolute measurement.

Research Gap

According to the existing literature, the NN method has a better performance than the conventional way. However, only limited studies used the NN model for EEV correlation. Thus, various limitations exist, and more work needs to be done in this field. First, since the criteria and the procedure varied in the literature, a clear conclusion cannot be made for parameter selections. Specifically, though parameter and transfer function studies were mentioned, the question of which combination of the transfer function and the inputs had the best performance has not been answered yet. Secondly, these studies all used the BP algorithm for data training, while other algorithms were neither mentioned nor compared.

To fill these gaps, the objective of this study is to develop an EEV modeling framework and optimize the input parameter number and hidden neuron number. The work is presented through a case study on a VRF system. The database was built based on the experiment results of a field test in the heating season. Models were built to predict the mass flow rate through the EEV in VRF systems operated with one indoor unit (IU). The system was equipped with a variable frequency compressor. A Principal-Component-Analysis (PCA)-based NN method was adapted to build the correlation and reduce the dimensions of the inputs. Besides commonly used input parameters in the literature, such as inlet and outlet pressure and temperature, other system parameters like the frequency of the compressor and the power consumption of the

indoor and outdoor units were also added in the modeling-built process. Optimization work was conducted to optimize input parameters, transfer function, and the number of hidden layer neurons of the NN method. A power-law correlation method was also developed to compare with the PCA-based NN method.

Methodologies

Field test results were used to build the model. The benefit of using the field test data is to get enough data sets available representing real-life operations. However, the quality of the data regarding stability may be lower than that from the laboratory. The field test was conducted on the third floor of a university office building in College Park, Maryland, U.S. Information about the building and the VRF system is provided in Table 3-4. Figure 3-8 shows the building floor plan. The VRF system consisted of seven indoor units (IU), one outdoor unit (OU), and one water heating unit. The system was controlled by each EEV in the IU and the inverter compressor in the OU. The indoor units were installed in five different rooms. The outdoor unit was installed on the fourth floor. To simplify the test and control the variables, only IU2 was operated during the test period, while all other IUs, including the water heating unit, were off. The data was saved from 6:20 PM, December 25th, 2017, to 10:40 AM, December 27th, 2017. The indoor unit was set at 20 °C. The data were saved every 2s.

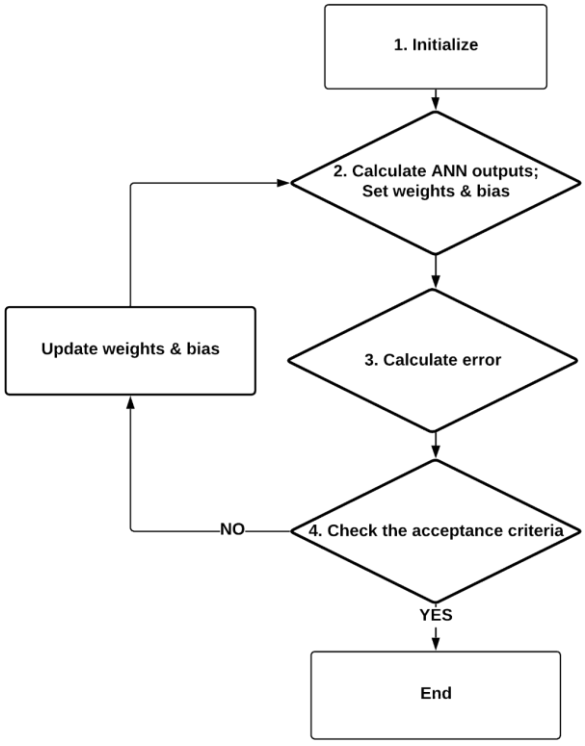

Figure 3-8 BP Algorithm Flow Chart

Table 3-4 Building and System Information

Field	Information
Location	College Park, MD, U.S.
Number of Rooms	5
Space area of Room B (m^2)	22.1
Number of occupants of Room B	7
Nominal heating capacity (Btu/h)	81,000
Refrigerant	R-410A

Seventeen groups of parameters were tested during the experiment, which was summarized in Table 3-5. The first group parameter is my target parameter, mass flow rate. The second group parameter is the frequency of the compressor, which was not discussed in most former research. All the parameters were tested directly except for the third and the twelfth. The third group is the target EEV opening degree, which was calculated by the current pulse number over the maximum pulse number of the EEV.

The twelfth group is the subcooling temperature before the EEV. It was calculated by the temperature before the EEV subtracted the saturated temperature.

Table 3-5 Test Parameters

Test parameter	Symbol (Unit)
Mass flow rate	q ($g \cdot s^{-1}$)
Frequency of compressor	f (Hz)
Target EEV opening degree	*X* (%)
Compressor suction pressure	P_s (kPa)
EEV inlet pressure	P_i (kPa)
EEV outlet pressure	P_o (kPa)
EEV inlet temperature	T_i (°C)
EEV outlet temperature	T_o (°C)
Ambient temperature	T_a (°C)
Suction temperature	T_s (°C)
Discharge temperature	T_d (°C)
Subcooling temperature	T_{sub} (°C)
IDU room temperature	T_{IDU} (°C)
Liquid Line temperature	T_l (°C)
Outdoor unit power	Pw_o (kW)
Indoor unit power	Pw_i (kW)
Outdoor Humidity	Rho (%)
Room Humidity	RHr (%)

Figure 2-1 shows the system layout and the position of all sensors. As described above, all the IUs except IU2 were set off during the test period. The water heating unit was also off. The EEV near the Sub-Cooling Heat Exchanger (SCHX), EEV A, and EEV B were kept at the same opening degree during the test to control the variable. Table 2-1 shows the specifications of the instruments used in the field test.

The traditional method (power-law correlation) and ANN method were adopted in this research to develop the correlation between parameters collected from the field test data and the mass flow rate of the target EEV. Only the steady-state data were considered in this research to guarantee the quality of the model. Methods to detect the steady-state of air conditioning and refrigerant cycle have been discussed (Lecompte et al., 2018b). The methodology developed by Kim et al. (2008) was adopted in this study. The standard deviation was monitored in a moving data window. If the standard deviation was below a threshold, the status of this moving data window could be considered steady. The threshold in this study was set as 5 %, and the moving data window was 20 seconds long, according to Kim's research. The data collection frequency was 0.5 Hz. Thus, the moving data window had 10 points. According to this standard, the sample number of my study was 10,851 for the IU2's steady-state data.

PCA method, which was proposed by Pearson (1901), is a statistical procedure that uses an orthogonal transformation to convert a set of observations of possibly correlated variables into a set of values of linearly uncorrelated variables into a set of values of linearly uncorrelated variables. PCA is usually used to select input parameters and reduce dimensions. The PCA method was adapted to reduce the dimensions of the input parameter matrix. In this way, the complexity of the NN training can be reduced.

To make all the input parameters comparable, the data was normalized by the following steps. If the input parameter matrix was B (n×14), the normalized matrix b could be given by:

$$b_{i,j} = 2\left(\frac{B_{i,j}-B_{min,\,j}}{B_{max,\,j}-B_{min,\,j}}\right) - 1 \tag{54}$$

Here, 1≤i≤n and 1≤j≤17. Some literature changed input parameters to dimensionless parameters (Tian et al., 2015). For example, they used P_i/P_c instead of P_i to substitute in the above equation. Nevertheless, this step was not necessary because if I put them into eq. 54, the same result was given due to the critical pressure of a certain refrigerant was constant.

In addition, in order to decrease the complexity of PCA, the centralization method was needed. This step aimed at changing the mean value of each column of matrix b to zero. The process could be expressed by:

$$c_{i,j} = b_{i,j} - b_{mean,j} \tag{55}$$

The next step was calculating the covariance matrix C (shown by eq. 57) of c (shown by eq. 56). I need to write matrix c as 17 groups of column vectors. Each column means the j[th] parameters of all the samples.

$$c = [\overline{c_1}, \overline{c_2}, \ldots, \overline{c_{14}}] \tag{56}$$

$$C = \begin{bmatrix} cov(\overline{c_1}, \overline{c_1}) & cov(\overline{c_1}, \overline{c_2}) & \cdots & cov(\overline{c_1}, \overline{c_{17}}) \\ cov(\overline{c_2}, \overline{c_1}) & cov(\overline{c_2}, \overline{c_2}) & \cdots & \vdots \\ \vdots & \vdots & \ddots & \vdots \\ cov(\overline{c_{17}}, \overline{c_1}) & cov(\overline{c_{17}}, \overline{c_2}) & \cdots & cov(\overline{c_{17}}, \overline{c_{17}}) \end{bmatrix} \tag{57}$$

Then I calculate the eigenvalue (E) and the eigenvector (V) of C and rearrange them into a descending order to get a new matrix V'. The more important the group was, the higher-order the group would be in the new eigenvector.

$$C = V \times E \times V^{-1} \tag{58}$$

In my study, I tried different numbers of input parameters based on the PCA to figure out the minimum number of input parameters for the ANN model building.

As for the NN modeling, I used the BP neural network prediction model in Matlab R2018a. The field test result of IU2 from Dec. 25 to Dec. 27, 2018, was used to build the NN model. 60 % of the data was used for training, 20 % of the data was used for testing, and 20 % of the data was used for validation. In the discussion and result part, I would further discuss selecting the transfer function pairs and deciding the hidden layer node numbers.

Discussions and Results

As shown in Figure 3-9, I used two methods for modeling: NN correlation and power-law correlation. As for NN modeling, I used PCA introduced above first to decrease the dimension of the input data matrix. I optimized the number of the input parameter groups and the number of the hidden layer nodes. In this study, I only consider the one-layer model since I tried two hidden layer models and found out a similar result but consuming a much longer training time. Using much more hidden layers is in the range of deep learning, like residual neural networks, with more than one hundred layers,

which is another topic and could be my future work. In addition, I also compared different transfer function pairs.

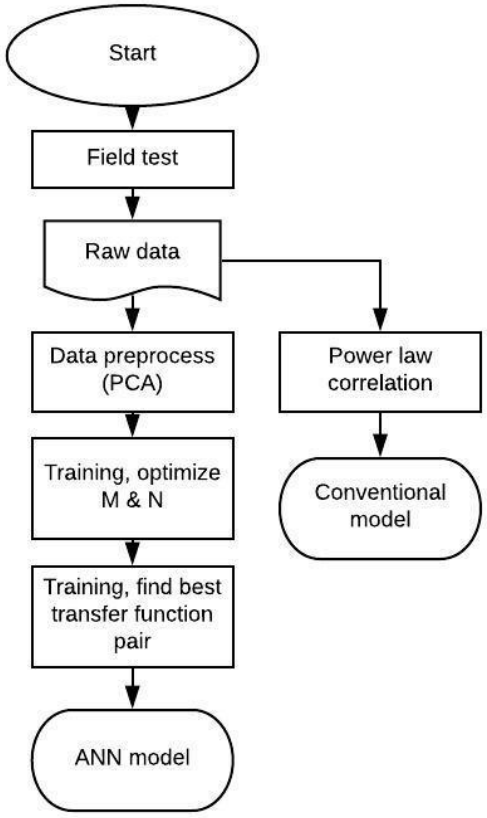

Figure 3-9 EEV Modeling Work Flowchart

The field test result of IU 2 was used to build the model. First, I optimized the number of the input parameter groups (N) and the number of the hidden layer nodes (M). The data was trained repeatedly with different N and M. The vectors in matrix V' were sorted by importance. Thus, it could be guaranteed that the first N vectors are chosen from V' would have the best result. In this research, N was set from 1 to 17.

Nevertheless, no standard exists for choosing M, the proper number of hidden neurons. Some literature mentioned M should be smaller than N (Tian et al., 2015). However, some other studies also considered the situation that M was larger than N (Cao et al., 2016b; Liu et al., 2017). The only certain rule was that M should be smaller than the number of samples used for training. Therefore, in this research, I would discuss the range of M from 1 to 25 to investigate what the result could be if M was larger than N.

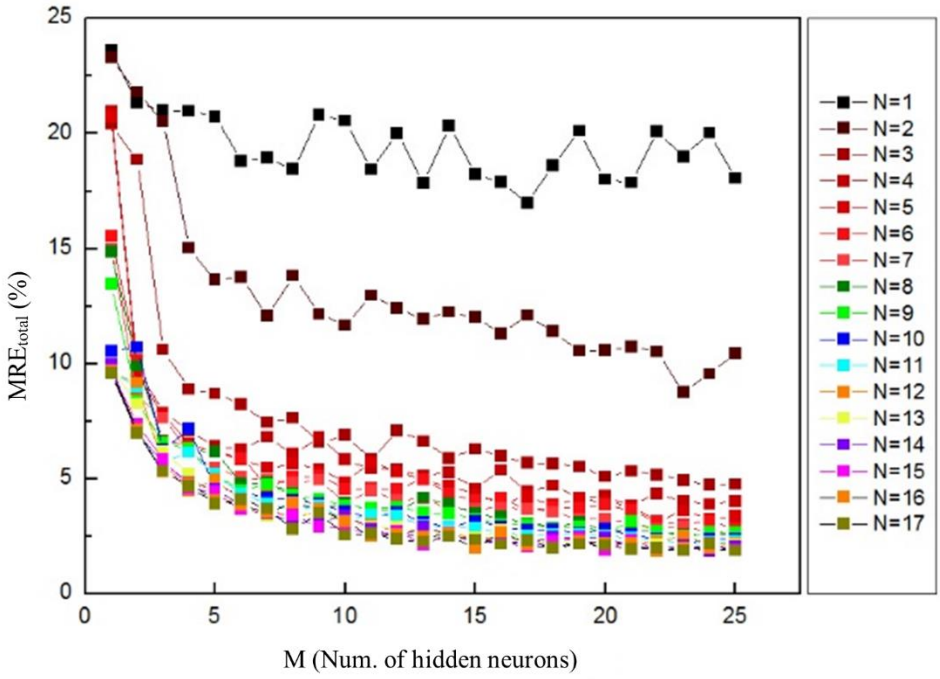

Figure 3-10 MRE with Different M and N

The transfer function pair used for the parameter study of this part was ‘tansig’ for the hidden layer and ‘purelin’ for the output layer. This was a proper assumption, and the reason would be given in the next section. Figure 3-10 shows the MRE of the results with different pairs of M and N. For each M and N pair, the data were trained six times, and the best one was kept and as shown in the figure. Since the training group,

the testing group, and the validation group data show the same trend. I only show the figures for all the samples.

In Figure 3-10, the y-axis of the graph is MRE, and the x-axis is M. Different lines in the graphs mean different N. When N was small, the ANN was large, which means the model accuracy was poor. When the N increased, the MRE decreased, which means the model improved. However, when N reached a threshold, in this case, around 15, the MRE decreased so small that I could ignore it. Therefore, I can conclude that a minimum number of N existed to guarantee the performance of the model. I always prefer a small N and M because large N and M would increase the complexity and the risk of over-fitting (Liu et al., 2017).

According to the analysis above, I used the model with N=15 and M=13. The performance parameter is given in Table 3-6.

Table 3-6 Performance Parameters when N=15, M=13

	MRE	RMSE	R^2
Total	2.16%	0.3954	0.9985
Training group	2.13%	0.3946	0.9985
Testing group	2.18%	0.3974	0.9985
Validation group	2.21%	0.3957	0.9985

Based on the conclusion from the previous discussion, I used N=15 and studied the different transfer function pairs. According to the literature, ‘tansig’, ‘logsig’ and ‘purelin’ are the most commonly used transfer function (Tian et al., 2015). In this study, I used these three transfer functions for the hidden layer and output layer, respectively. Thus, I had 9 different transfer function pairs: ‘tansig-tansig’, ‘tansig-logsig’, ‘tansig-

purelin', 'logsig-tansig', 'logsig-logsig', 'logsig-purelin', 'purelin-tansig', 'purelin-logsig' and 'purelin-purelin'. Each pair was trained with a different range of M. I also trained each case 6 times and kept the one with the best performance.

Similar to what I discussed in the previous section, in Figure 3-11, the y-axis of the graph was MRE, and the x-axis was M. Different lines in the graphs mean different transfer function pairs. The lines could be separated into three different groups, as shown in the graphs. The pairs of 'tansig-logsig', 'logsig-logsig' and 'purelin-logsig' were the first group. The MRE was higher than 70 % whenever the M changed. That meant the 'logsig' transfer function was not good enough to be chosen as the output layer transfer function. Furthermore, the 'purelin-tansig' and 'purelin-logsig' pairs were in the second group. The MRE was higher than 20 %, which means 'purelin' transfer function was not proper to be chosen as the hidden layer transfer function. In addition, for the rest pairs, they were the third group with similar performance. The 'tansig-tansig', 'tansig-purelin', 'logsig-tansig' and 'logsig-purelin' pairs were all proper for EEV NN training. I could also find out that for those pairs in the third group, M increased inversely with MRE. When the M was large enough (around 13), the MRE only decreased a little. This conclusion was in accordance with what I discussed in the previous section.

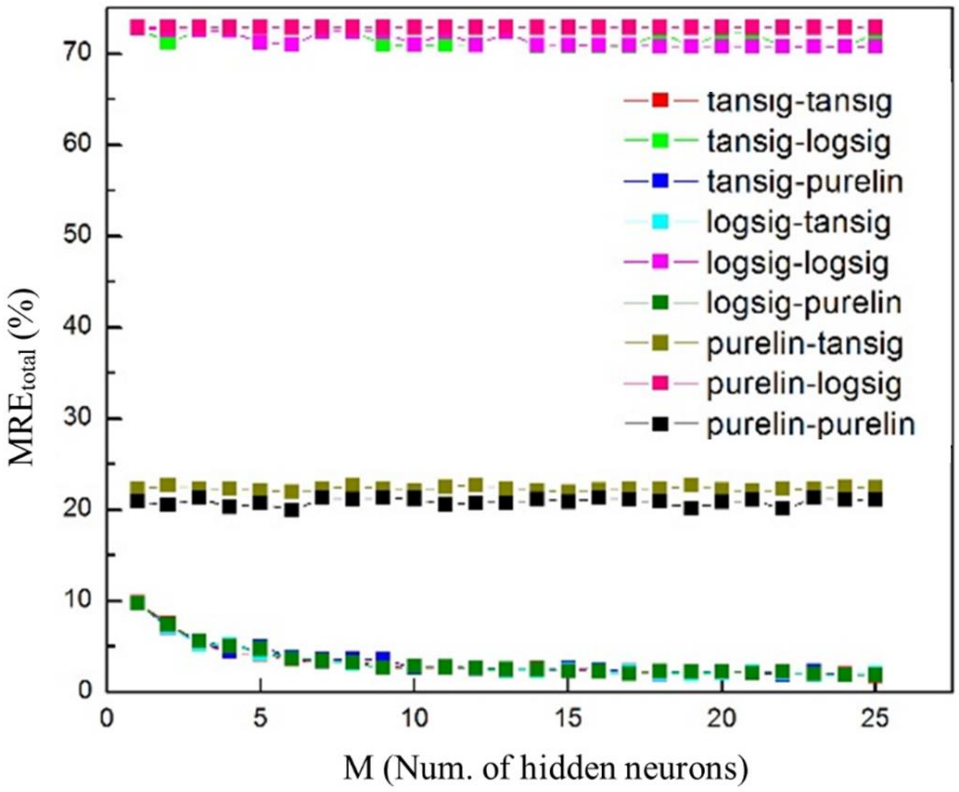

Figure 3-11 MRE with Different M and Transfer Function Pair

According to the analysis, my assumption to use 'tansig-purelin' transfer function pair was reasonable. When I did ANN training, I could choose one from the third group.

Figure 3-12 shows the JointPlot when N=15 and M=13, which provide information about the regression and distribution of the data between the predicted value and experiment value. The x-axis is the experiment value, and the y-axis is the predicted value. Except for limited data points (1 % among all data), my model has a decent performance in that the predicted value exactly matches the experiment value. In addition, I can find out data mostly focused at 0 $g \cdot s^{-1}$ and 15 $g \cdot s^{-1}$. The reason is that the database is from a field test. In the field test, the two most commonly observed conditions for the system are when the compressor is off and when the system is working under-designed conditions. Due to the concentration of the data, one drawback

of my model is the limited confidence of the points between the two points. This problem can be solved by adding some data points of the same system working in a lab experiment under these conditions, which is considered as future work.

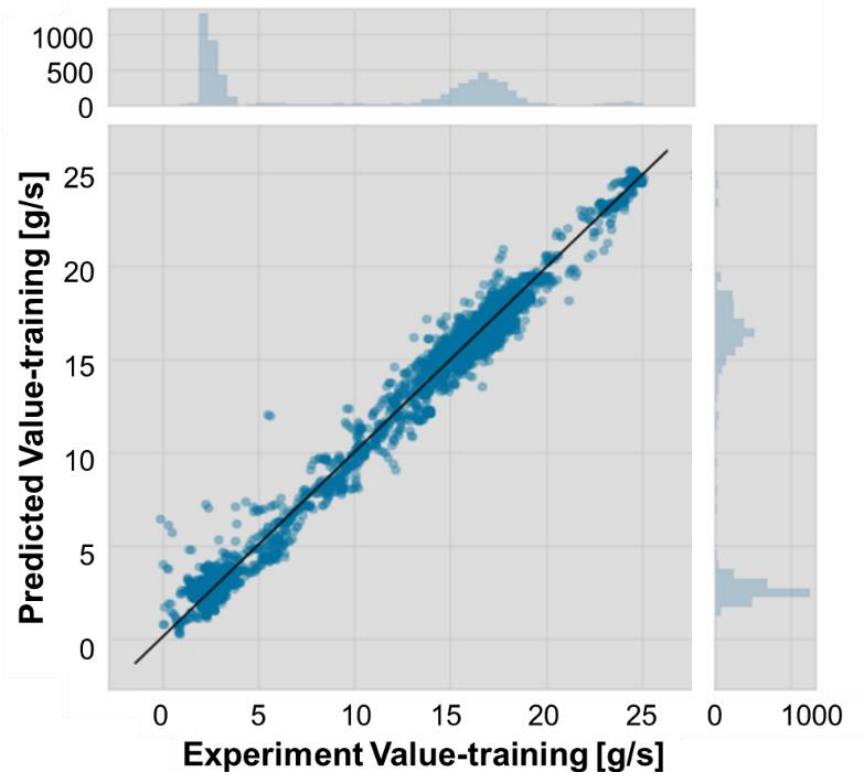

Figure 3-12 Cross-Validation JointPlot

Uncertainty Analysis

I used the same method for uncertainty analysis as chapter 3.1.2. The uncertainty on the variable y was calculated as a function of uncertainties U_{xi} on each measured variable xi:

$$U_y = \sqrt{\sum_i \left(\frac{\partial y}{\partial xi}\right)^2 {U_{xi}}^2} \tag{59}$$

Table 3-7 Uncertainty Analysis

Parameter	Unit	Point 1	Point 2
Mass flow rate absolute uncertainty (ANN model)	$g \cdot s^{-1}$	0.15	0.17
Experiment Mass flow rate	$g \cdot s^{-1}$	21.37	13.80
ANN predicted Mass flow rate	$g \cdot s^{-1}$	22.48	13.38
Frequency of compressor	Hz	20	31
Target EEV opening degree	%	11	6.5
EEV inlet pressure	kPa	3014	2360
EEV outlet pressure	kPa	1182	841
EEV inlet temperature	°C	49.7	39.2
EEV outlet temperature	°C	41.1	30.5
Ambient temperature	°C	-0.5	4.1
Suction temperature	°C	0.5	4.8
Discharge temperature	°C	71.0	77.0
IDU room temperature	°C	17.8	22.4
Outdoor unit power	kW	2.50	2.65
Indoor unit power	kW	0.06	0.06
Outdoor relative humidity	%	36	27
Room relative humidity	%	12	10

The accuracy of the measurement equipment used is given in Table 2-1. Since the correlation obtained from ANN regression was complicated, the value of the partial derivative was derived by numerical differentiation. The uncertainty of compressor frequency and the opening degree of target EEV were considered as zeros. The uncertainty of the mass flow rate varied when the input point varied. I gave the absolute uncertainty of the mass flow rate at two points in Table 3-7.

Comparisons

I studied and compared the conventional method, which is a power-law correlation, with the NN method. The same data as I used for the NN training was used to build the power-law correlation model. Two different power-law correlation methods were adopted. For the first one, I used the same input parameter groups as I used for the NN training. In the second one, I adopted the most commonly used model, Park's model (Park et al., 2007b). Since I only considered one IU, which means the EEV would not be changed, the π group for geometry in their model was not considered. To compare these methods, I used the same performance parameter as I used for ANN performance evaluation. I calculated MRE, RMSE, and R^2 for each case. Table 3-8 summarizes the results. According to Park's experiment data, the RD was between -4.2 % and 11.4 %, and their MRE was 0.76 %. My result in Table 3-8 shows the MRE of power-law correlation, which is 5.72%, which is worse than Park's result. That might be due to their experiment was conducted in the laboratory, but my data was from the field test. In addition, I could find that my NN work has a little bit better performance than Tian's work (Tian et al., 2015b) since I optimized the input parameters and hidden neurons. As I mentioned in the beginning, the compressor frequency was considered as an important parameter in the modeling work. I can validate this by deleting the column of the compressor frequency in the raw data sheet and repeating the process introduced in my manuscript. I still used N=15, M=13, and 'tansig-purelin' as transfer function pairs. The result was MRE=3.92%, RMES=0.6683 $g \cdot s^{-1}$, R^2=0.995. This result was close to Tian's work but worse than the result I showed with the compressor frequency

data. Overall, the PCA-based NN method had a better performance than the power-law correlation methods and previous NN correlation work.

Table 3-8 Comparison of the Conventional Method and NN Method

Method	MRE	RMSE ($g \cdot s^{-1}$)	R^2
Power-law correlation 1 (same input parameter groups as NN)	5.40%	1.5873	0.9756
Power-law correlation 2 (input parameter groups Park suggested)	5.72%	1.0566	0.9889
NN (N=15, M=13)	2.16%	0.3954	0.9985
Tian's work (Tian et al., 2015b)	3.62%	0.6611	0.994
Park's work (Park et al., 2007b)	0.76%	Not mentioned	Not mentioned

Summary

I proposed an EEV modeling framework with a case study on VRF systems. In particular, I developed an NN correlation for the EEV used in VRF systems and optimized the input parameter number and hidden neuron number. In this study, I used the field test data of a VRF system to build the models and applied PCA in optimizing the NN input parameter number. Furthermore, I also discussed the proper number of hidden neurons and different transfer functions. The performances of the power-law correlation and the NN correlation in existing literature were compared to my work, and my model has a better performance. I found that the performance parameters of the NN modeling wouldn't change a lot when the number of the input parameter and hidden neurons reached a threshold. In my case, when I used 15 input parameters and 13 hidden neurons, the model performance was acceptable. I also gave three recommended transfer function pairs for this case. When I compared my NN model

and the conventional method, my NN model improved the accuracy by having the 2.2 % MRE, 0.395 $g \cdot s^{-1}$ RMSE, and 0.999 R^2, while those of the conventional methods are 5.7 % MRE, 1.057 $g \cdot s^{-1}$ RMSE and 0.989 R^2.

Therefore, the PCA-based NN regression method proposed in the manuscript is more practical and accurate for EEV correlation development than the conventional method when a number of data is available. Since no certain criteria in NN model parameter optimization exist, my work gave the following strategies in utilization of NN modeling in HP EEV model development, which has never been discussed in previous NN EEV modeling works. First, a threshold exists for hidden neuron numbers. Second, 'purelin' function cannot be used as a hidden neuron layer function, while 'logsig' function cannot be used as an output layer function. Third, the more input parameters used, the better performance a model can have. But after a threshold, the performance cannot be improved a lot. The model development process and observation presented here are applicable to EEV modeling for other HP systems. Future research could focus more on using different machine learning algorithms to model other parts of the refrigerant system, like compressor and heat exchanger, and compare the performance of these different algorithms.

3.2.2. Steady-state Compressor Model

Background

The compressor is the central part of the HP system. The power consumption of the compressor accounts for 70% of the total energy consumption, according to my field

test. Compressor models were widely used in cycle design, control strategy, and fault detection. Compressor models mainly include the mass flow rate prediction model, the power consumption prediction model, and the current prediction model. In this thesis, I discuss the mass flow rate prediction model since the mass flow rate is the core of capacity calculation, which leads to energy efficiency directly.

In this study, I mainly focus on compressor performance in the whole system. First, I conducted field tests in an office building that installed a ductless VRF system with seven indoor units. I used the moving window method to get a QSS data set from the field test data. In addition, I compared this data set with the one from the manufactures. Furthermore, I summarized three compressor mass flow rate prediction methods from the literature. I compared the performance of these methods. I also applied three machine-learning-based methods to analyze the data set from the field test and the data set from the manufactures. Finally, I compared the performance of all the six methods to predict transient data. Uncertainty analysis was also conducted for the experiment test and the models I built.

Methodologies

I conducted a field test in a campus office building in College Park, MD, U.S. The target ductless VRF system had 7 indoor units and 1 outdoor unit. The test time period was from November 2019 to February 2020. The pressure sensors were installed to measure the suction and discharge pressure of the compressor. The compressor frequency was directly read from the system's control software. Thermocouples were

used to measure the suction and discharge temperature. The accuracy of the instruments could be found in Table 2-1. The mass flow rate was measured by a mass flow meter. The sampling time was 2 seconds. The nominal heating capacity of this system was 23.74 kW. The refrigerant of the system was R-410A. The average heating area for each indoor unit was 11 m^2. The shell volume of the compressor was 48 cc.

Only heating mode data were considered in this study. Simultaneous heating and cooling mode were not considered. The screening method was checking the operation mode of each indoor unit. A QSS filter introduced in chapter 2 was applied in this study. Δt equals 60 seconds. The "threshold" is that the relative deviation of each parameter should be smaller than 1%. The mean value of every parameter in this minute was used to represent the target value of this data point. In this study, the accuracy of the mass flow meter was 0.9 $g \cdot s^{-1}$. When the system was operating in low frequency, the mass flow rate through the system could be as low as 10 $g \cdot s^{-1}$. Thus, the uncertainty from the measurement was already nearly 10%. Therefore, for the steady-state filter, I didn't use the '1%' requirement for the mass flow rate.

In this study, I only considered the case in which the pressure ratio was smaller than 6. The purpose was to guarantee the characteristics of the compressor performance. Based on my test experience, the compressor would show a large difference when the pressure ratio is either low or high. First, I introduce three concepts in machine learning. "Training data set" is the data set I used to build the model. "Testing data set" is the data set I used to optimize the parameters set in the model. "Validation data set" is the

data set that I used to verify the model. Based on the literature review (Wan et al., 2020), two existing modeling methods are physics-based and knowledge-based models. Physics-based methods can reflect physics and thus is more reliable. However, physics-based methods are complicated, and sometimes even no physics equation exists. If the physics-based method was used in dynamic modeling, it might take a long time for the solver to get a result due to the non-linear property. Knowledge-based methods are easy to adapt. Since the knowledge-based model relied on the data, the accuracy was always better. Nevertheless, knowledge-based methods had a problem called "overfitting", which meant such models only work well in the range of the training data set. Strictly speaking, no completely physics-based model was used in practice. The difference was how much this model relied on physics.

Traditional modeling tools used physics-based methods. While nowadays, knowledge-based methods using machine learning algorithms have become popular. However, limited research reported the differences between different methods. In this research, I first compare several physics-based methods. Then I compare these methods with three different machine-learning-based methods.

Method 1: 20-coefficient Polynomial Correlation Methods

$$\begin{aligned}\dot{m} &= f(F, T_{dis}, T_{suc}) \\ &= M_1 + M_2 T_{dis} + M_3 T_{suc} + M_4 F + M_5 T_{dis} T_{suc} + \cdots + M_{20} T_{suc}^3\end{aligned} \tag{60}$$

This method was widely used in the industry to predict the performance of variable speed compressors (Guo et al., 2017b). Hereafter, I use the '20-c' to represent this method. In the equation, M is the correlation factor. T_{dis} is the discharge temperature,

which can be calculated by the discharge pressure I measured. T_{suc} can be obtained by the suction pressure. F is the frequency of the compressor, which is directly obtained from the control software.

The benefit of this method is that this method is easy to use and has a good performance in the range of the training database. However, if the predicting point is beyond this range, the performance would decrease sharply. Obviously, this is a knowledge-based method.

Method 2: Efficiency-based Model

This is another method widely used in both industry and academic fields (Jähnig et al., 2000; Li, 2013a). The mass flow rate could be represented by the compressor frequency, suction density, compressor volume, and volumetric efficiency (eqs. 61 and 62). Except for the efficiency, other parameters required could be obtained directly from the test. There are several different ways to calculate volumetric efficiency. According to Li (2013c), the volumetric efficiency had a strong linear relationship with the pressure ratio, especially when the pressure ratio was low. Besides, the frequency had a second-order polynomial relationship with volumetric efficiency. Thus, I derived a model using linear regression to obtain the volumetric efficiency first (63). I use the 'eff' in the following study to represent this method. This was a highly physics-based method.

$$\dot{m} = \left\{1 - C_{comp,1}\left[\left(\frac{P_{dis}}{P_{suc}}\right)^{1/k} - 1\right]\right\} \cdot \frac{V \cdot RPM}{v_{suc} \cdot 60} \tag{61}$$

$$\frac{\dot{m}}{f\rho_{suc}V} = \eta_{vol} = f(f, P_{dis}, P_{suc}) \tag{62}$$

$$\eta_{vol} = M_1 + M_2F + M_3F^2 + (M_4 + M_5F + M_6F^2)(b_1 + b_2\left(\frac{P_{dis}}{P_{suc}}\right)^{1/k}) \tag{63}$$

Method 3: Efficiency-based Model, using 20-coefficient Polynomial Correlation for Volumetric Efficiency

Of course, a polynomial correlation was always a choice to develop a correlation. Thus, I derived a 20-coefficient model to predict volumetric efficiency (64).

$$\begin{aligned}\eta_{vol} &= f(F, T_{dis}, T_{suc}) \\ &= M_1 + M_2T_{dis} + M_3T_{suc} + M_4F + M_5T_{dis}T_{suc} + \cdots + M_{20}T_{suc}^3\end{aligned} \tag{64}$$

The difference between this method and the 'method 1: 20-c' was that this method was based on the efficiency calculation. Applying this method did not require correction with different suction conditions. I use 'eff-20c' to represent this method. This method relied on physics, but it also used a knowledge-based approach to predict the parameters.

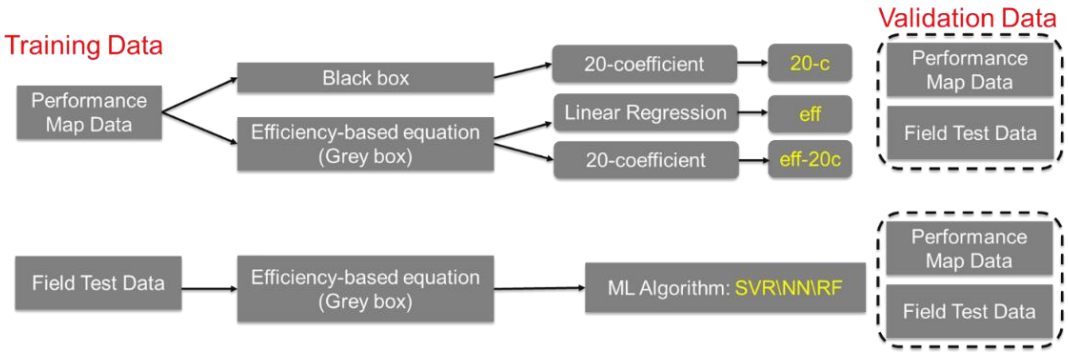

Figure 3-13 Structure of the Compressor Model Study

The structure of this study is shown in Figure 3-13. Nowadays, machine-learning-based methods are widely used in compressor modeling and air condition system modeling. I am not introducing too many details of each method. Interested readers can read the reference (Chen et al., 2020; Cho et al., 2020; Hipple et al., 2020).

For every method mentioned in this part, I divided the original database into three parts: training set, testing set, and validation set. The ratios of every data set were 60%, 20%, and 20%. The data were normalized before the training process. I used MATLAB as the platform. Toolboxes: 'Fitrsvm', 'net', and 'fitrensemble' were used for SVR, NN, and RF, respectively. Like my previous methods, I used discharge temperature, suction temperature, and compressor frequency as the input parameters. Output was the mass flow rate.

Method 4: Support Vector Regression (SVR)

SVR is a regression method using the Support Vector Machine algorithm. This is a linear regression method. Several groups of researchers already used this method to predict the performance of the compressor (Li et al., 2018) or for the fault diagnosis (Qin et al., 2012). The main parameter in the modeling work is the ε value. I optimized the ε in the modeling. I changed ε from 0.01 to 1.00 and found that when ε was 0.16, the accuracy of the model was the best in this study. Eq. (65) shows the equation that SVR generally solved:

$$Min(\frac{1}{2}\|w\|^2 + C\sum_{i=1}^{N}(\xi_i + \xi_i^*)) \quad (65)$$

where symbols w and b are weighting factor and bias, respectively. C and ξ are two crucial parameters that would affect the performance of the algorithm.

Method 5: Neural Network (NN)

Neural Network is also a common method for compressor modeling (Ghorbanian and Gholamrezaei, 2009). In this study, the network had one hidden layer with 7 neurons.

I changed the number of hidden neurons from 1 to 10 and found that when the number was larger than 7 the performance didn't improve a lot. Transfer function pairs used were 'tansig-tansig'. I also tried other pairs like 'tansig-logsig'. The 'tansig-tansig' pair had the best performance. The maximum epochs were 2,000. The following equation could explain the one-hidden-layer NN model. y was the output. "g" were the transfer functions. "w" were the weights and "b" are the bias.

$$y_k = g_{output}\left\{\sum_{j=1}^{n} w'_{jk} \times \left[g_{hidden}\left(\sum_{i=1}^{N} w_{ij}x_i + b_j\right)\right] + b'_k\right\} \quad (66)$$

Method 6: Random Forest (RF)

Yu et al. (2017) used Random Forest (RF) to predict the COP of a chiller. RF was also used to do fault detection work (Aravinth and Sugumaran, 2018). I used the default setting in MATLAB. RF method-based model was hard to write in a simple equation. Interesting readers can read the reference for details (Aravinth and Sugumaran, 2018).

Discussions

Most previous research used the data obtained in the laboratory to build the compressor model. Limited research used the data from the field test. The main reason was that a steady state was hard to be achieved in the field test. The uncertainty of the data brought difficulties in building a model. The conventional approach to build the models, including polynomial regression, had poor performance when dealing with high uncertainty data. While field test data is easy to access, conducting experiments in the laboratory is expensive. Normally, when researchers collected the data from the laboratory, they would test the compressor in a refrigerant cycle. After the system reached a steady-state, they would record the evaporating and condensing temperature

(or pressure), the frequency of the compressor, the target information they need (mass flow rate, power consumption, or capacity), and the suction condition. When they conducted the experiments, they would keep the suction condition (especially superheat) to be the same. In contrast, in field tests, people always recorded all the information time by time.

By the way, in the laboratory test, research always cared about the distribution and the range of the data samples. They would evenly distribute the data sample points. They would also choose several frequencies to do the test. Nevertheless, in the field test, the data points would distribute concentrating on several ranges. The ranges were the '0' point and the points which match with the capacities of the user's requirements. Table 3-9 shows a detailed comparison between data from the laboratory and the data from the field test.

Table 3-9 Comparison between Performance Map Test and Field Test

Parameter	Performance map test	Field test
Input	T_E, T_C, F_{comp}, CD_{suc}	T_E, T_C, F_{comp}…
Distribution	Evenly distributed	Heterogeneously distributed
Distribution Range	Large	Small
Lower bound	30 Hz	0 Hz
Data number	128	1,000 for steady state 624,476 for transient

First, I compare the three traditional methods.

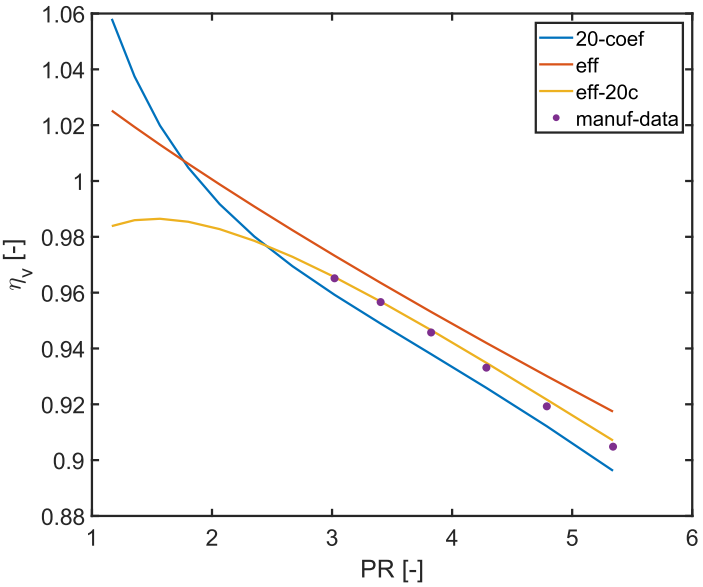

Figure 3-14 Pressure Ratio and Volumetric Efficiency

In Figure 3-14, the x-axis is the pressure ratio. The y-axis is the volumetric efficiency of the compressor. As shown in the figure, the shapes of the models are different. First, the 'eff' method is consistent with my model assumption. For the '20-coef' method, when the pressure ratio decreases below 2, the efficiency would increase sharply. However, for the actual compressor, when the pressure ratio was meager, for example, at the start-up period, the efficiency was not so high. For 'eff-20c' method, when the pressure ratio decreased below 1.5, the efficiency started to decrease. As for the accuracy, the '20-c' and 'eff-20c' methods had better performance than the 'eff' method.

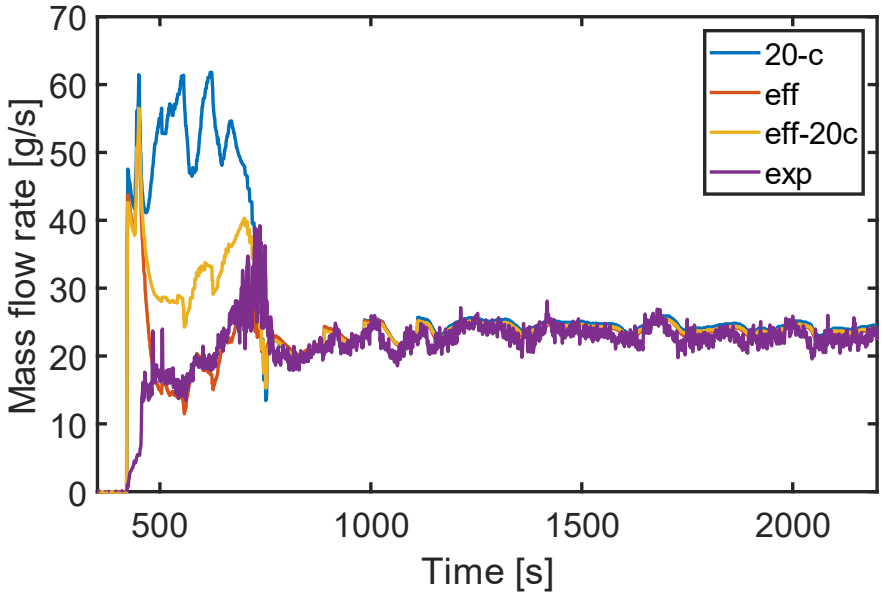

Figure 3-15 Transient Validation

Figure 3-15 shows a comparison between these modeling results and the field test results. The x-axis is the time. The y-axis is the mass flow rate. I could find that at the steady-state, all these methods had similar performance. However, at the beginning of the startup period, all methods failed to predict. The reason could be that at first when the compressor frequency increased, the mass flow rate needed a few seconds to increase due to inertia. After these periods, only the 'eff' method could predict the value well. During these periods, the compressor frequency was low, which was also beyond the training data set range of the data obtained from the manufacture.

The above work all used the data from the manufacture. Then, I would use the field test data set to build the model.

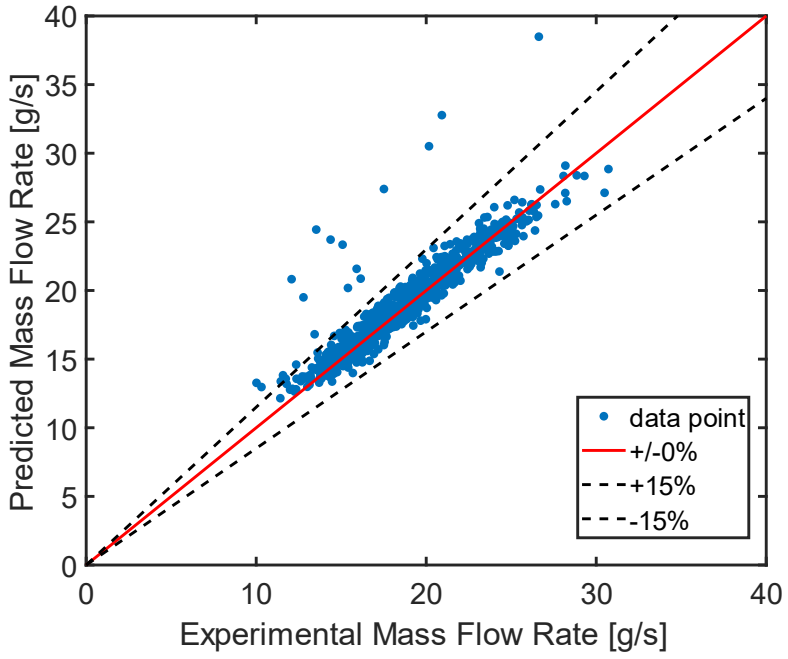

Figure 3-16 Validation by Field Test Data (eff)

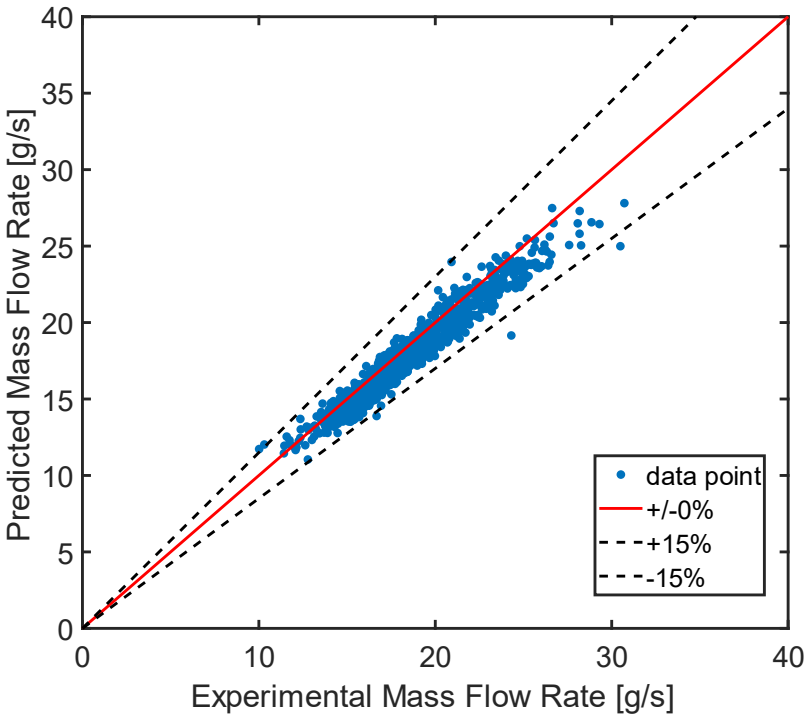

Figure 3-17 Validation by Field Test Data (SVR)

First, I used the model ‘eff’, which had the best overall performance, to predict the field test database, as shown in Figure 3-16. The x-axis is the value of the experiment (field test). The y-axis is the expected value from the model. Most of the data was within the 15% range. As I could find in the figure, there were several points with larger deviations than 15%. In fact, for these data points, the evaporating temperature was around -21 °C. However, in my training database, the lowest evaporating temperature was -10 °C. Thus, it was beyond this range.

The next step was applying machine learning algorithms. I used the SVR method as an example to treat the same data set, as shown in Figure 3-17. Applying other machine learning algorithms would be similar. I could see that for this data set, the SVR method had a better performance than the ‘eff’ method.

Then, I tried other machine learning algorithms, including neural network (NN) and random forest (RF). The Relative Mean Error (RME) and Relative Mean Square Error (RMSE) were given in Table 3-10.

Table 3-10 Machine Learning Algorithm Comparisons

Algorithm	**SVR**	**NN**	**RF**
RME [-]	0.0357	0.0295	0.0237
RMSE [-]	0.0381	0.0328	0.0267

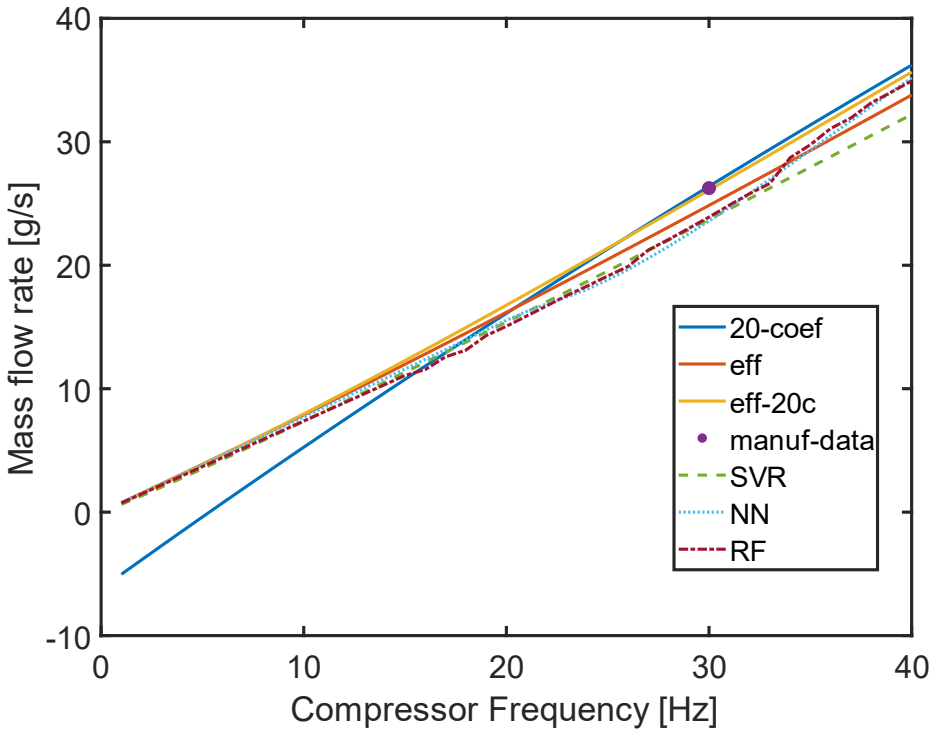

Figure 3-18 Compressor Frequency versus Mass Flow Rate

Figure 3-18 shows the relationship between the mass flow rate and compressor frequency. All approaches show that the mass flow rate has a nearly linear relationship with the compressor frequency. I could find that ’20-c’ had abysmal performance when the compressor frequency was lower than 20 Hz. It predicted the mass flow rate below

0. For other methods, NN and RF methods would predict the slope of the value decrease first and increase later. The slope values were not continuous. These results did not follow the physics.

I also compared all these methods in the startup period in Figure 3-19.

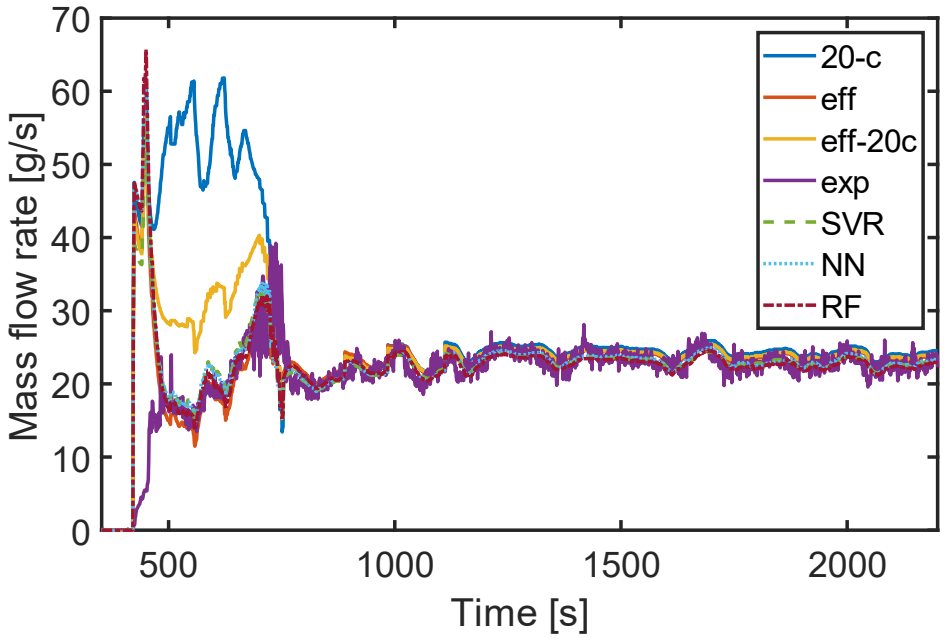

Figure 3-19 Transient Validation (Six Methods)

The performance of 'eff', SVR, NN, and RF were all acceptable.

Table 3-11 Summary of Different Modeling Methods

Modeling method	eff	eff-20c	20-c	SVR	NN	RF
Reflect the physics	Highly	Medium	No	Lowly	No	No
Accuracy	Relatively low	Normal	Normal	Normal	High	High
Complexity	Simple	Medium	Medium	Medium	Complicated	Complicated
Uncertainty	Medium	Small	Small	Medium	Large	Large
Recommend	Yes	Yes	No	Yes	No	No

Uncertainty Analysis

The uncertainty of the data from the manufacture was not accessible. In this part, I would focus on the field test uncertainty and uncertainty analysis of every model I built.

For the field test, I also used the method introduced by Lecompte et al. (2018) to do uncertainty analysis:

$$U_y = \sqrt{\sum_i \left(\frac{\partial y}{\partial xi}\right)^2 {U_{xi}}^2} \tag{67}$$

The accuracy of the measurement equipment used was given in the methodology part of the thesis.

Table 3-12 Uncertainty Experiment part

	High pressure [kPa]		Low pressure [kPa]		Suction Temperature [°C]		Mass flow rate (Exp) [g·s^{-1}]	
	Test	Uncertainty	Test	Uncertainty	Test	Uncertainty	Test	Uncertainty
1	2867	6	901	6	10.2	0.5	18	1
2	2951	8	525	5	6.4	0.5	25	1

Table 3-13 Uncertainty Analysis Modeling part

	20-c [g·s^{-1}]		eff-20c [g·s^{-1}]		eff [g·s^{-1}]	
	Predicted	Uncertainty	Predicted	Uncertainty	Predicted	Uncertainty
1	18.3	0.1	19.2	0.1	20.0	0.1
2	27.4	0.1	25.4	0.1	23.4	0.2
	SVR [g·s^{-1}]		NN [g·s^{-1}]		RF [g·s^{-1}]	
	Predicted	Uncertainty	Predicted	Uncertainty	Predicted	Uncertainty
1	18.2	0.1	19.0	0.1	19.3	0.1
2	23.9	0.2	24.6	0.2	24.5	0.3

For the modeling work, the value of the partial derivative was derived by numerical differentiation. The uncertainty of compressor frequency was considered as zeros. The uncertainty of the mass flow rate varied when the input point varied. I gave the absolute

uncertainty of the mass flow rate at two points. The frequency of each is 15 Hz and 30 Hz, respectively. Table 3-12 shows the experiment part of uncertainty analysis. Table 3-13 shows the modeling part of uncertainty analysis. From this table, I could find that when the frequency increased, the mass flow rate increased, and the uncertainty of the value predicted also increased. Though the value predicted for the NN and RF methods were close to the experiment values, the uncertainty was also large. The uncertainty of the '20-c' method was small, but the value predicted was far from the experiment data point.

Summary

In this study, I built compressor models by both manufactures' data and field test data. I compared different methods to build the models. First, '20-c' method has the best accuracy within the range of the training database, but when the frequency was low, this method failed to predict the MFR. In addition, 'eff' method reflects the physics best. Finally, ML methods have excellent performance if the prediction data point is within the training data set range. As for the uncertainty, the '20-c' and 'eff-20c' methods had lower uncertainty but sometimes failed to predict the accurate value. The NN and RF methods had higher accuracy but also higher uncertainty. In conclusion, I recommended the 'eff' method and SVR method for ductless VRF system compressor mass flow rate prediction. For future work, people may apply the Bayesian-Neural-Network algorithm since this algorithm was reported for excellent performance on high uncertainty data. People may also build a knowledge-based heat exchanger model. Then people need to test the full cycle performance.

3.2.3. Transient Compressor Model

Methodologies

The compressor model in the transient state was different from that in steady-state. If I used the steady-state compressor model to predict transient field test data, some gaps between the experiment values and simulation values would exist. The mass flow rate I tested might not reflect the value everywhere in the system since, in the transient case, the mass flow rate might not be consent in the system.

In order to simplify the case, I only consider the situation in which only one indoor unit was used. EEV opening degree, compressor suction pressure, compressor discharge pressure, condenser outlet temperature, condenser outlet density, evaporator inlet temperature, and compressor frequency were used as the input parameters. The outlet parameter was the mass flow rate through the system. The input data also had another dimension, which was the time. I considered 80 s (40 test data points) in this study. Each input data slot was an 8-by-40 matrix. The x-dimension was the eight parameters I studied. The y-dimension was the time. An example was shown in Figure 3-20. It was an image generated by MATLAB. Columns from left to right meant EEV opening degree, condenser outlet temperature, compressor discharge pressure, evaporator inlet temperature, compressor suction pressure, subcooling of the condenser, condenser outlet density, and compressor frequency, respectively. There were 40 rows. The first row was the time 80 s ago. The last row was the current time. All the values were normalized to 0-1. In the example (Figure 3-20), the last figure was in QSS. Thus, the top side color was very closed to the downside color.

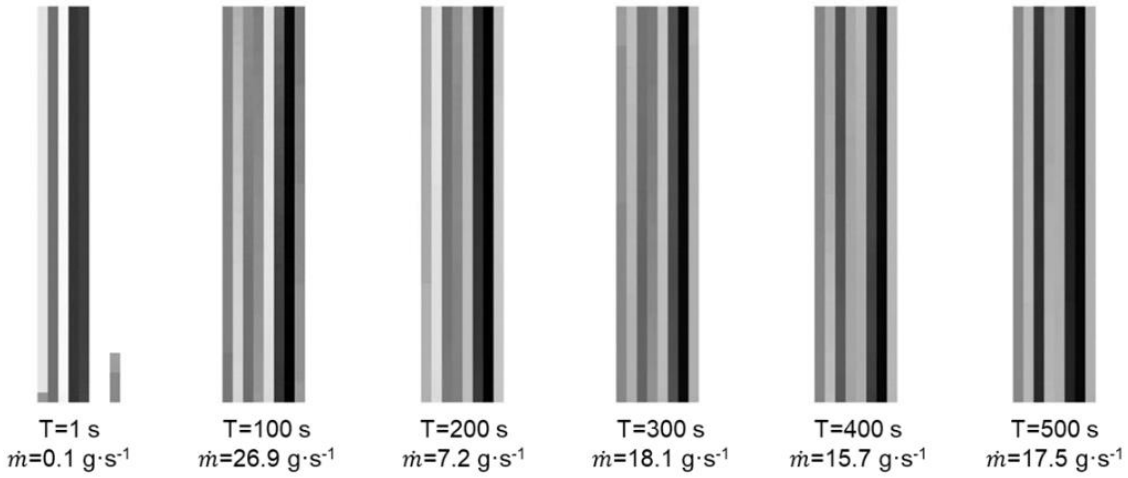

Figure 3-20 Input Example

I had a set of images, as shown in the example. For each image, I also had a matching value, which was the mass flow rate at the current time, the output of my model. CNN was a common method for image recognition. I used the 'trainNetwork' toolbox in MATLAB to build the CNN model. In my model, I set 6 hidden layers. I had 57,456 input data images. 30,000 were used as the training data set. 10,000 were used as the testing data set. The remaining images were used as the validation data set.

The parameters of the model setting were listing below: (ReLU was Rectified Linear Unit, and Table 3-14 was a set format of MATLAB toolbox)

Table 3-14 Parameters of Model Setting

No.	Layer	Note
1	Image Input	12x6x1 images with 'zerocenter' normalization
2	Convolution	8 3x3 convolutions with stride [1 1] and padding 'same'
3	Batch Normalization	-
4	ReLU	-
5	Average Pooling	2x2 average pooling with stride [2 2] and padding [0 0 0 0]
6	Convolution	16 3x3 convolutions with stride [1 1] and padding 'same'
7	Batch Normalization	-
8	ReLU	-
9	Average Pooling	2x2 average pooling with stride [2 2] and padding [0 0 0 0]
10	Convolution	32 2x2 convolutions with stride [1 1] and padding 'same'
11	Batch Normalization	-
12	ReLU	-
13	Convolution	32 2x2 convolutions with stride [1 1] and padding 'same'
14	Batch Normalization	
15	ReLU	
16	Dropout	20% dropout
17	Fully Connected	1 fully connected layer
18	Regression Output	Mean-Squared-Error

Discussions

Figure 3-21 shows the startup period of the VRF system when only one indoor unit was working. This test data was generated at 9:16 am on July 11th, 2019. The x-axis for all the subfigures is the time. This lasts for 500 s, which also means there are 250 data points in each subfigure. The first subfigure shows the condensing temperature and evaporating temperature. The condensing pressure increased at first and then decreased, and then increased again, and kept at a constant value. The evaporating pressure decreased and then kept at a constant value. The reason was the high pressure was

controlled by the frequency of the compressor. As I could see in the second subfigure, the compressor frequency also increased at first and then decreased and increased again. The third subfigure shows the EEV opening degree of the target IU. The trending for that was similar to the high pressure and the compressor frequency. In this example, there were 500 seconds. At the end of this period, I could find that the system went into QSS. In this figure, the pressure changes and mass flow rate change had some delay compared with the control parameters like compressor frequency and EEV opening degree. This was the truth in the field test since the system needed some time to reflect control and operation by the users. Another main reason could be the thermal mass of the refrigerant and heat exchangers.

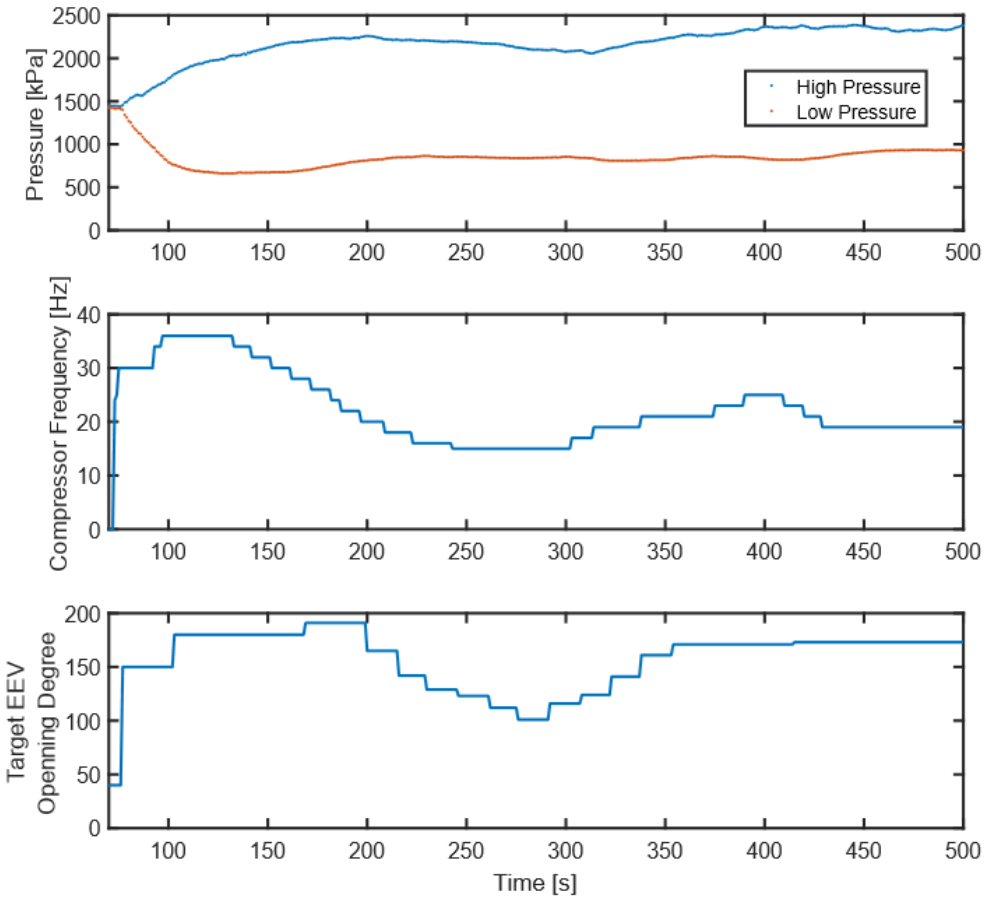

Figure 3-21 VRF System Startup

I used the compressor map from the manufacture to predict the mass flow rate of the system and compared the result with my experiment data. The compressor map I used was a 20-coefficients compressor map. This method was widely used to evaluate the compressor mass flow rate for VRF systems. This method was also a knowledge-based method since no physics rules were used in this approach. This method could only be used for steady-state data or quasi-steady-state data. My following result also proved this. Figure 3-22 shows the experiment mass flow rate value and predicted value from the compressor map. The blue line is the experiment result, and the red line is the modeling result. This 500-second period was the same period as I showed in Figure 3-22. The y-axis is the mass flow rate. The x-axis is the time. The experiment mass flow rate trend is in accordance with the compressor frequency trend and the EEV opening pulse trend. The mass flow rate increased sharply at first and then decreased, and then increased, and kept at a constant value. From Figure 3-21, I could find that the liquid mass flow rate and the mass flow rate showed different behaviors. For those parts where the mass flow rate varied a lot, the gaps were obvious between the experiment value and the predicted value.

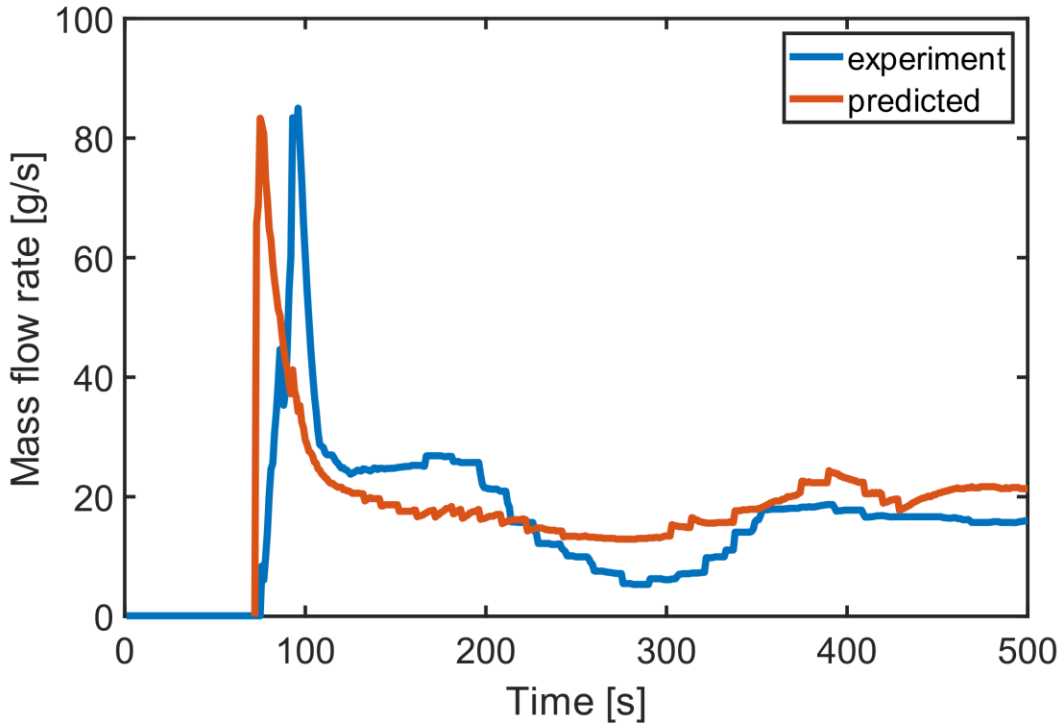

Figure 3-22 Mass Flow Rate Comparisons (Compressor Map versus Experiment)

I applied the CNN-based modeling method introduced in the methodology part to predict the mass flow rate at the same time. Figure 3-23 was the result. Similar to Figure 3-23, the y-axis is the mass flow rate. The x-axis is the time. The blue line is the experiment result, and the red line is the modeling result. As shown in Figure 3-23, the CNN-based model could solve the mismatch problem. However, in the very first part of this period, the mass flow rate predicted was larger than the experiment value. At the peak point, the predicted value was smaller than that experiment value. The current Mean Relative Error (MRE) of this model was 2%. In my study, I didn't optimize the structure of the network. I also didn't study which activation functions were the best in this case. Thus, there would still be some space for this model to be improved. Another drawback of this method was the 0-value shifting. As shown in Figure 3-23, in the first

several seconds before the system startup, the predicted mass flow rate value was not exactly 0. The training time for building the model was 5 min 44 seconds using one single CPU, but after one-time training, the prediction work could be complete immediately. The uncertainty analysis of the CNN model was complicated since the input parameters had two dimensions. Traditional uncertainty analysis was not approvable for this approach. This could be my future work.

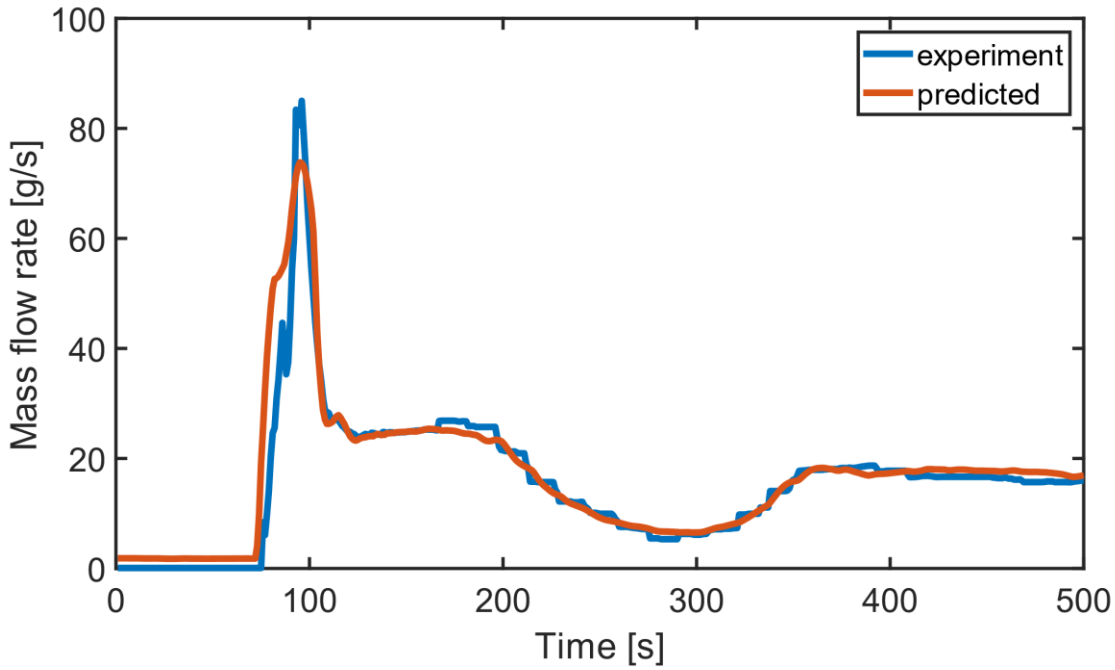

Figure 3-23 Mass Flow Rate Comparisons (CNN-based Model versus Experiment)

3.3. Summary

In this chapter, the authors introduced a large number of modeling methods and compared them in HP system performance prediction. These models could be used to predict the overall performance of the system, like power consumption or pressures. They can also be used to predict the performance of the subcomponents in the system

like the EEV and compressor. Table 3-15 summarized these methods and compared the characteristics of these methods.

Choosing an appropriate method and setting the parameters in the model are important. Figure 3-24 shows a general process to select models and set the parameters in the model. Like field test data analysis, goals (the purpose of the modeling) and computer performance need to be considered when choosing the method.

Table 3-15 Comparisons of Different Data-driven Modeling Methods

Modeling Methods	Physics	Statistic	Machine learning			Deep learning
	Physics-based	Power-law/Polynomial Correlation	SVR (SVM)	RF (decision tree)	NN (SNN)	CNN (Multiple-time-step NN)
Example	Compressor efficiency-based model	EEV MFR correlation, compressor map	Power model, compressor model	Compressor model	EEV model, compressor model	Compressor model
Risk of overfitting	Very low	Very high	Low	Normal	Normal	Normal
Uncertainty	Medium	Small	Small	Large	Large	-
Accuracy	Low	Low	Normal	Normal	Normal	High
Complex setting	-	Simple	Medium	Medium	Medium	Complex
Training time	Very short	Short	Short	Medium	Medium	Very long
Dealing Large Data	Yes	Yes	PCA	PCA	PCA	Yes
Continuous	Yes	Yes	Yes	No	Yes	Yes

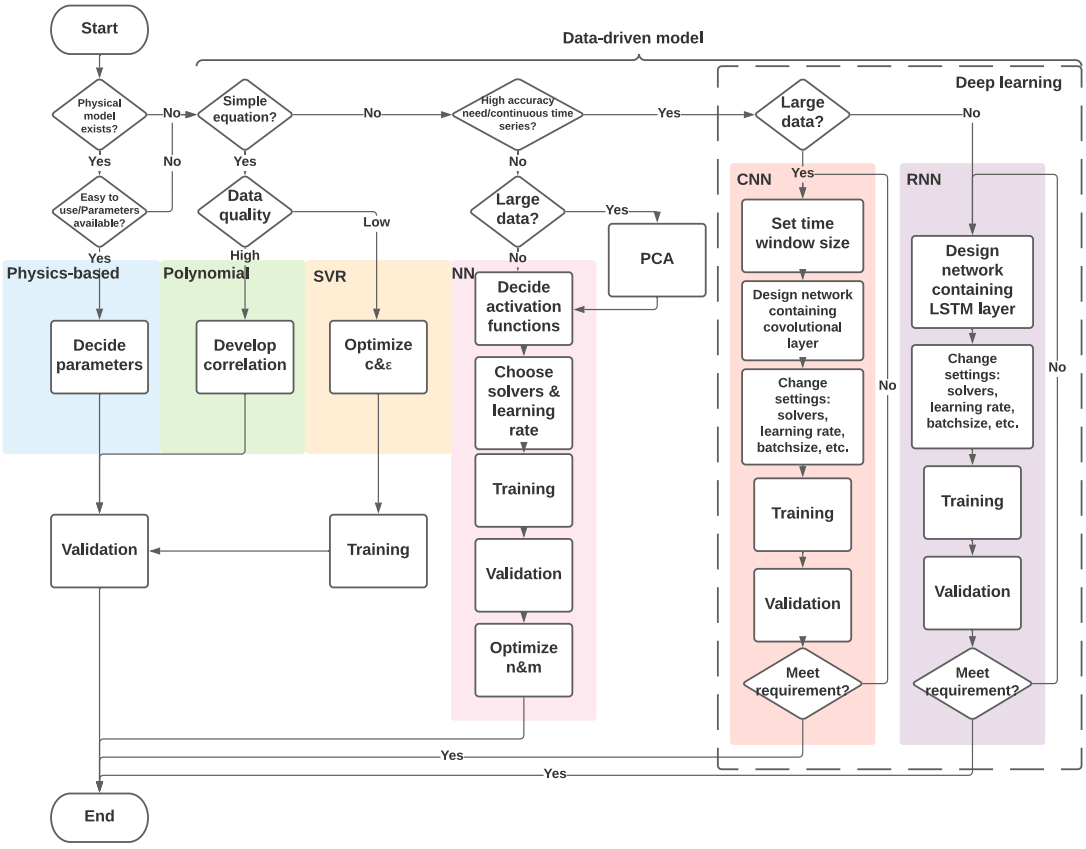

Figure 3-24 Flow Chart to Select and Set Data-driven Models

4. Enhanced Life Cycle Climate Performance Evaluation

4.1. LCCP in Different Regions for Different Refrigerants

Long-term usage of halogenated refrigerants in refrigeration and air conditioning systems has caused severe environmental damages. With the phasing down of high-GWP refrigerants, the replacement of currently used refrigerants requires safe, energy-efficient, and environmentally friendly characteristics. Nevertheless, no perfect alternative refrigerant exists, satisfying all these requirements (Venkatarathnam and Murthy, 2012). Many target parameters are involved, including flammability, GWP, compressor efficiency, compressor and system cost, heat transfer, and pressure drop. A trade-off map among these can be drawn, as shown in Figure 4-1 (Gilmour and McNally, 2010).

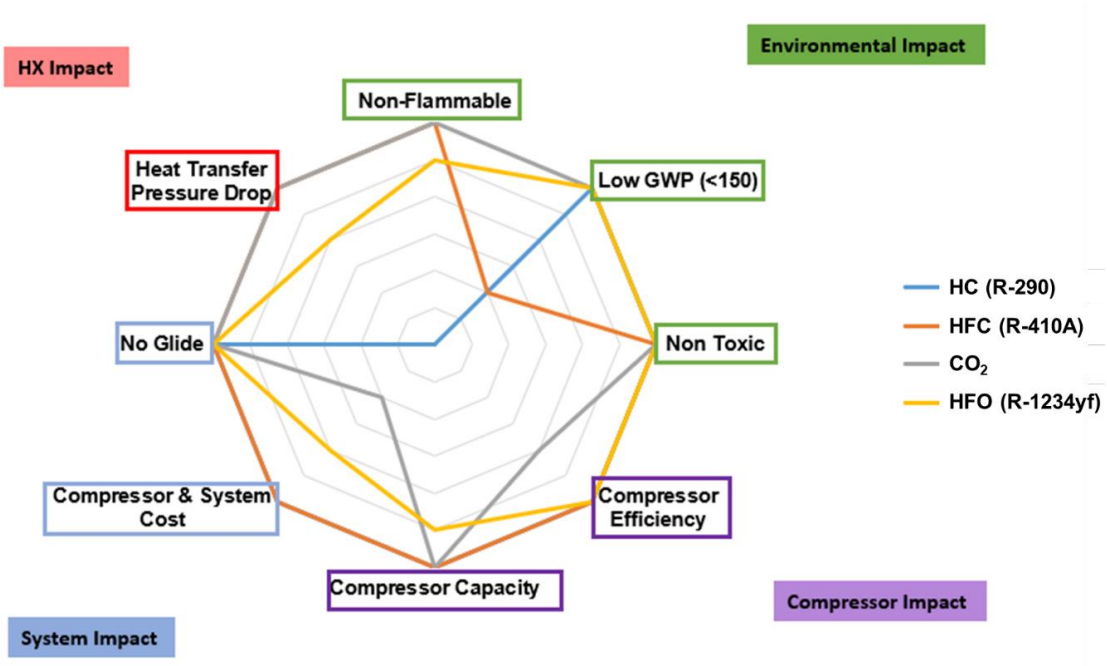

Figure 4-1 An Example of the Target Parameter Trade-offs Involved in Choosing the Ideal Refrigerant

Therefore, how to choose an appropriate refrigerant is significant. I need some metrics to combine these criteria. LCCP is a reasonable way to evaluate the performance, including system efficiency and environmental impact at the same time. Table 1-3 summarizes the refrigerants evaluated in the LCCP calculation. Till now, the manufacturing emissions of R-466A and R-454B have not been reported. In the results part, I discuss R-466A and R-454B manufacturing emissions' effects on the LCCP with different assumption values. In this chapter, the tested VRF system was not evaluated since the material usage data was confidential. A unitary system was used as a substitution. The process to analyze the two systems would be the same.

4.1.1. System Annual Energy Consumption

The Annual Energy Consumption (AEC) consists of the cooling power consumption and heating power consumption of the target system throughout the year. In real-life applications, field tests and energy surveys can help determine the HVAC system's annual energy consumption. However, the field test is not always available. To estimate power consumption, I need to know the cooling and heating loads and the system performance at a given ambient temperature. In this study, to compare the LCCP in different countries for different refrigerants, I used the simulation method to estimate the AEC.

System Performance

I simulated the HP systems of a 10.55 kW and 115 kg-weight system (Alabdulkarem et al., 2014, 2015) using an in-house component-based steady-state vapor compression

cycle modeling tool, VapCyc (Winkler et al., 2008). The models were validated by experiments using R-410A and R-32.

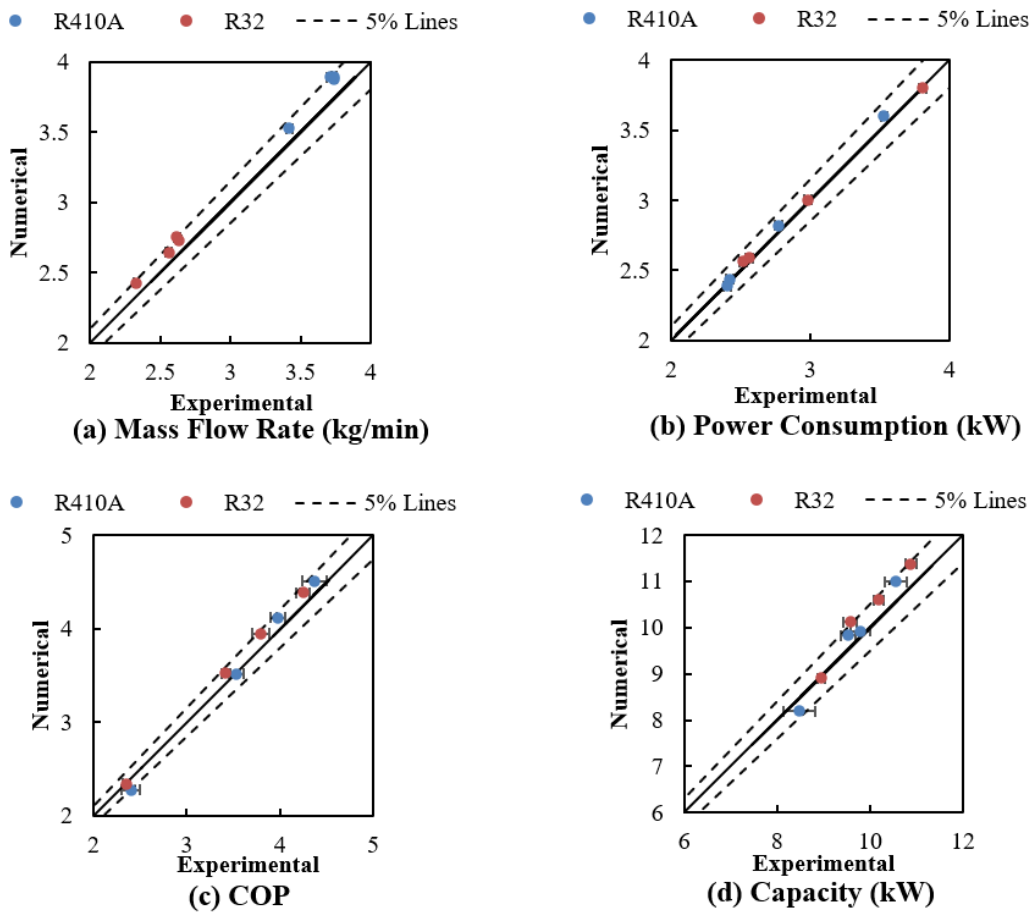

Figure 4-2 Cooling Experiments Validation Results (Alabdulkarem et al., 2014)

The validation results of cooling experiments are shown in Figure 4-2. All the results agree with the experimental test data within 5% deviations. I used this model to predict the system performance in different ambient environments. In the model, an assumption of 2.1 K superheat at suction was assumed for these tests. An assumption of 2.8 K subcooling was used to predict the charge level. A constant isentropic and volumetric efficiency compressor model was used. The volumetric efficiency, isentropic efficiency, and mechanical efficiency were assumed to be 0.8, 0.75, and 0.95,

respectively. The assumptions were based on my previous experiments (Alabdulkarem et al., 2015).

Table 4-1 Design Compressor Displacement Volume and Predicted Charge Level

Capacity	Refrigerant	Compressor RPM	Compressor Displacement Volume (cm^3)	Charge (kg)
10.5 kW	R-410A	4,700	34	4
	R-290	7,300	43	1.2
	R-32	4,000	34	3.5
	R-452B	4,700	34	3.8
	R-454B	4,700	34	3.8
	R-466A	4,800	34	4.2
12.3 kW	R-410A	4,700	47	4.1
	R-290	7,300	61	1.8
	R-32	4,000	47	3.6
	R-452B	4,700	47	3.9
	R-454B	4,700	47	3.9
	R-466A	4,800	34	4.3

Table 4-1 shows the compressor's Revolutions Per Minute (RPM) and displacement volume for different refrigerants and the predicted charge level. The charge level was consistent with the density of each refrigerant. The RPM and displacement volume were set to optimize the system performance with the capacity constraints. I also designed the system for the 12.3 kW system since for cities in hot climate regions like Miami and Phoenix, the 10.5 kW system could not match the load requirement for a similar size room in other areas. My study focused on office buildings with relatively higher occupants' density and equipment loads than residential buildings. Thus, for cold countries in winter like Switzerland and Sweden, the systems could also be designed for the cooling season.

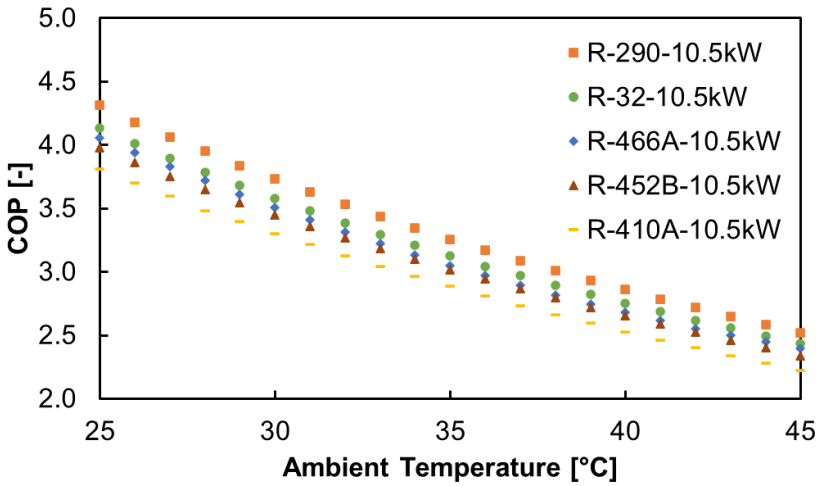

Figure 4-3 Cooling COP Comparisons for Different Refrigerants

Figure 4-3 shows the simulation results of 10.5 kW capacity systems' COP for five refrigerants with different ambient temperatures in the range of 25 °C to 45 °C. R-290 has the best performance, while R-410A has the worst performance. R-32, R-466A, and R-452B have similar performances. R-454B has the same performance as R-452B and is not drawn on the figure. From my modeling results, R-32 has a better performance than R-466A, while R-466A has a better performance than R-452B. When the ambient temperature increases, the performance of the three refrigerants gets even closer.

Some researchers studied different refrigerants' performances with different ambient temperatures. Kujak (2019) reported that R-32 had a lower COP than R-452B when the ambient temperature was lower than 47 °C and higher COP when the ambient temperature was higher than 47 °C. Binbin et al. (2020) studied tens of alternatives for R-410A and concluded that the COPs for R-290, R-32, R-466A, and R-452B were 5%,

1%, 1%, and 1%, respectively, higher than the R-410A. My results are consistent with the literature.

Since my study only considered a cooling-season-based design (high-density occupants and equipment), the system performances would be very close (within 1% differences) for different refrigerants at the same ambient temperature. The reason was that the heating loads were from 3 kW to 6 kW for different cities, which were less than half of the design capacity.

Load Prediction

AHRI standard 210/240 (2017) provides an approach to estimate the air conditioning load. This approach is called the temperature bin method. However, this approach is applicable to a fixed speed system. If the system had a variable speed compressor, the compressor frequency's control logic would also affect the result. With the development of data-driven methods, some researchers used machine-learning-based models for load forecasting (Madonna and Bazzocchi, 2013). The data-driven approach requires a large amount of test power data. When the weather data is available, I could use a physics-based method to simulate the target building's load or a room by following the ASHRAE standard (ANSI/ASHRAE Standard 34-2019). In this study, I chose the physics-based method to estimate the load since this method controls the variables, which are the regions and refrigerants. I considered a 10 m × 10 m room facing south in the Northern Hemisphere. Two windows were installed facing south and north. The ceiling and floor were assumed to be adiabatic. Other parameters can be found in Table 4-2. I also made the following assumptions to eliminate other factors'

impact on LCCP calculation: the optical depth parameters for the location were assumed to be constants through the year; windows had no shading. I used the model introduced by Wijeysundera (2015) to estimate the cooling and heating load of the target room.

Table 4-2 Parameters for Simulation

Item	Value
Height	3 [m]
Window to Wall Ratio	0.6 [-]
Ground Reflectivity	0.25 [-]
Solar Absorptivity of Wall	0.8 [-]
Wall	Brick and a layer of insulation board
U-value of Wall	0.58 [$Wm^{-2}K^{-1}$]
Window	Double-glazed
Occupant	75 W for sensible heat, 55 W for latent heat
Occupant per unit floor area	0.1 [m^{-2}]
Equipment per unit floor area	13.5 [m^{-2}]
Light per unit floor area	4.5 [Wm^{-2}]
Working Hours	9:00-19:00

Grid Electricity Emission Factor and Material Embodied Carbon Coefficients

The emissions due to energy consumption are a dominant factor in the LCCP calculation. Different countries and regions have different power plant emission factors due to the resource portion difference (Choi et al., 2017). Carbon Footprint (2019) summarizes the country-specific electricity grid carbon emission factor in June 2019. The data for Asian countries is from G20 Green Report 2018 (Transparency, 2018), for European countries is from the Association of Issuing Bodies (European Residual Mix | AIB, 2012), and for the U.S. is from the Environment Protect Agency database (U.S. EPA, 2020). The second column of Table 4-3 shows the Grid Emission Factors (GEFs) used in this study.

Table 4-3 GEEF, Material Usage, and ECCs

Weight: 115 [kg]		GEEF [kg CO_2e/kWh]	ECCs [kg CO_2e/kg]			
Material (% usage)			Aluminum (12%)	Copper (19%)	Plastic (23%)	Steel (46%)
Average around world		0.623	13.1	2.71	3.31	3.02
EU	UK	0.277	6.58	2.71	-	1.80-2.89
	Sweden (SE)	0.012				
	Switzerland (CH)	0.014				
NA	US FL	0.467	5.65	3.00	2.80	1.80
	US AZ	0.425				
	US GA	0.457				
AS	JP	0.492	10.60	-	-	1.64
	KR	0.517	11.90	-	-	-
	CN	0.623	14.60	-	-	3.50-4.50

The carbon emission during the system's manufacturing phase is another factor that affects the LCCP calculation. Some previous studies used the same emissions values for the material in every country. For example, Choi et al. (2017) used the IIR's LCCP guideline (Life Cycle Climate Performance Working Group, 2015) to estimate the LCCP in Korea. However, IIR's LCCP guideline only provides the recommended values in the U.S. Some researchers, especially those working on Life Cycle Assessment of buildings, have developed a database for different material's Embodied Carbon Coefficients (ECC) in different countries (De Wolf et al., 2016). For this study, I used the Inventory of Carbon and Energy database developed by Hammond et al. (2011). For plastic and steel, I used the general values for these two materials. Some ECCs were not found in the literature for some countries. The average value around the work was used as a substitute in this study. As shown in Table 4-3, the ECC for aluminum in the U.S. is around one-third of China's value. Thus, ECCs could be a crucial factor in the LCCP calculation for different countries.

4.1.2. Weather Station Data and On-site Weather Data

Most building simulation studies utilize data collected from weather stations. The most commonly used database includes the EnergyPlus built-in weather data, NOAA weather data, and TMY3 weather data. The first two datasets are the Actual Multi-Year (AMY) dataset, while the last one is a Typical Meteorological Year (TMY) dataset. Some researchers studied the difference between the AMY dataset and the TMY dataset (Kamel and Sheikh, 2020). They concluded that the dry-bulb ambient temperature had a significant impact on the simulation results. Most of the weather station data were collected around the airports. Some studies pointed out the temperature gaps between a city and an airport. Such a temperature gap in an urban area or metropolitan area due to human activities is called urban heat islands (UHI) effect (Kotharkar et al., 2018). This effect's leading cause is from modifying land surfaces (Solecki et al., 2005) and waste heat generated (Li and Zhao, 2012). Santamouris et al. (2017) studied the UHI effect from 220 projects and found that 31% of the analyzed projects resulted in a peak temperature drop below 1 °C, 62% below 2 °C, 82 % below 3 °C, and 90 % below 4 °C. Munck et al. (2013) found that the increase in temperature was 0.5 °C in the situation with current heat releases, 1 °C with recent releases converted to only sensible heat, and 2 °C for the future doubling of air conditioning waste heat released to air in Paris. This temperature gap could bring some differences in LCCP calculation. Thus, I would compare the LCCP results using both weather station data and weather data corrected by Santamouris's statistics (2017).

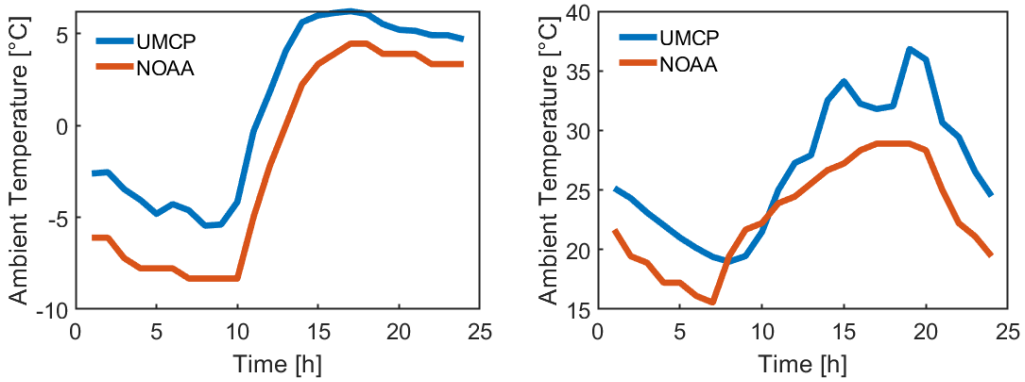

(a) January 15th Ambient Temperature (b) July 1st Ambient Temperature

Figure 4-4 Comparison of Ambient Temperatures in 2019

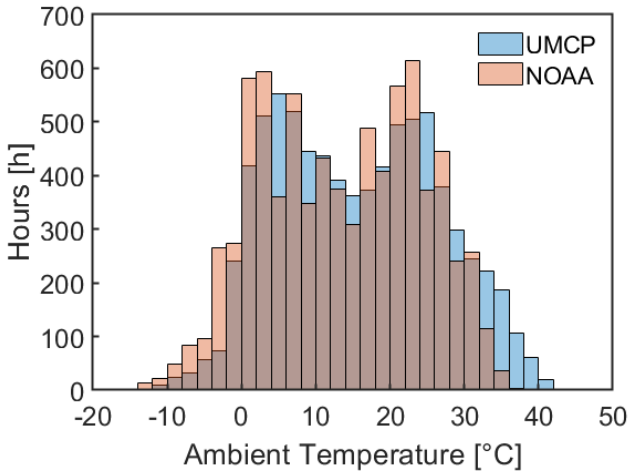

Figure 4-5 Histogram of the Year 2019 Ambient Air Temperature in College Park, MD, U.S.

I also measured the local ambient temperature. Thermocouples were installed next to the outdoor unit in the campus building at UMD, College Park, U.S. introduced in chapter 2.1. The thermocouples were exposed in the air facing north and had no shadings. The ambient temperature tested was compared with the temperature data from Airport, College Park, U.S. The distance between the two places is 1.8 km. Figure 4-4 shows the comparisons between the two data. Figure 4-4 (a) shows the daily temperature measured on January 15th, 2019. Figure 4-4 (b) shows the daily

temperature tested on July 1st, 2019. The blue line is the temperature tested in the campus reading through LabView, marked as UMCP. The red line is the temperature tested in the airport from the NOAA database. I could find that in winter, the UMCP campus temperature was 10-20 °C higher than the airport's temperature. Since the campus building sensors had no shading, solar radiation would have a significant effect on them. As a comparison, the weather stations' temperature sensors were usually stored in a shaded structure, which had less impact on the radiation. In the field test, the built-in sensors of the outdoor units are usually exposed to the air directly. Thus, the UMCP campus case should be closer to the field test case. This temperature gap could also be caused by human activity and other HP outdoor unit outlet waste heat. However, during the summer, the UMCP campus temperature had a higher peak but lower valley than the airport's temperature. Figure 4-5 shows a histogram of the two temperatures in the year 2019. 118-hour data points in the campus testing dataset and 43-hour data points in the airport dataset were not validated due to the power outage or broken database. I excluded these data points when I drew Figure 4-5. Thus, 8,599 data points exist in this figure. I used these two datasets separately to calculate the LCCP and discussed the differences. The finding is that the gap between the on-site data and the weather station data is much larger than what previous researchers assumed.

4.1.3. Different Countries and Regions

Figure 4-6 shows the LCCP results in different areas for R-410A as an example. "CollegePark1" and "CollegePark2" show the calculation results using UMCP campus weather data and College Park airport weather data, respectively. From Figure 4-6, I

can find that the LCCP results for Basel and Kallax are very small. The reason is that the GEFs of Sweden and Switzerland are very small. Only for the two countries, the annual leakage is the primary factor of the LCCP. For all other countries, annual energy consumption is the main factor affecting the LCCP. Li (2015b) concluded that the SEER rating had a far more significant impact on lowering CO_{2e}. Nevertheless, based on my study, this conclusion is only valid in the countries with a high GEEF.

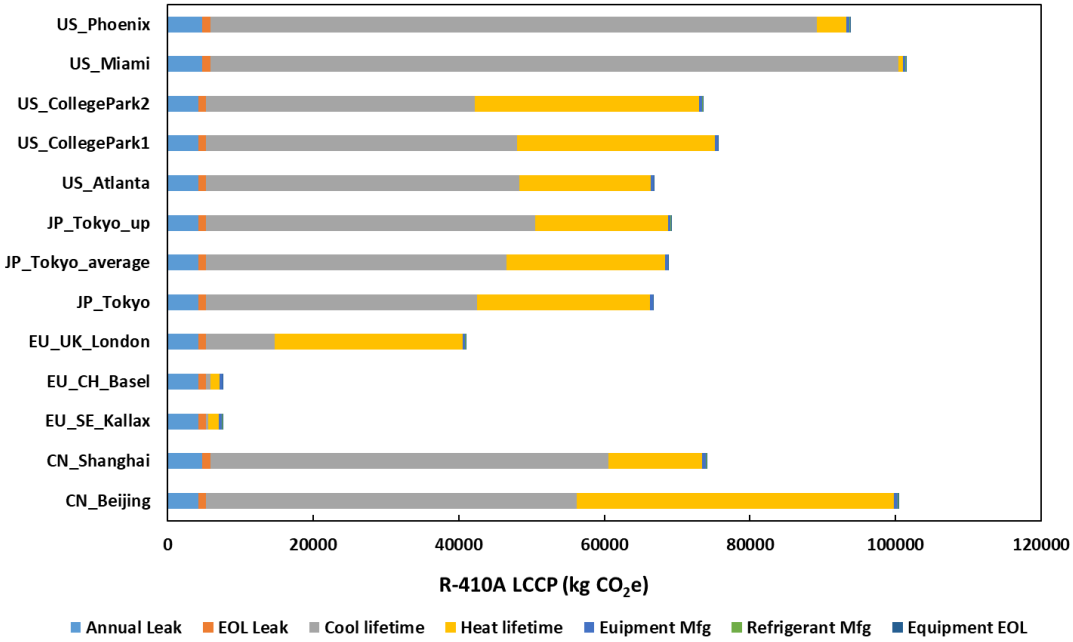

Figure 4-6 LCCP Results for R-410A at Various Cities

4.1.4. Different Refrigerants

Figure 4-7 shows the LCCP in four different cities for six different refrigerants (The RFM values for R-466A and R-454B were assumed to be 31 and 9 kg $CO_{2}e$/kg). The readers can see that R-290, R-32, R-452B, R-454B, and R-466A are good alternatives for R-410A with lower LCCP. R-454B has a bit better performance than R-452B due to a smaller GWP value. For Kallax, the annual leakage is the major contributor to

emissions since its GEEF is low. Thus, the LCCP could be decreased by 60% for this city if R-290 substituted R-410A. As for the previous studies, Choi et al. (2017) compared the LCCP of R-290, R-410A, and R-32 for five different cities in Korea. They found that the LCCP of R-410A was 9% higher than that of R-32 and 21% higher than that of R-290 in Seoul, Korea. Lee et al. (2016) calculated the LCCPs for R-410A, R-32, R-290, and R-452B, and the results were 126, 119, 111, and 120 MT of CO_{2e}, respectively. The LCCP order of different refrigerants was consistent with the current study.

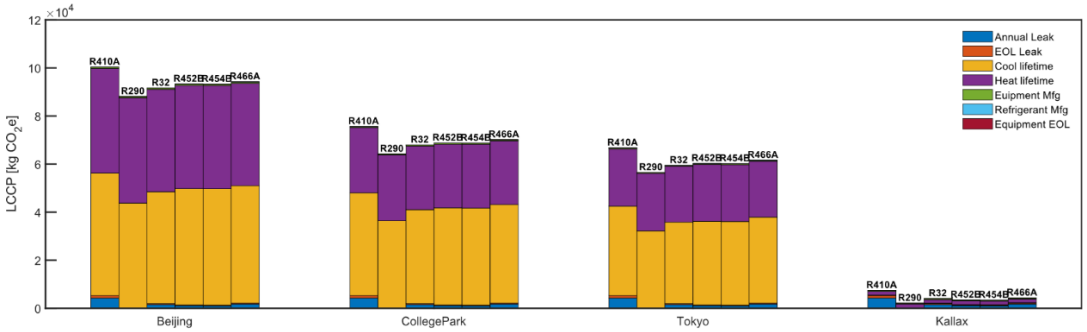

Figure 4-7 Different Refrigerant LCCP Results for Four Selected Cities

As for R-466A and R-454B, the emission from the refrigerant manufacturing process had not been reported until now. Thus, I made three assumptions for the values and studied whether different emissions in the refrigerant manufacture phase would bring some differences in the LCCP calculation. According to the IIR guideline (Life Cycle Climate Performance Working Group, 2015), the emissions from the refrigerant manufacturing process for HFC refrigerants range from 5 to 20 kg of CO_{2e} per kg. I assumed the value to be 5, 10, and 20 kg of CO_{2e} per kg for assumptions 1, 2, and 3, respectively. The LCCP calculation results are shown in Table 4-4. The three columns for each assumption are the emissions during the refrigerant manufacturing process,

the total LCCP result, and the percentage of the emissions from the refrigerant manufacturing process in the total LCCP. I can find that even for low emission cities like Basel and Kallax, the emissions from the refrigerant manufacturing process are only 3% of the total LCCP. Thus, I concluded that the refrigerant manufacturing phase's effect is insignificant in the LCCP calculation. Furthermore, when I compare the LCCP calculation results for R-466A (assumption 1) with other refrigerants' results in Figure 4-7, I can find that the LCCP of R-466A is 1.6% higher than that of R-452B but 8% lower than that of R-410A for College Park, U.S. as an example. Thus, R-466A is also a good substitute for R-410A from the LCCP perspective. R-454B can be analyzed using the same approach.

Table 4-4 R-466A Refrigerant Manufacturing Process Emission Effect

(kg CO_2e)	Assumption 1			Assumption 2			Assumption 3		
City	RFM	LCCP	Percentage	RFM	LCCP	Percentage	RFM	LCCP	Percentage
Beijing, CN	31	94164	0.03%	62	94195	0.07%	124	94257	0.13%
Shanghai, CN	31	69482	0.04%	62	69513	0.09%	124	69575	0.18%
Tokyo, JP	31	61524	0.05%	62	61555	0.10%	124	61617	0.20%
Kallax, SE	31	4246	0.73%	62	4277	1.45%	124	4339	2.85%
Basel, CH	31	4314	0.72%	62	4345	1.42%	124	4407	2.81%
London, UK	31	61524	0.05%	62	61555	0.10%	124	61617	0.20%
Atlanta, US	31	61518	0.05%	62	61549	0.10%	124	61610	0.20%
College Park, US	31	70087	0.04%	62	70118	0.09%	124	70180	0.18%
Miami, US	34	98865	0.03%	69	98899	0.07%	138	98968	0.14%
Phoenix, US	34	91276	0.04%	69	91311	0.08%	138	91379	0.15%

4.1.5. Weather Data Source and LCCP

I compared the LCCP results using weather data from the UMCP campus field tests and the local airport weather station. Figure 4-8 shows the results. From Figure 4-8, the UMCP campus ambient temperature was always higher than that from the College Park

airport due to the UHI effect. This brings a higher emission in the summer but a lower emission in the winter. Figure 4-8 shows that the decrease in heating is smaller than the increase in cooling. This brings a total increase in the final LCCP result. Compared with the airport data, the LCCP results using the campus data are up 8.1%, 2.4%, 2.8%, and 0.6% for R-454B, R-32, R-410A, and R-290, respectively. This result means that using local airport weather data can result in an up to 8% decrease for LCCP calculation. If onsite ambient data is not available, a correction on the ambient temperature is recommended.

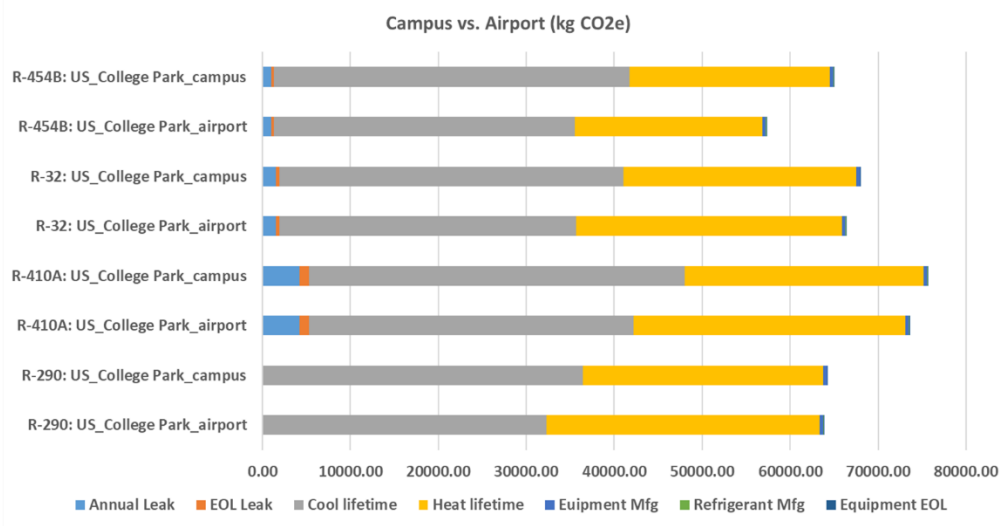

Figure 4-8 Comparison of LCCPs based on Weather Data from UMCP Campus and College Park Airport

4.1.6. Summary

A comprehensive LCCP assessment was conducted for a 10.5 kW capacity unitary heat pump working in cooling mode with five refrigerants using various influencing parameters in 11 cities. The conclusions from the study are as follows:

1) The system efficiency has a 10 to 100 times greater impact on HVAC system's emissions than refrigerant leakage only in higher GEEF countries. For lower

GEEF countries like Sweden and Switzerland, annual leakage is the major factor.

2) The refrigerant manufacturing process, which takes up to 3% in LCCP emissions, is a minor factor compared with emissions from annual energy consumption and annual leakage. While no data was reported on the emissions from the R-466A manufacturing phase, the LCCP can still be estimated by assuming equivalent values to typical HFC value.
3) R-290, R-32, R-452B, R-454B, and R-466A are all excellent alternatives for R-410A. The LCCPs of R-32, R-452B, R-454B, and R-466A are close to each other. The LCCP of R-410A is the highest, while the LCCP of R-290 is the lowest. In the low-GEEF countries, the LCCP can be decreased by 60% by substituting R-410A with R-290.
4) The ambient temperature weather data from the UMCP campus field test and College Park airport weather station are different up to 5 °C, possibly due to the UHI effect. This effect can cause up to an 8% difference in LCCP calculation. Thus, researchers are suggested to carefully consider the ambient temperature when conducting LCCP calculations for high-population-density regions. Some correction factors could be needed if the weather station database and local ambient temperature show measurable differences.

4.2. Enhanced LCCP Evaluation

The environmental performance of HP systems has been widely studied. Several hot topics exist. First, several studies discussed the breakdown of total LCCP (Lee et al., 2016; Li, 2015b; Yang et al., 2021). Second, some scholars pointed out the current

challenge of LCCP calculation (Andersen et al., 2018; Li, 2017). Finally, different studies may also use LCCP for different purposes (Fricke et al., 2017; Troch, 2016). In Figure 1-11, I summarized several factors for LCCP evaluation, including refrigerant effects, energy consumption, and material embodied emissions. This chapter discusses how to consider these factors in LCCP calculation using realistic assumptions. In addition, green power impact and data limitation will also be discussed.

4.2.1. Refrigerants Effects

The refrigerants used in ACs have evolved over several decades from ozone-depleting R-22 GHG to chlorine-free/ozone-safe hydrofluorocarbon (HFC) R-410A GHG and now to lower GWP R-32. The U.S. Environmental Protection Agency (EPA) reported that current HP systems using HFC-410A still contribute 36.7 million metric tons of carbon dioxide equivalent (EPA, 2015). Selecting an appropriate refrigerant for the HP system is a trade-off involving heat transfer characteristics, compressor efficiency, flammability, and cost (Gilmour and McNally, 2010). LCCP provides a tool for selecting alternative working fluids that reduce GHG emissions from HP systems.

Since limited nations use R-22 nowadays, this review used R-410A as the baseline. I discussed several replacements for R-410A based on ASHARE Standard 34 (2019) for refrigerant safety, namely A1, A2L, A3, and B groups. Table 4-5 shows some common refrigerants and their properties. The refrigerant leakage, emissions associated with the refrigerant manufacture phase, and emissions due to disposal of the refrigerant can affect LCCP calculation.

Table 4-5 Refrigerants of Interests

ASHRAE safety classification	Refrigerant	GWP (kg CO_{2e}/kg)	Adp.GWP (kg CO_{2e}/kg)	Concerns	Introduced Year	Reference
A1	R-410A	2,088	-	High GWP	Honeywell, 1991	Goto et al., 2001; Wang et al., 2009
A1	R-466A	730	-	High cost	Honeywell, 2018	Cooling Post, 2018a, 2018b; Devecioğlu and Oruç, 2020
A1	R-1234yf	< 1	3.3	Low pressure	DuPont, 2011	Baral et al., 2013; Myhre et al., 2014
A1	R-134a	1,300	1.6	High GWP	DuPont, 1930	Baral et al., 2013; Myhre et al., 2014
A1	R-404A	3,943	-	High GWP	-	ASHRAE Standards, 2019
A1	R-22	1,760	-	High GWP Mild ODP	General Motors, 1928	ASHRAE Standards, 2019
A2L	R-32	675	-	Mildly Flammable	Japan Ministry of Economy, Trade, and Industry (METI), 2011	Mota-Babiloni et al., 2017; Pham and Rajendran, 2012; Xu et al., 2013
A2L	R-452B	676	-	Mildly Flammable	Ingersoll Rand, 2015	Kedzierski and Kang, 2016; Kujak et al., 2014
A2L	R-454B	466	-	Mildly Flammable	Carrier, 2018	Devecioğlu and Oruç, 2020
A3	R-290	<1	-	Highly Flammable	-	Wu et al., 2012

Refrigerants Leakage

The main factors that affect direct emissions are the annual leakage rate (ALR) of the refrigerant, the GWP of the refrigerant, and the GWP of the Atmospheric Degradation Product of the Refrigerant. Direct emissions are the refrigerant emissions during the usage phase and End Of Life (EOL) phase. By expanding the terms in eq. (3), direct emissions can be calculated by eq. (68):

$$E_{direct} = C \times (L \times ALR + EOL) \times (GWP + Adp.GWP) \quad (68)$$

where C means refrigerant charge (kg); L means average life of the equipment (yr); ALR means annual leakage rate (percentage of refrigerant charge); EOL means End of Life refrigerant leakage (percentage of refrigerant charge); GWP means Global Warming Potential (kg CO_{2e}/kg); Adp.GWP means GWP of Atmospheric Degradation Products of the Refrigerant (kg CO_{2e}/kg). GWP and Adp.GWP were widely reported

in the literature (Bobbo et al., 2018). C is usually marked on the HP system's label. C could also be reached directly by using simulation methods.

Global Warming Potential

Global Warming Potential (GWP) of a refrigerant is an index to compare the relative radiative forcing of different gases relative to the reference gas CO_2, which is set equal to 1. A significant number of researchers studied the refrigerants' GWP (Bobbo et al., 2018; Lin and Kedzierski, 2019). However, Adp.GWP was rarely mentioned. Though previous research all pointed out Adp.GWP needed to be considered in LCCP calculation (Yang et al., 2021; Andersen et al., 2018; Choi et al., 2017), only Baral et al. reported the Adp.GWP values for R1234yf and R134a (Baral et al., 2013). Yang et al. (Yang et al., 2021) used 0 for R-410A and R-32 but didn't mention the reference or reason. Thus, more work is needed to perfect Adp.GWP values.

Unit Lifespans, Annual Leakage Rate, and EOL Leakage Rate

The most accurate values for L, EOL, and ALR in stationary applications can often be obtained from the manufactures. Average unit lifetimes could be taken from AR4, AR5 reports, or from the United Nation, Environmental Program (UNEP) Montreal Protocol Refrigeration, Air Conditioning and Heat Pumps Technical Options Committee (RTOC) 2002 report (Troch, 2016). The U.S. limits the amount of refrigerant released from an appliance to 15% for units with a charge of 22.7 kg (Troch, 2016). Troch summarized the recommended value for ALR, EOL, and L for different types of HP systems (Troch, 2016). Table 4-6 shows these values for stationary applications. It is worth noting that SAE International Standard J-2727 prescribes a method to estimate the leak rate based on a standard configuration and taking into account fittings, seals, and refrigeration

permeation of flexible hoses for mobile air conditioning systems (SAE International, 2012).

Table 4-6 Recommended ALR, EOL, and L Values (Troch, 2016)

System Type	ALR (%)	EOL (%)	L (yr)
Residential Packaged HP Units	2.5	15	15
Residential Split HP Units	4	15	15
Packaged Refrigeration System	2	15	15
Supermarket Direct HP System	18	10	7-10
Supermarket Indirect HP System	12	10	7-10
Commercial Refrigeration System	5	15	15
Commercial Packaged HP Units	5	15	10
Commercial Split HP Units	5	15	10
Chillers	5	15	15
Marine	20	15	15

Refrigerants Manufacturing

Refrigerant leakage contributes to direct emissions, while the refrigerant manufacturing phase and refrigerant disposal phase is related to indirect emissions from the energy used to recover, transport, and recycle or destroy the refrigerant. The leakage in these two phases is counted in the leakage calculation in chapter 3.2. The emissions I discussed here are from the energy usage in these two phases. The $E_{ref,man}$ can be calculated by:

$$E_{ref,man} = C \times (1 + L \times ALR) \times (1 - R) \times RFM \quad (69)$$

where RFM means refrigerant manufacturing emission (kg CO_{2e}/kg); R means the fraction of the refrigerant in the system, which is reclaimed refrigerant. Refrigerant manufacturing emissions rates are shown in Table 4-7 for selected refrigerants. They will be updated as more efficient methods of manufacturing are developed. So far, the

manufacturing emissions for R-466A and R-454B have not been reported. As we proved in chapter 4.1.4, appropriate assumptions could be used as substitutions.

Table 4-7 Refrigerant Manufacturing Emission of Refrigerants of Interests

Refrigerant	RFM (kg CO_2e/kg)	Reference
R-410A	10.7	Spatz and Motta, 2004
R-466A	n/a	n/a
R-32	7.2	Spatz and Motta, 2004
R-452B	8.9	Troch, 2016
R-454B	n/a	n/a
R-290	0.05	Hill and Papasavva, 2005
R-1234yf	13.7	Hill and Papasavva, 2005
R-134a	5	Banks and Sharratt, 1996
R-404A	16.7	Papasavva et al., 2010
R-22	390	Chen, 2008

Refrigerant Disposal

Similar to chapter 3.3, $E_{ref,EOL}$ can be calculated by eq. (70):

$$E_{ref,EOL} = C \times (1 - EOL) \times RFD \quad (70)$$

where RFD means refrigerant disposal emissions (kg CO_{2e}/kg). This process also includes the recovery of the refrigerant. Though RFM values were widely reported, nearly no study reported RFD values. This may explain why almost all the literature mentioned emissions from the refrigerant disposal phase but not counted in their calculation.

Summary

The refrigerant environmental impact has been widely studied. The current challenge is data limitation. First, the Adp.GWP values were rarely mentioned. Second, for the emissions caused by the refrigerant manufacture, the RFM values for novel refrigerants like R-466A were seldom reported. Third, many researchers noted the emissions during

the refrigerant disposal or recycling process. However, only GREEN-MAC-LCCP adds the refrigerant disposal emissions in the LCCP calculation (Rhoads, 2020).

4.2.2. Energy Consumption

Eq. (71) shows a commonly used approach to estimate emissions from energy consumption:

$$E_{Energy} = L \times AEC \times EM \tag{71}$$

where AEC means Annual Energy Consumption. EM means CO_2 produced/kWh (kg CO_{2e}/kWh), which is the grid electricity emission factor (GEEF) if electricity is the only energy source. The central part of AEC consists of the cooling power consumption and heating power consumption of the target system throughout the year. Field tests and energy surveys could help determine the HP system's annual energy consumption in real-life applications. However, the field test would not always be available. One need to know the room's load and the system performance at a given ambient temperature to estimate power consumption. As for indirect emissions, AEC would show large differences in different climate regions for the same system (Choi et al., 2017). This was reported to be the most significant part of the LCCP calculation (Li, 2015b). AEC was usually estimated from the simulation result using EnergyPlus or other software (Hong et al., 2016b; Li, 2015b). AHRI 210/240 2017 also provided a method to estimate the AEC of UAC (Alabdulkarem et al., 2014). Furthermore, the energy consumption and emissions depend on the time-of-day incremental carbon intensity of electricity as delivered to the equipment after taking into account the effects

of ambient temperature and grid capacity on electricity generation, transmission and distribution (Andersen et al., 2018).

Load Prediction

As we mentioned in chapter 4.1.1, AHRI Standard 210/240 (2017) provides the "temperature bin method" to estimate the load, power consumption, and energy efficiency. However, this approach is only applicable to a fixed-speed system. If the system had a variable speed compressor, the compressor frequency's control logic would affect the result. ASHRAE Handbook (2001), chapter 28, provides a detailed process to calculate the load using a physics-based method. With the development of data-driven approaches, some researchers also use machine-learning-based methods for load forecasting.

Temperature Bin Method

To calculate the thermal load using the temperature bin method, Troch et al. (2016) and Lee et al. (2016) gave a clear description in their papers. Engaging readers can also use AHRI 210/240 (Standards, 2017) as references. The temperature bin definition is different in different regions. China (GB 21455-2019), Japan (JIS C 9612:2013), and EU (NO 206/2012) use an interval of 1 ℃ for each temperature bin. However, U.S. (AHRI Standard 210/240-2017) uses an interval of around 2.7 °C (5 °F). Figure 4-9 shows a comparison of the bin temperature used in different countries. The weather data was from the NOAA Integrated Surface Database (ISD) (Smith et al., 2011). Many countries in Europe and elsewhere have relatively lower temperatures in the cooling season. Thus, the lowest bin temperature for Europe (17 °C) is 5 °C lower than that for

China and Japan (24 °C). Similarly, very hot climates require consideration of even higher bin temperatures and consideration of global warming from rapidly increasing greenhouse gas concentrations in the atmosphere. When conducting the LCCP calculation, using different temperature bins will bring different results.

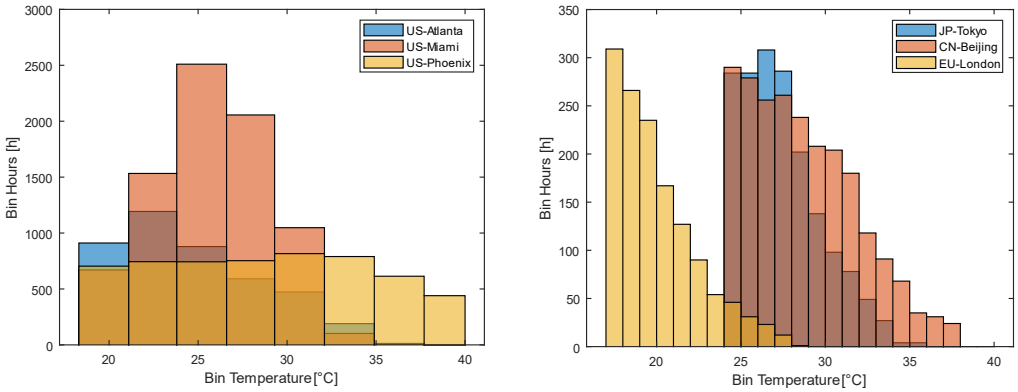

(a) US (b) China, Japan, and EU

Figure 4-9 Bin Hours Distributions

Different countries use different standards, which define different temperature bins. The energy efficiency metrics are also different. Seasonal Energy Efficiency Ratio (SEER) and Cooling Seasonal Performance Factor (CSPF) are used for cooling, while the Heating Seasonal Performance Factor (HSPF) and Seasonal COP (SCOP) are used for heating. Annual Performance Factor (APF) is used for the whole year. These metrics are summarized in Table 1-1.

Simulation-based Method

As the weather data is available, I can use a physics-based method to simulate the target building's load of a room that follows the ASHRAE Standard 34 (2019). This method is able to control the variables, like the regions and refrigerants. As the application, Wijeysundera (2015) developed models in MATLAB to estimate the cooling and

heating load of the target room. The new challenge is to accurately adjust ambient weather data collected at locations unaffected by human activity to account for urban heat islands and clustering and stacking of the outside heat exchangers that can drastically impact both heating and cooling efficiency.

Data-driven Method

As NN-based techniques develop, a data-driven method is widely used to predict the building load. Zhao and Magoules (2012) reviewed the papers using Neural Networks and Support Vector Machines in building energy prediction. Kadir and Nora (2018) studied 78 different prediction models for different types of buildings and summarized eight other metrics to evaluate the models' performance. The benefit of the data-driven method is that the process is straightforward and requires fewer labor efforts. However, the data-driven approach requires a large amount of data to guarantee the quality of the model results. Plus, the model built for one building design is usually unable to predict the performance for other, significantly different building designs.

Grid Effect

In the previous studies (Choi et al., 2017; Lee et al., 2016; Yang et al., 2021), the AEC was only calculated from HP systems, and EM was considered as a constant. With this assumption, the emissions due to electricity generation are a dominant factor in the LCCP calculation. Different regions have various power plant emission factors due to the resource portion difference (Choi et al., 2017). Carbon Footprint summarizes the country-specific GEEF in June 2019 (Carbon Footprint, 2019). Table 4-3 shows the grid electricity emission factors. The data for Asian countries is from G20 Green Report

2018 (Transparency, 2018), for European countries is from the Association of Issuing Bodies (AIB, 2019), and for the U.S. is from the Environment Protect Agency database (U.S. EPA, 2020).

However, more realistic assumptions related to the grid are required, including local seasonal and time-of-day carbon intensity of electricity sources (Khan, 2018), electricity transmission and distribution losses (Sadovskaia et al., 2019), energy embodied in water used for power plant cooling (Torcellini et al., 2003), and black-and-brown carbon power plant emissions (Jacobson, 2014). It is vital to use incremental carbon intensity of electricity, mindful that dispatching is usually based on cost considerations that can ignore the carbon footprint implications. Plus, promoting the development and utilization of renewable energy is the current trend globally (Xu et al., 2019). LCCP could be different depending on the power mix ratio.

Time-variation Carbon Intensity

Though previous research treated EM as a constant, this value was reported to have a 15% deviation throughout a year in Bangladesh (Khan, 2018). The reason is that each energy source can have different greenhouse gas emissions and with variation from ambient temperature, capacity factor, and availability of thermal power plant cooling. If the data from the local power supplier is available, using this data is the first choice. Khan et al. (2017) proposed a method to calculate a time-vary carbon intensity. This approach was based on each country's GHG inventory. However, this approach was very complicated since hundreds of categories were involved in the GHG inventory (Eggleston et al., 2006). Coskun et al. (2019) used a simpler method, only considering

14 major categories like natural gas and coal. This is a more practical method for HP LCCP evaluation. Besides the impact of energy source components, ambient conditions were reported to affect the power plant carbon emissions as well (Arrieta and Lora, 2005; Kehlhofer et al., 2009). González-Díaz et al. (2017) summarized correction curves for power plant carbon emissions prediction under different ambient temperatures.

Electricity Transmission, Distribution, and Transformer Losses

Transmission, distribution, and transformer grid losses typically account for about 4–15% of grid generation (Saminathan et al., 2016), with higher losses at high ambient temperatures when the equipment is operating at maximum capacity (minimum efficiency) and more power is required to cool transformers. Thus, these losses are unignorable in LCCP calculations. Technical power losses can be divided into two main categories: power line losses (Amemiya et al., 2011) and transformer losses (Lakervi and Holmes, 1995). Poveda (1999) presented a method to break down, by subsystem and cause, power distribution losses in electrical systems. Nadira et al. (2003) proposed an approach to compute distribution losses without the complete set of data. Sadovskaia et al. (2019) created a holistic and analytic function for describing the transmission and distribution grid power loss for all countries globally based on economic, geographical, political, and technical available data.

Energy Embodied in Cooling Water

Water abstractions from the natural environment often achieve the cooling of thermoelectric plants. In industrialized countries, the electricity sector abstractions can

be 40% from freshwater sources (Pan et al., 2012). Thus, the carbon emission from water consumption is unignorable. Byers et al. (2014) built a model and predicted the 'carbon dioxide intensity' ($MTCO_2$/TWh) for water consumption of the six pathways averaged over the grid's full capacity in the UK from 2010 to 2050. Lohrmann et al. (2019) used satellite imagery to calculate the cooling water consumption around the world. Furthermore, consider that in the future, there may not be enough water for power plant cooling during high ambient temperatures when people and agricultural and urban landscapes also need more water.

Renewable Energy as Power Sources

Promoting the development and utilization of renewable energy has become a common consensus (Xu et al., 2019). This effect outperforms the power mix ratio and brings lower EM. Thus, the LCCP would be lower as the source of electricity became "greener". I can achieve several power mix scenarios with current and future power mix ratios according to EIA's projections (U.S. EIA, 2021). In Table 4-8, the ratio of renewable energy in the residential sector in the U.S. is expected to increase from 20% to 41% in the next thirty years.

Table 4-8 Percentage of Material Use

Author	Systems	Steel	Aluminum	Copper	Plastic
Yang et al., 2021, Troch, 2016	Residential Heat Pump	46%	12%	19%	23%
Fricke et al., 2017	Supermarket Refrigeration System	10%	55%	30%	5%

The last column of Table 4-8 shows the average EM for each source from the literature (Amponsah et al., 2014; Lenzen, 2008; U.S. EPA, 2020). I can simulate the equivalent

EM value for each year by calculating the weighted mean using the ratios as weights. The last row in Table 4-8 shows the result. Due to the renewable energy ratio increase, carbon emissions from energy consumption are expected to decrease by 26% in 2050.

Summary

Almost all the past studies assumed the energy source was electricity. However, natural gas and petroleum fossil fuels are also used in HP systems. Thus, more research on non-electric HP system environment performance needs further study. Different countries could show more than 100 times the difference for EM (Ryan et al., 2016). However, limited studies show a specific dataset for these values. Unique calculation methods are also required for district heating and cooling with and without electricity co-generation and waste heat utilization. For example, in colder climates where heat is rejected from supermarket food, refrigeration is used to heat occupied spaces or anywhere both sides of a heat pump are put to a useful purpose or where other co-benefits are captured. Examples include vending machines with both hot and cold drinks, heat pump condensing clothes dryers with water recovery, and air conditioners that provide the desired level of comfort at high ambient temperature by intentional control of humidity and air movement.

It is well known that energy consumption is the main contributor to the carbon footprint of refrigeration and air conditioning equipment, but this can be evaluated very differently depending on how "green" the electricity is defined. This effect outperforms everything else. I can simulate the power emission factors according to several power

mix scenarios like the current power mix ratio and future power mix ratio according to EIA's projections. This will be valuable information to HP society. For electric HP systems, I recommend an updated approach to calculate emissions caused by energy consumption given by eq. (72):

$$E_{Energy} = L \times \sum_{i=1}^{8760} (EC_i \times EM_i) = L \times \sum_{i=1}^{8760} [(C_i + C_{trans} + C_{water}) \times EM_0 \times p(t_i)] \quad (72)$$

where i stands for the hour in one year; EC_i is the energy consumption in hour i; EM_i is the emission factor in hour i; C_i is the electrical energy consumption in hour i; C_{trans} is the energy loss during transmission and transform process; C_{water} is the energy embodied in the power plant cooling water; EM_0 is the local nominal grid emission factor; p is the penalty factor for time-vary carbon intensity, which is a function of the ambient temperature.

4.2.3. Material Embodied Emissions

The carbon emissions due to the material used in the HP system are another factor that may affect the LCCP calculation. Different systems have different percentages of material usage. In the previous LCCP studies, most researchers used the detailed calculation method. Most LCCP studies calculate the carbon emissions from the system manufacture phase and the EOL phase. Another approach is searching the Embodied Carbon Coefficients (ECC) database directly.

Percentage of Material Usage

Four materials, including steel, aluminum, copper, and plastic, were discussed in previous research. The percentage of composition data was limited due to confidential

reasons. Studies rarely elaborated the data they used. Plus, some researchers applied the same composition data for different types of systems (Fricke et al., 2017). Table 4-3 shows the information in the open literature. According to some studies (Lee et al., 2016), the material embodied emissions only take 1% of the total LCCP. Thus, it's reasonable to estimate values if the composition data is not available. However, for a more accurate calculation, the information still needs to be achieved from the manufacture. The emissions embodied in materials may be more important as composite plastics replace metal or as battery storage becomes part of equipment design (to level peak power).

Detailed Calculation

The carbon emissions due to the material used can be calculated by adding the emissions from the system manufacture phase and EOL phase. These emissions can be calculated by eq.73 and eq.74:

$$E_{sys,man} = \sum (m \times MM) \tag{73}$$

$$E_{sys,EOL} = \sum (mr \times RM) \tag{74}$$

where m means the mass of unit (kg); MM means CO_2 Produced/Material (kg CO_{2e}/kg), which is also known as ECC; mr means the mass of recycling material (kg); RM means CO_2 produced/ recycled material (kg CO_{2e}/kg);

In many cases, recycled materials are used for economic and environmental reasons in the manufacture of HP units rather than pure virgin materials (Troch, 2016). Most recycled materials require considerably less energy to manufacture (Troch, 2016).

Many materials today are manufactured with a mixture of virgin and recycled materials. The average values of virgin materials and recycled materials were usually used in LCCP calculation. Material disposal emissions include all emissions up to the production of recycled material. For metals and plastics, this consists of the shredding of the material (Zhang et al., 2011). These emissions may be included in the manufacturing emissions if the material is produced from recycled materials. A public records search was conducted to determine the amounts of emissions were generated by shredding metals and plastics.

However, some drawbacks exist. First, this method ignored the emissions from the material transportation and installation phase. Second, some previous studies used the same emissions values for the material in every country. For example, Choi et al. (2017) used the IIR guideline to estimate Korea's LCCP. However, IIR only provides the recommended values in the U.S. According to some studies, MM values could show 50% differences in different regions (Ibn-Mohammed et al., 2013).

Searching Database

Some researchers working on LCA of buildings have developed a database for different material's Embodied Carbon Coefficients (ECC) in different countries (Vilches et al., 2017). Table 4-3 shows the virgin ECCs for the four material Inventory of Carbon & Energy database developed by Hammond et al. (2011). If the recycled material is used, the recycled material database needs to be used. The data is missing for some material in some regions. The average value around the world can be used for substitution. As I can find in Table 4-3, the ECC for Aluminum in the U.S. is around one-third of China's

value. Thus, ECCs could be a crucial factor in the LCCP calculation for different countries.

Summary

The biggest challenge to estimate the material embodied emissions is the data limitation. Since this part takes 0.1%-1% of the total LCCP (Troch, 2016), some estimation could be used if data is not available. Researchers working on buildings or other products have developed an ECC database. This is a simple approach to calculate the system material embodied emissions.

4.2.4. Green Power Impact

According to the previous studies, emissions due to energy consumption are a major part of an HP system's total emissions. Many researchers concluded that the emissions caused by cooling and heating represent around 70%-80% in the total LCCP calculation (Lee et al., 2016; Li, 2015b; Yang et al., 2021). Direct emissions caused by refrigerant leakage represent around 1%-10%, depending on what kind of refrigerants are used (Lee et al., 2016; Yang et al., 2021). Material-embodied emissions only represent around 1%-5% (Choi et al., 2017; Lee et al., 2016; Zhang and Muehlbauer, 2012). However, these conclusions cannot be generalized for all regions. Nearly all of the LCCP studies were conducted in the U.S., Korea, and China. These regions have a relatively high GEEF in Table 4-3. This can lead to the result that energy consumption is more important than the other two emission parts. For some European countries like Sweden, the GEEF is only 1/40 of the GEEF of the U.S. This will make the emissions caused by energy consumption in Sweden decreased by 40 times, with the result that

direct emissions become the crucial part of total emissions. Promoting the development and utilization of renewable energy has become widely accepted (Xu et al., 2019). Clean renewable energy such as hydroelectric, solar, and wind outperforms the power mix ratio and brings lower EM for the regions with high GEEF values. The LCCP would be lower as the source of electricity becomes "greener." I can achieve several power mix scenarios with current and future power mix ratios according to EIA's projections (U.S. EIA, 2021).

In Table 4-9, the ratio of renewable energy in the residential sector in the U.S. is expected to increase from 20% to 41% in the next thirty years.

Table 4-9 U.S. Residential Energy Structure and Carbon Intensity Projections

		Projections of Residential Grid Sources in U.S. [-] (U.S. EIA, 2021)							EM [kg CO_2e/kWh]
Year		2020	2025	2030	2035	2040	2045	2050	
Renewable Energy (Amponsah et al., 2014)	Hydro	8%	7%	7%	7%	7%	6%	6%	0.004
	Geothermal	0%	0%	1%	1%	1%	1%	1%	0.045
	Waste treatment	0%	1%	1%	1%	1%	1%	1%	0.200
	Dedicated biomass	1%	1%	1%	1%	1%	1%	0%	0.025
	Solar thermal	0%	0%	0%	0%	0%	0%	0%	0.075
	Photovoltaic	2%	6%	10%	12%	14%	15%	17%	0.046
	Wind-onshore	9%	16%	16%	15%	15%	15%	14%	0.020
	Wind-offshore	0%	0%	1%	2%	2%	2%	2%	0.010
Fossil Fuel (U.S. EPA, 2020)	Coal	20%	17%	17%	15%	14%	13%	12%	0.991
	Petroleum	0%	0%	0%	0%	0%	0%	0%	0.717
	Natural gas	37%	33%	32%	31%	33%	34%	34%	0.405
Nuclear Power (Lenzen, 2008)		21%	19%	16%	15%	14%	13%	12%	0.065
Equivalent EM [kg CO_2e/kWh]									
Year		2020	2025	2030	2035	2040	2045	2050	
Values		0.375	0.327	0.317	0.300	0.291	0.283	0.277	

The last column of Table 4-9 shows the average EM for each source from the literature (Amponsah et al., 2014; Lenzen, 2008; U.S. EPA, 2020). I can simulate the equivalent EM value for each year by calculating the weighted mean using the ratios as weights. The last row in Table 4-9 shows the result. Due to the renewable energy ratio increase, carbon emissions from residential energy consumption in the U.S. are expected to decrease by 26% in 2050.

Table 4-10 Grid Electricity Emission Factor Sensitivity Analysis

Location	Phoenix, AZ						
Year	2020	2025	2030	2035	2040	2045	2050
GEEF (kg CO_2e/kWh)	0.375	0.327	0.317	0.300	0.291	0.283	0.277
Total Lifetime Emission (kg CO_2e)	60,265	53,003	51,490	48,918	47,557	46,346	45,439
Total Direct Emission (kg CO_2e)	3,047	3,047	3,047	3,047	3,047	3,047	3,047
Annual Refrigerant Leakage (kg CO_2e)	2,437	2,437	2,437	2,437	2,437	2,437	2,437
EOL Refrigerant Leakage (kg CO_2e)	609	609	609	609	609	609	609
Total Indirect Emissions (kg CO_2e)	57,219	49,957	48,444	45,872	44,510	43,300	42,392
Energy Consumption (kg CO_2e)	56,735	49,473	47,960	45,388	44,026	42,816	41,908
Equipment Manufacturing (kg CO_2e)	409	409	409	409	409	409	409
Equipment EOL (kg CO_2e)	6	6	6	6	6	6	6
Refrigerant Manufacturing (kg CO_2e)	69	69	69	69	69	69	69

A sensitivity analysis for these different GEEF values is shown in Table 4-10. The 10-kW unitary system performance and Phoenix weather data reported in chapter 4.1 were used as the baseline. As shown, indirect energy emissions become less important as fossil fuels are phased out from power generation, and electricity is supplied entirely from low-carbon sources like hydro, nuclear, solar, and wind sources from 2020 to 2050. The corresponding LCCP value will decrease by 25% for this unitary system in

Phoenix till 2050. However, keep in mind that the incremental carbon intensity of electricity will be from the fossil fuel and biomass plants whenever they are operating in otherwise clean energy electric utilities.

4.2.5. Data Limitation

Data limitation is the main challenge in LCCP calculations. The data include real, local ambient temperature data, local power plant carbon intensity data, and percentage of material usage data. Though each of these factors alone wouldn't affect the LCCP result too much, the result could be different if multiple conditions were estimated. One possible solution is using the prediction method (Amasyali and El-Gohary, 2018). A correlation could be developed using data from monitored buildings to calibrate the prediction model. Then, for the case without available data, such correlation can be used for prediction. An example is a data-driven method I introduce in chapter 2.3.1. Plus, some systems were rarely mentioned in previous publications, which also had the data-limitation challenge. For example, the variable speed system applied different control logics to the compressor and fan speed (Cheung and Braun, 2014). Nevertheless, no study reported how to evaluate this effect in LCCP calculation uniformly.

4.2.6. Summary

The invention and evolution of LCCP have been reviewed in this study first. Then, I discuss the application of LCCP to select replacements of HFC-134a. In addition, I compared the conceptual frameworks and the operational estimation methods. Finally,

I summarized the drawbacks of current LCCP research and recommended ways to improve the calculations. The conclusions are listed below:

1) Energy consumption caused emissions are a significant part (70%-80%) of total LCCP calculation. However, current studies are not perfect on these calculations. Non-electric HP system was rarely studied before. Plus, almost all the literature discussed only one region. Limited studies compared multiple regions with different standards and grid effects.
2) The emissions from the refrigerant manufacture phase, which takes up to 1%-5% in LCCP emissions, are a minor factor compared with emissions from annual energy consumption and annual leakage. Thus, though no research reported the emissions from the R466A manufacturing phase, the LCCP can still be estimated with a general HFC value.
3) The data limitation is the current major challenge in LCCP calculation. Realistic assumptions could lead to an accurate result, but the data is usually unavailable. Appropriate estimation values could be used when they are reasonable for given purposes.
4) LCCP could be used for multiple purposes. Thus, the assumptions could be made depending on the application conditions. For the purpose of selecting refrigerants, the percentage of material use values and ECC values could be used approximation, but if the purpose is to use LCCP design or optimizing system, the percentage of material use values and ECC values need to be careful.

4.3. Summary

The En-LCCP evaluation method is discussed in this chapter. I improved the current En-LCCP calculation by proposing a more detailed energy consumption model (as shown in eq.72) and providing substitutions for unachievable values (discussed in chapter 4.2.1, 4.2.3, and 4.2.5). The improved approach is closer to reality and can be used for HP using green power. Moreover, the improved method considering the data limitation problem, so it is able to analyze novel systems with limited open-source data (like systems using R-466A and R-454B).

Appropriate estimation values could be used when they are reasonable for given purposes. Figure 4-10 shows the improved process for the En-LCCP evaluation. Field tests and modeling results for the annual energy consumption can be used in the LCCP calculation. Emissions from the material and refrigerant manufacturing process only take up to 1-5% in LCCP and are a minor factor as compared to those from annual energy consumption and annual leakage. Thus, if the data related to the material embodied emissions or refrigerant manufacturing emissions is unavailable, the average value around the world could be used as a substitution. If the power source structure is known, the green power impact could be considered in the calculation. If the power source structure is unknown, the emission values from the local power supplier could be used as an approximation.

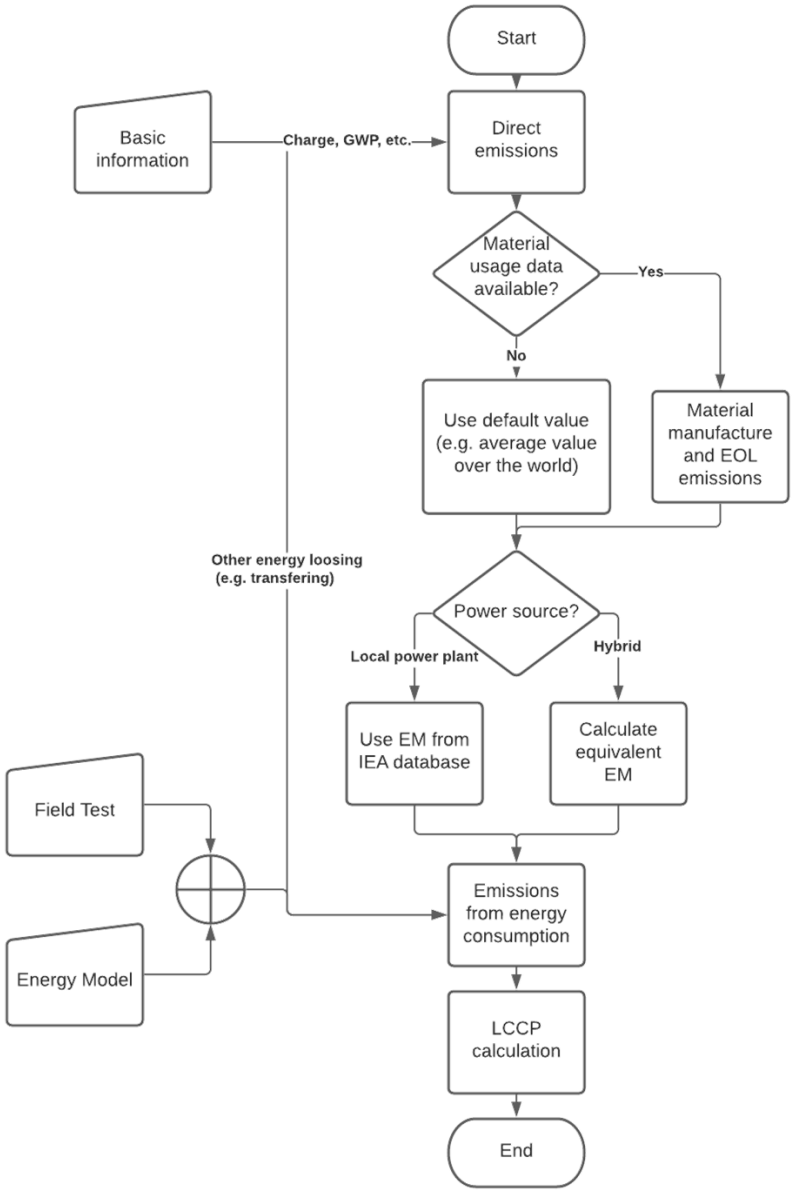

Figure 4-10 Flow Chart of En-LCCP Evaluation

5. Conclusions and Future Work

5.1. Conclusions

An experimental, emulational, and environmental (EEE) evaluation method is developed for HP systems in this dissertation. The whole process could be divided into three sub-modules: field test, modeling, and LCCP evaluation. The processes for the three sub-modules are provided in the summary parts from chapter 2 to chapter 4. By combining Figure 1-12, Figure 2-29, Figure 3-24, and Figure 4-10, the process of the next generation HP system evaluation method could be explained as shown in Figure 5-1.

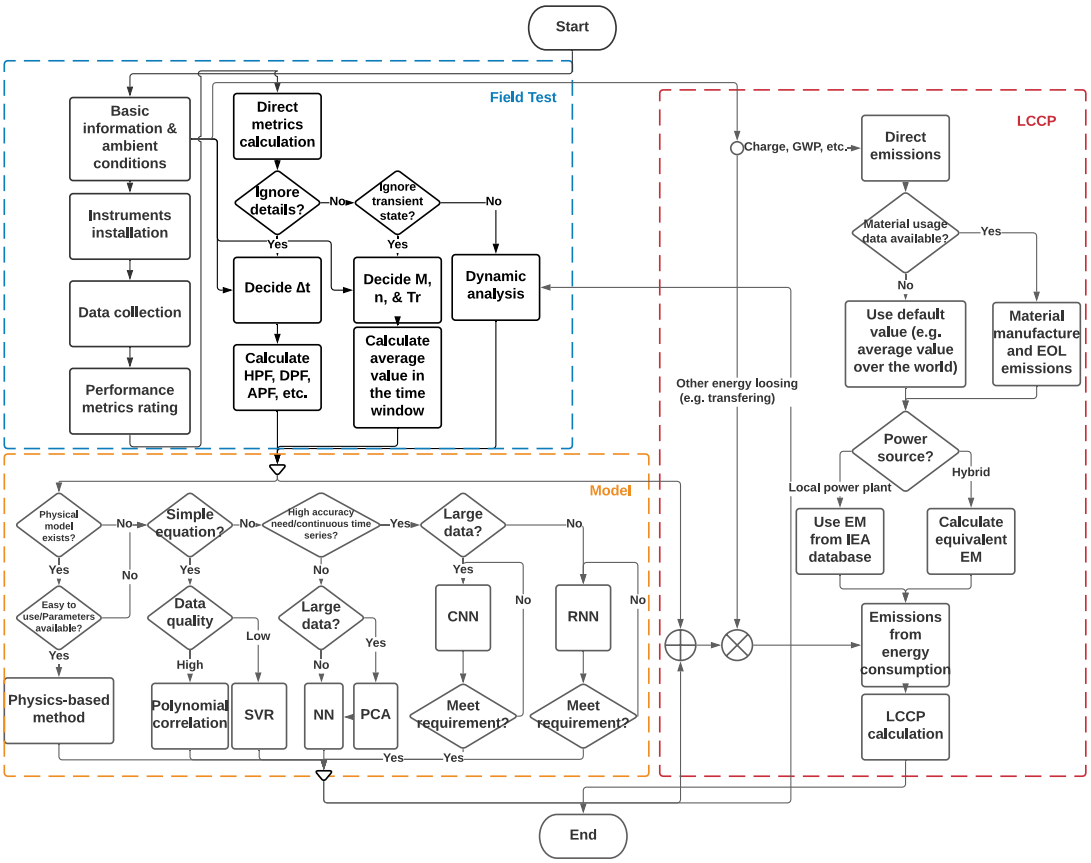

Figure 5-1 Flow Chart of the EEE Evaluation Method

The novel evaluation method can reflect the thermodynamic characteristics of the system by calculating QSS performance metrics and save time in extensive data calculation by calculating time-average performance. In addition, a database was developed for a VRF system over four years and the yearly performance was compared. Moreover, different modeling approaches were compared, and deep-learning-based algorithms were found to have higher accuracy than conventional modeling approaches and could be used to analyze the system's dynamic performance. However, the complicated structure of the networks, numerous parameters needing to be optimized, and longer training time are the main challenges of these methods. Furthermore, the new evaluation method improved the current En-LCCP calculation considering ambient conditions variation, local grid source structure, and next-generation low-GWP refrigerants, which led the LCCP results closer to reality and provided alternative methods for determining LCCP input parameters with limited-data cases. It was also able to analyze novel systems with limited open-source data (like systems using R-466A). The detailed conclusions are listed below:

For the field test and data analysis:

1. The first step for field test data analysis is the direct metrics calculation, including part load ratio, usage ratio, cooling combination ratio, operating unit ratio, etc. The next step is to decide whether the details could be ignored or not. If the study doesn’t care about the system performance details, the time-average performance metrics are recommended to be used. If the study needs some details of the system, for example, showing the cycle on the P-h diagram, then the QSS performance method is recommended to be used. The final step is to

check whether transient data analysis is needed. If the transient performance needs to be studied, some modeling tools might be needed for prediction.

2. QSS performance is compared with time-average performance. The moving window size, target function, and target threshold are the most important parameters for QSS performance. The Δt is the most significant parameter for time-average performance. The benefits of using the QSS metric include reflecting the heist performance of the system and reflecting the relationship among different tested parameters. In contrast, the benefits of using time-average performance are saving time when Δt is large and reflecting the transient phase performance to some extent.
3. Parameters setting could be made depending on the specific purpose and cost constraints. Choosing an appropriate method also needs to consider a lot of similar factors. Thus, the rule is not invariable. Changes could be made based on the accidental event in the field tests.

For the data-driven modeling:

4. Classification model of two controls was developed using PCA. First three dimensions can explain 98.7% of the data. Thus, only the first three dimensions need to be considered in the classification. The two groups of data for the two control modes are at different sides in the new space.
5. The total uncertainty of power consumption prediction was 0.7%. The condensing temperature, which also meant the high-side pressure, had the most critical impact on the outdoor power consumption when the frequency and outdoor fan speed were fixed.

6. The PCA-based NN regression method proposed is more practical and accurate for EEV correlation development than the conventional method when a number of data is available. Since no certain criteria in NN model parameter optimization exist, my work provides the following strategies in utilization NN modeling in EEV model development, which has not been discussed in previous NN EEV model works.
7. Compressor models were built by both manufactures' data and field test data. I compared different methods to build the models. First, '20-c' method has the best accuracy within the range of the training database, but when the frequency was low, this method fails to predict the MFR. In addition, 'eff' method reflects the physics best. Finally, ML methods have excellent performance if the prediction data point is within the training data set range. As for the uncertainty, the '20-c' and 'eff-20c' methods had lower uncertainty but sometimes failed to predict the accurate value. The NN and RF methods had higher accuracy but also higher uncertainty. As conclusion, I recommend the 'eff' method and SVR method for predicting the compressor mass flow rate of ductless VRF systems.
8. A CNN-based model for dynamic compressor model was developed. The current MRE for MFR prediction is 2%.
9. Overall, for the MFR prediction, physics-based and SVR-based methods are recommended with low uncertainty and high accuracy.
10. As for deep learning methods, CNN can be used to reduce input dimensions, while RNN has very high accuracy in predicting time-series data.

For the Enhanced-LCCP evaluation:

11. The system efficiency has a 10 to 100 times greater impact on HVAC system's emissions than the refrigerant leakage only in higher GEEF countries. For lower GEEF countries like Sweden and Switzerland, annual leakage is the major factor.
12. R-290, R-32, R-452B, R-454B, and R-466A are all excellent alternatives for R-410A. The LCCPs of R-32, R-452B, R-454B, and R-466A are close to each other. The LCCP of R-410A is the highest, while the LCCP of R-290 is the lowest. In the low-GEEF countries, the LCCP can be decreased by 60% by substituting R-410A with R-290.
13. The ambient temperature weather data from the UMCP campus field test and College Park airport weather station are different up to 5 °C, possibly due to the UHI effect. This effect can cause up to an 8% difference in LCCP calculation. Thus, researchers are suggested to carefully consider the ambient temperature when conducting the LCCP calculation for high-population-density regions. Some correction factors could be needed if the weather station database and local ambient temperature show measurable differences.
14. Energy consumption caused emissions are a significant part (70%-80%) of total LCCP calculation. However, current studies are not perfect on these calculations. Non-electric HP system was rarely studied before. Plus, almost all the literature discussed only one region. Limited studies compared multiple regions with different standards and grid effects.
15. The emissions from the refrigerant manufacturing phase, which takes up to 1%-5% in LCCP emissions, are a minor factor compared with emissions from

annual energy consumption and annual leakage. Thus, though no research reported the emissions from the R-466A and R-454B manufacturing phase, the LCCP can still be estimated with a general HFC value.

16. The data limitation is the current major challenge in LCCP calculation. Realistic assumptions could lead to an accurate result, but the data is usually unavailable. Appropriate estimation values could be used when they are reasonable for given purposes.
17. LCCP could be used for multiple purposes. Thus, the assumptions could be made depending on the application conditions. For the purpose of selecting refrigerants, the percentage of material use values and ECC values could be used approximation, but if the purpose is to use LCCP design or optimizing system, the percentage of material use values and ECC values need to be careful.

5.2. Future Work

As for possible future works, people can study the uncertainty within the deep learning networks and finding a general process for modeling settings. Since the uncertainty within the deep learning networks is still unknown, people can link the weights, bias, and activation functions with the physics background and try to explain the settings. People may apply the Bayesian-Neural-Network algorithm since this algorithm was reported for excellent performance on data with high uncertainty. For the environmental impact, people can develop a multi-objective optimization model for HP system design while considering both the LCCP and cost.

5.3. Contributions

5.3.1. List of Contributions

Contributions	Chapter in Dissertation	Publication
• Review current HP systems field tests, data analysis, and modeling methods	1.3.1-1.3.3	J2, C5
• Review Life Cycle Climate Performance works	1.3.4	J5
• Develop a ten-year field test database and dig information for large data sets	2.1.2	J7
• Compare time-average performance metrics with QSS performance metrics • Develop a general data analysis method for field tests data	2.1.3-2.1.5	J7
• Develop an online data monitoring system with low capital cost • Compare RACs performance with different installation and refrigerants	-	J6, C6
• Compare SNN, Multiple-time-step NN, and RNN in temperature data recovery	-	J6
• Develop a NN-based IDU MFR model • Develop an IDU MFR test method with one MFR meter installation • Compare NN model with polynomial regression	3.2.1	J1
• Develop machine-learning-based and deep-learning-based compressor models • Compare NN, RF, SVR, CNN, and polynomial regression methods	3.2.2, 3.2.3	C1, J3
• Develop an SVR-based energy model for VRF system	3.1.2	C2
• Compare LCCP of a UAC in different regions for different refrigerants	4.1	J4
• Improve current LCCP evaluation method with more realistic assumptions	4.2	J5
• Design and simulate a novel UAC using flammable refrigerants	-	C3, C4

5.3.2. List of Publications

Journal Publications

1. Wan H, Cao T, Hwang Y, et al. Machine-Learning-Based Compressor Models: A Case Study for Variable Refrigerant Flow Systems International Journal of Refrigeration [J]. International Journal of Refrigeration, 2021, 123: 23-33 https://doi.org/10.1016/j.ijrefrig.2020.12.003 (J1)
2. Wan H, Cao T, Hwang Y, et al. A review of recent advancements of variable refrigerant flow air-conditioning systems[J]. Applied Thermal Engineering, 2020, 169: 114893. https://doi.org/10.1016/j.ijrefrig.2019.08.018 (J2)
3. Wan H, Cao T, Hwang Y, et al. An electronic expansion valve modeling framework development using artificial neural network: A case study on VRF systems[J]. International Journal of Refrigeration, 2019, 107: 114-127. https://doi.org/10.1016/j.applthermaleng.2019.114893 (J3)
4. Wan H, Cao T, Hwang Y, et al. Comprehensive Investigations on Life Cycle Climate Performance of Unitary Air-Conditioners International Journal of Refrigeration [J]. https://doi.org/10.1016/j.ijrefrig.2021.04.033 (J4)
5. Wan H, Cao T, Hwang Y, et al. Life Cycle Climate Performance Analysis in Different Regions: A Review; International Journal of Refrigeration [J]. https://doi.org/10.1016/j.ijrefrig.2021.06.026 (J5)
6. Wan H, Cao T, Hwang Y, et al. Field Test and Life Cycle Climate Performance Comparisons in Marrakech; International Journal of Refrigeration [J]. (99%) (J6)

7. Wan H, Cao T, Hwang Y, et al. Variable Refrigerant Flow Systems Field Test Database Development; International Journal of Refrigeration [J]. (70%) (J7)

Conference Publications

1. Wan H, Cao T, Hwang Y, et al. Development of Dynamic Modeling Framework Using Convolution Neuron Network for Variable Refrigerant Flow Systems; Purdue Conference 2020, May 2021 (C1)
2. Wan H, Cao T, Hwang Y, et al. “Investigation of VRF System under Cooling Mode through Field Testing and Machine Learning-based Modeling.” 13th IEA Heat Pump Conference, Jeju, April 2021 (C2)
3. Wan H, Cao T, Hwang Y, et al. Dynamic performance comparison of three refrigerants in a novel unitary air condition system; 14th IIR-Gustav Lorentzen Conference, December 2020, http://dx.doi.org/10.18462/iir.gl.2020.1079 (C3)
4. Wan H, Cao T, Hwang Y, et al. "A Novel Unitary Air Condition System Design for Flammable Refrigerants and Building Ventilation." ICR 2019. Montreal, Canada. August 2019, https://doi.org/10.18462/iir.icr.2019.0565 (C4)
5. Wan H, Cao T, Hwang Y, et al. "A Review of Electronic Expansion Valve Correlations for Air-conditioning and Heat Pump Systems." Purdue Conference 2018. Illinois, U.S. July 2018 https://docs.lib.purdue.edu/iracc/1984/ (C5)

6. Hwang Y, Wan H. "R-32 Super-Efficient Room ACs Replacement Field Tests." ASHRAE Conference 2022 (99%) (C6)

Bibliography

AIB, 2019. European Residual Mix [WWW Document]. Association of Issuing Bodies. URL https://www.aib-net.org/facts/european-residual-mix (accessed 8.20.20).

Alabdulkarem, A., Eldeeb, R., Hwang, Y., Aute, V., Radermacher, R., 2015. Testing, simulation and soft-optimization of R410A low-GWP alternatives in heat pump system. International Journal of Refrigeration 60, 106–117.

Alabdulkarem, A., Eldeeb, R., Hwang, Y., Aute, V., Radermacher, R., 2014. Evaluation and soft-optimization for R410A low-GWP replacement candidates through testing and simulation, in: 15th International Refrigeration and Air Conditioning Conference at Purdue, West Lafayette, Indiana.

Amasyali, K., El-Gohary, N.M., 2018. A review of data-driven building energy consumption prediction studies. Renewable and Sustainable Energy Reviews 81, 1192–1205.

Amemiya, N., Li, Q., Nishino, R., Takeuchi, K., Nakamura, T., Ohmatsu, K., Ohya, M., Maruyama, O., Okuma, T., Izumi, T., 2011. Lateral critical current density distributions degraded near edges of coated conductors through cutting processes and their influence on ac loss characteristics of power transmission cables. Physica C: Superconductivity and its Applications 471, 990–994.

Amponsah, N.Y., Troldborg, M., Kington, B., Aalders, I., Hough, R.L., 2014. Greenhouse gas emissions from renewable energy sources: A review of

lifecycle considerations. Renewable and Sustainable Energy Reviews 39, 461–475. https://doi.org/10.1016/j.rser.2014.07.087

Andersen, S.O., Halberstadt, M.L., Borgford-Parnell, N., 2013. Stratospheric ozone, global warming, and the principle of unintended consequences—An ongoing science and policy success story. Journal of the Air & Waste Management Association 63, 607–647. https://doi.org/10.1080/10962247.2013.791349

Andersen, S.O., Wolf, J., Hwang, Y., Ling, J., 2018. Life-Cycle Climate Performance Metrics and Room AC Carbon Footprint. ASHRAE Journal 25.

ANSI/ASHRAE Standard 34-2019, 52.

Aprea, C., Greco, A., Maiorino, A., Masselli, C., Metallo, A., 2016. HFO1234yf as a Drop-in Replacement for R134a in Domestic Refrigerators: A Life Cycle Climate Performance Analysis. IJHT 34, S212–S218. https://doi.org/10.18280/ijht.34S204

Aravinth, S., Sugumaran, V., 2018. Air compressor fault diagnosis through statistical feature extraction and random forest classifier. Progress in Industrial Ecology, an International Journal 12, 192–205.

Arrieta, F.R.P., Lora, E.E.S., 2005. Influence of ambient temperature on combined-cycle power-plant performance. Applied energy 80, 261–272.

ASHRAE Standards, 2019. Designation and safety classification of refrigerants. ANSI/ASHRAE Standard 34-2019.

Aynur, T.N., 2010. Variable refrigerant flow systems: A review. Energy and Buildings 42, 1106–1112. https://doi.org/10.1016/j.enbuild.2010.01.024

Bachmann, J., Hidalgo, C., Bricout, S., 2017. Environmental analysis of innovative sustainable composites with potential use in aviation sector—A life cycle assessment review. Science China Technological Sciences 60, 1301–1317.

Banks, R.E., Sharratt, P.N., 1996. Environmental Impacts of the Manufacture of HFC-134a. Department of Chemical Engineering, UMIST, Manchester, United Kingdom.

Baral, A., Minjares, R., Urban, R., 2013. Upstream climate impacts from production of R-134a and R-1234yf refrigerants used in mobile air conditioning systems. International Council on Clean Transportation.

Bejarano, G., Rodríguez, D., Alfaya, J.A., Ortega, M.G., Castaño, F., 2016. On identifying steady-state parameters of an experimental mechanical-compression refrigeration plant. Applied Thermal Engineering 109, 318–333. https://doi.org/10.1016/j.applthermaleng.2016.08.021

Bergman, T.L., Incropera, F.P., DeWitt, D.P., Lavine, A.S., 2011. Fundamentals of Heat and Mass Transfer. John Wiley & Sons.

Bethea, R.M., Rhinehart, R.R., 1991. Applied engineering statistics. CRC Press.

Bianchi, M., Branchini, L., De Pascale, A., Orlandini, V., Ottaviano, S., Peretto, A., Melino, F., Pinelli, M., Spina, P.R., Suman, A., 2017. Experimental Investigation with Steady-State Detection in a Micro-ORC Test Bench. Energy Procedia 126, 469–476. https://doi.org/10.1016/j.egypro.2017.08.222

Bilal, M., Oyedele, L.O., Qadir, J., Munir, K., Ajayi, S.O., Akinade, O.O., Owolabi, H.A., Alaka, H.A., Pasha, M., 2016. Big Data in the construction industry: A review of present status, opportunities, and future trends. Advanced

Engineering Informatics 30, 500–521. https://doi.org/10.1016/j.aei.2016.07.001

Bobbo, S., Nicola, G.D., Zilio, C., Brown, J.S., Fedele, L., 2018. Low GWP halocarbon refrigerants: A review of thermophysical properties. International Journal of Refrigeration 90, 181–201. https://doi.org/10.1016/j.ijrefrig.2018.03.027

Breiman, L., 2001. Statistical Modeling: The Two Cultures (with comments and a rejoinder by the author). Statist. Sci. 16, 199–231. https://doi.org/10.1214/ss/1009213726

Brodrick, J., 2002. Energy Consumption Characteristics of Commercial Building HVAC Systems Volume III: Energy Savings Potential. New York: Department of Energy 19–155.

Byers, E.A., Hall, J.W., Amezaga, J.M., 2014. Electricity generation and cooling water use: UK pathways to 2050. Global Environmental Change 25, 16–30. https://doi.org/10.1016/j.gloenvcha.2014.01.005

Cao, S., Rhinehart, R.R., 1995. An efficient method for on-line identification of steady state. Journal of Process Control, 1995, 5(6): 363-374

Cao, X., Li, Z.-Y., Shao, L.-L., Zhang, C.-L., 2016. Refrigerant flow through electronic expansion valve: Experiment and neural network modeling. Applied Thermal Engineering 92, 210–218. https://doi.org/10.1016/j.applthermaleng.2015.09.062

Capozzoli, A., Piscitelli, M.S., Gorrino, A., Ballarini, I., Corrado, V., 2017. Data analytics for occupancy pattern learning to reduce the energy consumption of

HVAC systems in office buildings. Sustainable Cities and Society 35, 191–208. https://doi.org/10.1016/j.scs.2017.07.016

Carbon Footprint, 2019. COUNTRY SPECIFIC ELECTRICITY GRID GREENHOUSE GAS EMISSION FACTORS [WWW Document]. URL https://www.carbonfootprint.com/docs/2019_06_emissions_factors_sources_for_2019_electricity.pdf (accessed 8.20.20).

Chau, C.K., Leung, T.M., Ng, W.Y., 2015. A review on Life Cycle Assessment, Life Cycle Energy Assessment and Life Cycle Carbon Emissions Assessment on buildings. Applied Energy 143, 395–413. https://doi.org/10.1016/j.apenergy.2015.01.023

Chen, L., Liu, J., Chen, J., Chen, Z., 2009. A new model of mass flow characteristics in electronic expansion valves considering metastability. International Journal of Thermal Sciences 48, 1235–1242.

Chen, T., Cha, D.A., Kwon, O.K., 2017. Experimental investigation on mass flow characteristics of R245fa through electronic expansion valve. Applied Thermal Engineering 125, 111–117. https://doi.org/10.1016/j.applthermaleng.2017.06.127

Chen, W., 2008. A comparative study on the performance and environmental characteristics of R410A and R22 residential air conditioners. Applied thermal engineering 28, 1–7.

Chen, Z., Zhu, X., Jin, X., Du, Z., 2020. Machine learning enhanced inverse modeling method for variable speed air conditioning systems. International Journal of Refrigeration 118, 311–324.

Cheung, H., Braun, J.E., 2014. Performance comparisons for variable-speed ductless and single-speed ducted residential heat pumps. International Journal of Refrigeration 47, 15–25. https://doi.org/10.1016/j.ijrefrig.2014.07.019

Cho, D., Yoo, C., Im, J., Cha, D.-H., 2020. Comparative assessment of various machine learning-based bias correction methods for numerical weather prediction model forecasts of extreme air temperatures in urban areas. Earth and Space Science 7, e2019EA000740.

Choi, J., Chung, J.T., Kim, Y., 2004. A generalized correlation for two-phase flow of alternative refrigerants through short tube orifices. International Journal of Refrigeration 27, 393–400. https://doi.org/10.1016/j.ijrefrig.2003.11.008

Choi, J.M., Kim, Y.C., 2003. Capacity modulation of an inverter-driven multi-air conditioner using electronic expansion valves. Energy 28, 141–155.

Choi, S., Oh, J., Hwang, Y., Lee, H., 2017. Life cycle climate performance evaluation (LCCP) on cooling and heating systems in South Korea. Applied Thermal Engineering 120, 88–98. https://doi.org/10.1016/j.applthermaleng.2017.03.105

Chung, M.H., Yang, Y.K., Lee, K.H., Lee, J.H., Moon, J.W., 2017. Application of artificial neural networks for determining energy-efficient operating set-points of the VRF cooling system. Building and Environment 125, 77–87. https://doi.org/10.1016/j.buildenv.2017.08.044

Cooling Post, 2018a. Honeywell announces R410A breakthrough [WWW Document]. Cooling Post. URL https://www.coolingpost.com/world-news/honeywell-announces-r410a-breakthrough/ (accessed 4.14.21).

Cooling Post, 2018b. Honeywell's N41 – a blast from the past [WWW Document]. Cooling Post. URL https://www.coolingpost.com/features/honeywells-n41-a-blast-from-the-past/ (accessed 4.14.21).

Cortes, C., Vapnik, V., 1995. Support-vector networks. Mach Learn 20, 273–297. https://doi.org/10.1007/BF00994018

Coskun, C., 2019. A time-varying carbon intensity approach for demand-side management strategies with respect to CO2 emission reduction in the electricity grid. International Journal of Global Warming 19, 3–23.

Crawley, D.B., Lawrie, L.K., Pedersen, C.O., Winkelmann, F.C., 2000. Energy plus: energy simulation program. ASHRAE journal 42, 49–56.

de Munck, C., Pigeon, G., Masson, V., Meunier, F., Bousquet, P., Tréméac, B., Merchat, M., Poeuf, P., Marchadier, C., 2013. How much can air conditioning increase air temperatures for a city like Paris, France? Int. J. Climatol. 33, 210–227. https://doi.org/10.1002/joc.3415

De Wolf, C., Yang, F., Cox, D., Charlson, A., Hattan, A.S., Ochsendorf, J., 2016. Material quantities and embodied carbon dioxide in structures. Proceedings of the Institution of Civil Engineers - Engineering Sustainability 169, 150–161. https://doi.org/10.1680/ensu.15.00033

Deng, S., Su, W., Zhao, L., 2016. A neural network for predicting normal boiling point of pure refrigerants using molecular groups and a topological index. International Journal of refrigeration 63, 63–71.

Devecioğlu, A.G., Oruç, V., 2020. Energetic performance analysis of R466A as an alternative to R410A in VRF systems. Engineering Science and Technology, an International Journal.

Dey, M., Rana, S.P., Dudley, S., 2018. Smart building creation in large scale HVAC environments through automated fault detection and diagnosis. Future Generation Computer Systems S0167739X17324287. https://doi.org/10.1016/j.future.2018.02.019

Eggleston, S., Buendia, L., Miwa, K., Ngara, T., Tanabe, K., 2006. 2006 IPCC guidelines for national greenhouse gas inventories. Institute for Global Environmental Strategies Hayama, Japan.

EPA, S.P., 2015. TRANSITIONING TO LOW-GWP ALTERNATIVES in Residential & Light Commercial Air Conditioning.

Fricke, B.A., Sharma, V., Abdelaziz, O., 2017. Low Global Warming Potential Refrigerants for Commercial Refrigeration Systems. Oak Ridge National Lab.(ORNL), Oak Ridge, TN (United States).

Ge, Y.T., Cropper, R., 2005. Performance evaluations of air-cooled condensers using pure and mixture refrigerants by four-section lumped modelling methods. Applied Thermal Engineering 25, 1549–1564. https://doi.org/10.1016/j.applthermaleng.2004.10.001

Ghorbanian, K., Gholamrezaei, M., 2009. An artificial neural network approach to compressor performance prediction. Applied Energy 86, 1210–1221. https://doi.org/10.1016/j.apenergy.2008.06.006

Gilmour, B., McNally, J., 2010. ACEEE Summer Study on Energy Efficiency in Buildings. Washington, DC: American Council for an Energy-Efficient Economy.

Goetzler, W., 2007. Variable refrigerant flow systems. Ashrae Journal 49, 24–31.

González-Díaz, A., Alcaráz-Calderón, A.M., González-Díaz, M.O., Méndez-Aranda, Á., Lucquiaud, M., González-Santaló, J.M., 2017. Effect of the ambient conditions on gas turbine combined cycle power plants with post-combustion CO2 capture. Energy 134, 221–233. https://doi.org/10.1016/j.energy.2017.05.020

Goto, M., Inoue, N., Ishiwatari, N., 2001. Condensation and evaporation heat transfer of R410A inside internally grooved horizontal tubes. International Journal of Refrigeration 24, 628–638.

Gu, B., Qian, C., Yang, L., Liu, F., 2015. Electronic expansion valve mass flow rate prediction based on dimensionless correlation and ANN model. International Journal of Refrigeration 57, 1–10. https://doi.org/10.1016/j.ijrefrig.2015.04.016

Guo, Y., Li, G., Chen, H., Hu, Y., Shen, L., Li, H., Hu, M., Li, J., 2017. Development of a virtual variable-speed compressor power sensor for variable refrigerant flow air conditioning system. International Journal of Refrigeration 74, 73–85. https://doi.org/10.1016/j.ijrefrig.2016.09.025

Hammond, G., Jones, C., Lowrie, E.F., Tse, P., 2011. Embodied carbon. The inventory of carbon and energy (ICE). Version (2.0).

Handbook, A.F., 2001. ASHRAE. Atlanta, Ga.

Herold, K.E., Radermacher, R., 1989. Advanced energy systems: absorption heat pumps. Mechanical engineering 111, 68.

Hill, W., Papasavva, S., 2005. Life cycle analysis framework; A comparison of HFC-134a, HFC-134a enhanced, HFC-152a, R744, R744 enhanced, and R290 automotive refrigerant systems. SAE Technical Paper.

Hipple, S.M., Bonilla-Alvarado, H., Pezzini, P., Shadle, L., Bryden, K.M., 2020. Using machine learning tools to predict compressor stall. Journal of Energy Resources Technology 142.

Holly, W., Cook, R., Crowe, C.M., 1989. Reconciliation of mass flow rate measurements in a chemical extraction plant. The Canadian Journal of Chemical Engineering 67, 595–601.

Hong, T., Pang, X., Schetrit, O., Wang, L., Kasahara, S., Yura, Y., Hinokuma, R., 2014. A new model to simulate energy performance of VRF systems. Microbiology 150, 2609–17.

Hong, T., Sun, K., Zhang, R., Hinokuma, R., Kasahara, S., Yura, Y., 2016. Development and validation of a new variable refrigerant flow system model in EnergyPlus. Energy and Buildings 117, 399–411. https://doi.org/10.1016/j.enbuild.2015.09.023

Horie, H., Kamiaka, T., Dang, C., Hihara, E., no Ha, K., 2010. Study on cycle property and LCCP evaluation of heat pump using HFO-1234yf, HFC-32, and HFC-410A as refrigerant, in: 2010 International Symposium on Next-Generation Air Conditioning and Refrigeration Technology, 17–19 February 2010, Tokyo, Japan.

Hou, Y., Liu, C., Ma, J., Cao, J., Chen, S., 2014. Mass flowrate characteristics of supercritical CO2 flowing through an electronic expansion valve. International Journal of Refrigeration 47, 134–140.

Ibn-Mohammed, T., Greenough, R., Taylor, S., Ozawa-Meida, L., Acquaye, A., 2013. Operational vs. embodied emissions in buildings—A review of current trends. Energy and Buildings 66, 232–245.

Integrated Surface Database (ISD) | National Centers for Environmental Information (NCEI) formerly known as National Climatic Data Center (NCDC) [WWW Document], 2020. URL https://www.ncdc.noaa.gov/isd (accessed 8.20.20).

Jacobson, M.Z., 2014. Effects of biomass burning on climate, accounting for heat and moisture fluxes, black and brown carbon, and cloud absorption effects. Journal of Geophysical Research: Atmospheres 119, 8980–9002.

Jähnig, D.I., Reindl, D.T., Klein, S.A., 2000. A Semi-Empirical Method for Representing Domestic Refrigerator/Freezer Compressor Calorimeter Test Data. ASHRAE Trans. 106(Pt. 2), 122–130.

Jiang, Y., Ge, T., Wang, R., 2014. Comparison study of a novel solid desiccant heat pump system with EnergyPlus. Building Simulation 7, 467–476. https://doi.org/10.1007/s12273-014-0166-7

Joo, Y., Kang, H., Ahn, J.H., Lee, M., Kim, Y., 2011. Performance characteristics of a simultaneous cooling and heating multi-heat pump at partial load conditions. international journal of refrigeration 34, 893–901.

Kamel, E., Sheikh, S., 2020. Typical Meteorological Year and Actual Weather Data in Data-Driven Machine Learning Models for Residential Building Energy Use (VC-20-C008), in: 2020 ASHRAE Virtual Conference. ASHRAE.

Kang, H., Joo, Y., Chung, H., Kim, Y., Choi, J., 2009. Experimental study on the performance of a simultaneous heating and cooling multi-heat pump with the variation of operation mode. international journal of refrigeration 32, 1452–1459.

Kang, I., Lee, K., Lee, J., Moon, J., 2018. Artificial Neural Network–Based Control of a Variable Refrigerant Flow System in the Cooling Season. Energies 11, 1643. https://doi.org/10.3390/en11071643

Kao, J.Y., 1992. HVAC functional inspection and testing guide. National Inst. of Standards and Technology (BFRL), Gaithersburg, MD (United ….

Kavanaugh, P.S., Simplified, H., 2006. American Society of Heating, Refrigerating and Air-Conditioning Engineers (ASHRAE). Atlanta.

Kedzierski, M.A., Kang, D., 2016. Horizontal convective boiling of R448A, R449A, and R452B within a micro-fin tube. Science and technology for the built environment 22, 1090–1103.

Kehlhofer, R., Hannemann, F., Rukes, B., Stirnimann, F., 2009. Combined-cycle gas & steam turbine power plants. Pennwell Books.

Kennett, R., Hwang, Y., Radermacher, R., 2016. Evaluation of an Extended-Duct Air Delivery System in Tall Spaces Conditioned by Rooftop Units, in: ASME International Mechanical Engineering Congress and Exposition. American Society of Mechanical Engineers, p. V06BT08A004.

Khan, I., 2018. Importance of GHG emissions assessment in the electricity grid expansion towards a low-carbon future: A time-varying carbon intensity approach. Journal of Cleaner Production 196, 1587–1599.

Khan, I., Jack, M.W., Stephenson, J., 2017. Use of time-varying carbon intensity estimation to evaluate GHG emission reduction opportunities in electricity sector, in: 2017 IEEE Conference on Technologies for Sustainability (SusTech). Presented at the 2017 IEEE Conference on Technologies for Sustainability (SusTech), pp. 1–2. https://doi.org/10.1109/SusTech.2017.8333479

Khatri, R., Joshi, A., 2017. Energy Performance Comparison of Inverter based Variable Refrigerant Flow Unitary AC with Constant Volume Unitary AC. Energy Procedia 109, 18–26. https://doi.org/10.1016/j.egypro.2017.03.038

Kim, D., Song, K.S., Lim, J., Kim, Y., 2018. Analysis of two-phase injection heat pump using artificial neural network considering APF and LCCP under various weather conditions. Energy 155, 117–127. https://doi.org/10.1016/j.energy.2018.05.046

Kim, M., Lee, Y.S., 2017. Development of Steady-State Reference Model for Heat Pump System Based on Real-time Machine Learning Algorithm 8.

Kim, M., Yoon, S.H., Domanski, P.A., Vance Payne, W., 2008. Design of a steady-state detector for fault detection and diagnosis of a residential air conditioner. International Journal of Refrigeration 31, 790–799. https://doi.org/10.1016/j.ijrefrig.2007.11.008

Kim, O.J., Choi, Y.-H., Yoon, S.H., 2010. Flow characteristics of electronic expansion valves for heat pump system using carbon dioxide as a refrigerant, in: ASME 2010 3rd Joint US-European Fluids Engineering Summer Meeting Collocated with 8th International Conference on Nanochannels, Microchannels, and Minichannels. American Society of Mechanical Engineers, pp. 1041–1046.

Kim, W., Jeon, S.W., Kim, Y., 2016. Model-based multi-objective optimal control of a VRF (variable refrigerant flow) combined system with DOAS (dedicated outdoor air system) using genetic algorithm under heating conditions. Energy 107, 196–204. https://doi.org/10.1016/j.energy.2016.03.139

Kocyigit, N., 2015. Fault and sensor error diagnostic strategies for a vapor compression refrigeration system by using fuzzy inference systems and artificial neural network. International Journal of Refrigeration 50, 69–79.

Kotharkar, R., Ramesh, A., Bagade, A., 2018. Urban Heat Island studies in South Asia: a critical review. Urban climate 24, 1011–1026.

Kovler, K., Haquin, G., Manasherov, V., Ne'eman, E., Lavi, N., 2002. Natural radionuclides in building materials available in Israel. Building and Environment 37, 531–537. https://doi.org/10.1016/S0360-1323(01)00048-8

Kujak, S., 2019. Examination of a Novel R410A Replacement. ASHRAE Transactions 125, 264–271.

Kujak, S.A., Srichai, P.R., Schultz, K.J., 2014. Assessment Of Life Cycle Climate Performance (LCCP) Tools For HVAC&R Applications With The Latest Next Generation Refrigerant Technology 11.

Kwon, L., Hwang, Y., Radermacher, R., Kim, B., 2012. Field performance measurements of a VRF system with sub-cooler in educational offices for the cooling season. Energy and Buildings 49, 300–305. https://doi.org/10.1016/j.enbuild.2012.02.027

Kwon, L., Lee, H., Hwang, Y., Radermacher, R., Kim, B., 2014. Experimental investigation of multifunctional VRF system in heating and shoulder seasons. Applied Thermal Engineering 66, 355–364. https://doi.org/10.1016/j.applthermaleng.2014.02.032

Lachhab, F., Malek, Youssef.N., Bakhouya, M., Ouladsine, R., Essaaidi, M., 2018. A Context-Driven Approach using IoT and Big Data Technologies for Controlling HVAC Systems, in: 2018 5th International Conference on Control, Decision and Information Technologies (CoDIT). Presented at the 2018 5th International Conference on Control, Decision and Information Technologies (CoDIT), IEEE, Thessaloniki, pp. 694–699. https://doi.org/10.1109/CoDIT.2018.8394823

Lakervi, E., Holmes, E.J., 1995. Electricity distribution network design. IET.

Lecompte, S., Gusev, S., Vanslambrouck, B., De Paepe, M., 2018. Experimental results of a small-scale organic Rankine cycle: Steady state identification and application to off-design model validation. Applied Energy 226, 82–106. https://doi.org/10.1016/j.apenergy.2018.05.103

Lee, H., Troch, S., Hwang, Y., Radermacher, R., 2016. LCCP evaluation on various vapor compression cycle options and low GWP refrigerants. International Journal of Refrigeration 70, 128–137.

Lenzen, M., 2008. Life cycle energy and greenhouse gas emissions of nuclear energy: A review. Energy Conversion and Management 49, 2178–2199. https://doi.org/10.1016/j.enconman.2008.01.033

Li, G., 2017. Comprehensive investigation of transport refrigeration life cycle climate performance. Sustainable Energy Technologies and Assessments 21, 33–49.

Li, G., 2015a. Investigations of life cycle climate performance and material life cycle assessment of packaged air conditioners for residential application. Sustainable Energy Technologies and Assessments 11, 114–125.

Li, G., 2015b. Comprehensive investigations of life cycle climate performance of packaged air source heat pumps for residential application. Renewable and Sustainable Energy Reviews 43, 702–710. https://doi.org/10.1016/j.rser.2014.11.078

Li, G., Hu, Y., Chen, H., Li, H., Hu, M., Guo, Y., Shi, S., Hu, W., 2016. A sensor fault detection and diagnosis strategy for screw chiller system using support vector data description-based D-statistic and DV-contribution plots. Energy and Buildings 133, 230–245.

Li, W., 2013a. Simplified modeling analysis of mass flow characteristics in electronic expansion valve. Applied Thermal Engineering 53, 8–12. https://doi.org/10.1016/j.applthermaleng.2012.12.035

Li, W., 2013b. Simplified steady-state modeling for variable speed compressor. Applied Thermal Engineering 50, 318–326. https://doi.org/10.1016/j.applthermaleng.2012.08.041

Li, W., Koo, C., Hong, T., Oh, J., Cha, S.H., Wang, S., 2020. A novel operation approach for the energy efficiency improvement of the HVAC system in office spaces through real-time big data analytics. Renewable and Sustainable Energy Reviews 127, 109885. https://doi.org/10.1016/j.rser.2020.109885

Li, X., Duan, F., Bennett, I., Mba, D., 2018. Canonical variate analysis, probability approach and support vector regression for fault identification and failure time prediction. Journal of Intelligent & Fuzzy Systems 34, 3771–3783. https://doi.org/10.3233/JIFS-169550

Li, Y., Zhao, X., 2012. An empirical study of the impact of human activity on long-term temperature change in China: A perspective from energy consumption. Journal of Geophysical Research: Atmospheres 117.

Li, Y.M., Wu, J.Y., 2010. Energy simulation and analysis of the heat recovery variable refrigerant flow system in winter. Energy and Buildings 42, 1093–1099.

Liang, C., Jiangping, C., Jinghui, L., Zhijiu, C., 2009. Experimental investigation on mass flow characteristics of electronic expansion valves with R22, R410A and R407C. Energy Conversion and Management 50, 1033–1039. https://doi.org/10.1016/j.enconman.2008.12.018

Life Cycle Climate Performance Working Group, 2015. Guideline for life cycle climate performance 2015 [WWW Document]. International Institute of Refrigeration. URL http://www.cold.org.gr/library/downloads/Docs/Guideline%20for%20life%20cycle%20climate%20performance%202015.pdf (accessed 8.18.20).

Lin, J.-L., Yeh, T.-J., 2007. Identification and control of multi-evaporator air-conditioning systems. International Journal of Refrigeration 30, 1374–1385. https://doi.org/10.1016/j.ijrefrig.2007.04.003

Lin, L., Kedzierski, M.A., 2019. Review of low-GWP refrigerant pool boiling heat transfer on enhanced surfaces. International journal of heat and mass transfer 131, 1279–1303.

Lin, X., Lee, H., Hwang, Y., Radermacher, R., 2015. A review of recent development in variable refrigerant flow systems. Science and Technology for the Built Environment 21, 917–933. https://doi.org/10.1080/23744731.2015.1071987

Lin, X., Lee, H., Hwang, Y., Radermacher, R., Oh, S., 2014. Experimental investigation of multi-functional variable refrigerant flow system.

Liu, C., Hou, Y., Ma, J., Liu, X., Chen, L., 2016. Experimental study on the CO2 flow characteristics through electronic expansion valves in heat pump. International Journal of Refrigeration 69, 106–113. https://doi.org/10.1016/j.ijrefrig.2016.05.005

Liu, J., Wang, J., Li, G., Chen, H., Shen, L., Xing, L., 2017. Evaluation of the energy performance of variable refrigerant flow systems using dynamic energy benchmarks based on data mining techniques. Applied Energy 208, 522–539. https://doi.org/10.1016/j.apenergy.2017.09.116

Liu, X., Hong, T., 2010. Comparison of energy efficiency between variable refrigerant flow systems and ground source heat pump systems. Energy and Buildings 42, 584–589.

Lohrmann, A., Farfan, J., Caldera, U., Lohrmann, C., Breyer, C., 2019. Global scenarios for significant water use reduction in thermal power plants based on cooling water demand estimation using satellite imagery. Nature Energy 4, 1040–1048. https://doi.org/10.1038/s41560-019-0501-4

Madonna, F., Bazzocchi, F., 2013. Annual performances of reversible air-to-water heat pumps in small residential buildings. Energy and Buildings 65, 299–309. https://doi.org/10.1016/j.enbuild.2013.06.016

Makhnatch, P., Khodabandeh, R., 2014. The role of environmental metrics (GWP, TEWI, LCCP) in the selection of low GWP refrigerant. Energy Procedia 61, 2460–2463.

Mota-Babiloni, A., Barbosa, J.R., Makhnatch, P., Lozano, J.A., 2020. Assessment of the utilization of equivalent warming impact metrics in refrigeration, air conditioning and heat pump systems. Renewable and Sustainable Energy Reviews 129, 109929. https://doi.org/10.1016/j.rser.2020.109929

Mota-Babiloni, A., Navarro-Esbrí, J., Makhnatch, P., Molés, F., 2017. Refrigerant R32 as lower GWP working fluid in residential air conditioning systems in Europe and the USA. Renewable and Sustainable Energy Reviews 80, 1031–1042. https://doi.org/10.1016/j.rser.2017.05.216

Müller-Steinhagen, H., Heck, K., 1986. A simple friction pressure drop correlation for two-phase flow in pipes. Chemical Engineering and Processing: Process Intensification 20, 297–308.

Myhre, G., Shindell, D., Pongratz, J., 2014. Anthropogenic and natural radiative forcing.

Nadira, R., Benchluch, S., Dortolina, C.A., 2003. A novel approach to computing distribution losses, in: 2003 IEEE PES Transmission and Distribution Conference and Exposition (IEEE Cat. No. 03CH37495). IEEE, pp. 659–663.

Narasimhan, S., Kao, C.S., Mah, R.S.H., 1987. Detecting changes of steady states using the mathematical theory of evidence. AIChE Journal 33, 1930–1932. https://doi.org/10.1002/aic.690331125

Nasrabadi, N.M., 2007. Pattern recognition and machine learning. Journal of electronic imaging 16, 049901.

Okochi, G.S., Yao, Y., 2016. A review of recent developments and technological advancements of variable-air-volume (VAV) air-conditioning systems. Renewable and Sustainable Energy Reviews 59, 784–817. https://doi.org/10.1016/j.rser.2015.12.328

Özahi, E., Abuşoğlu, A., Kutlar, A.İ., Dağcı, O., 2017. A comparative thermodynamic and economic analysis and assessment of a conventional HVAC and a VRF system in a social and cultural center building. Energy and Buildings 140, 196–209. https://doi.org/10.1016/j.enbuild.2017.02.008

Pan, L., Liu, P., Ma, L., Li, Z., 2012. A supply chain based assessment of water issues in the coal industry in China. Energy Policy 48, 93–102.

Papasavva, S., Hill, W.R., Andersen, S.O., 2010. GREEN-MAC-LCCP: A Tool for Assessing the Life Cycle Climate Performance of MAC Systems. Environ. Sci. Technol. 44, 7666–7672. https://doi.org/10.1021/es100849g

Park, C., Cho, H., Lee, Y., Kim, Y., 2007. Mass flow characteristics and empirical modeling of R22 and R410A flowing through electronic expansion valves.

International Journal of Refrigeration 30, 1401–1407. https://doi.org/10.1016/j.ijrefrig.2007.03.011

Park, D.Y., Yun, G., Kim, K.S., 2017. Experimental evaluation and simulation of a variable refrigerant- flow (VRF) air-conditioning system with outdoor air processing unit. Energy and Buildings 146, 122–140. https://doi.org/10.1016/j.enbuild.2017.04.026

Park, Y.C., Kim, Y.C., Min, M.-K., 2001. Performance analysis on a multi-type inverter air conditioner. Energy Conversion and Management 42, 1607–1621. https://doi.org/10.1016/S0196-8904(00)00147-3

Pearson, K., 1901. LIII. On lines and planes of closest fit to systems of points in space. The London, Edinburgh, and Dublin Philosophical Magazine and Journal of Science 2, 559–572.

Perez, C.F.A., 2018. Systems and methods for steady state detection. Google Patents.

Pérez-Lombard, L., Ortiz, J., Pout, C., 2008. A review on buildings energy consumption information. Energy and Buildings 40, 394–398. https://doi.org/10.1016/j.enbuild.2007.03.007

Pham, H.M., Rajendran, R., 2012. R32 And HFOs As Low-GWP Refrigerants For Air Conditioning 11.

Qian, M., Yan, D., Hong, T., Liu, H., 2021. Operation and performance of VRF systems: Mining a large-scale dataset. Energy and Buildings 230, 110519. https://doi.org/10.1016/j.enbuild.2020.110519

Qiao, H., Laughman, C.R., Burns, D.J., Bortoff, S.A., 2017. Dynamic Characteristics of an R-410A Multi-split Variable Refrigerant Flow Air-conditioning System 11.

Qiao, H., Radermacher, R., Aute, V., 2010. A review for numerical simulation of vapor compression systems.

Qin, Q., Jiang, Z.-N., Feng, K., He, W., 2012. A novel scheme for fault detection of reciprocating compressor valves based on basis pursuit, wave matching and support vector machine. Measurement 45, 897–908. https://doi.org/10.1016/j.measurement.2012.02.005

Qiu, T., 2018. Refrigerant charge distribution in unitary air-conditioning units.

Raustad, R., Nigusse, B., Domitrovic, R., 2013. Technical Subtopic 2.1: Modeling Variable Refrigerant Flow Heat Pump and Heat Recovery Equipment in EnergyPlus. Univ. of Central Florida, Orlando, FL (United States).

Rhoads, Adam. A Study of the Effect of Weather Data and Other Assumptions on MAC LCCP. No. 2020-01-0152. SAE Technical Paper, 2020. https://doi.org/10.4271/2020-01-0152

Rovelli, C., Smolin, L., 1990. Loop space representation of quantum general relativity. Nuclear Physics B 331, 80–152. https://doi.org/10.1016/0550-3213(90)90019-A

Ryan, N.A., Johnson, J.X., Keoleian, G.A., 2016. Comparative assessment of models and methods to calculate grid electricity emissions. Environmental science & technology 50, 8937–8953.

Saab, R., Ali, M.I.H., 2017. Variable-Refrigerant-Flow Cooling-Systems Performance at Different Operation-Pressures and Types-of-Refrigerants. Energy Procedia 119, 426–432. https://doi.org/10.1016/j.egypro.2017.07.041

Sadovskaia, K., Bogdanov, D., Honkapuro, S., Breyer, C., 2019. Power transmission and distribution losses–A model based on available empirical data and future trends for all countries globally. International Journal of Electrical Power & Energy Systems 107, 98–109.

SAE International, 2012. Mobile Air Conditioning System Refrigerant Emission Charts for R-134a and R-1234yf [WWW Document]. SAE Mobilus. URL https://saemobilus.sae.org/content/j2727_201202 (accessed 3.24.21).

SAE International, 2009. Life Cycle Analysis to Estimate the CO2-Equivalent Emissions from MAC Operation [WWW Document]. URL https://saemobilus.sae.org/content/j2766_200902 (accessed 3.24.21).

Saminathan, M., Rana, R., Ramakrishnan, M.A., Karthik, K., Malik, Y.S., Dhama, K., 2016. Prevalence, diagnosis, management and control of important diseases of ruminants with special reference to Indian scenario. J Exp Biol Agric Sci 4, 3338–3367.

Sand, J.R., Fischer, S.K., Baxter, V.D., 1997. Energy and global warming impacts of HFC refrigerants and emerging technologies. Citeseer.

Santamouris, M., Ding, L., Fiorito, F., Oldfield, P., Osmond, P., Paolini, R., Prasad, D., Synnefa, A., 2017. Passive and active cooling for the outdoor built environment – Analysis and assessment of the cooling potential of mitigation

technologies using performance data from 220 large scale projects. Solar Energy 154, 14–33. https://doi.org/10.1016/j.solener.2016.12.006

Shah, R., Alleyne, A.G., Bullard, C.W., 2004. Dynamic modeling and control of multi-evaporator air-conditioning systems. ASHRAE transactions 110, 109.

Shanwei, M., Chuan, Z., Jiangping, C., Zhiujiu, C., 2005. Experimental research on refrigerant mass flow coefficient of electronic expansion valve. Applied Thermal Engineering 25, 2351–2366. https://doi.org/10.1016/j.applthermaleng.2004.12.005

Shao, S., Xu, H., Tian, C., 2012. Dynamic simulation of multi-unit air conditioners based on two-phase fluid network model. Applied Thermal Engineering 40, 378–388. https://doi.org/10.1016/j.applthermaleng.2012.02.022

Sharma, A., Saxena, A., Sethi, M., Shree, V., 2011. Life cycle assessment of buildings: a review. Renewable and Sustainable Energy Reviews 15, 871–875.

Shen, B., Rice, C.K., 2012. Multiple-Zone Variable Refrigerant Flow System Modeling and Equipment Performance Mapping. ASHRAE Transactions 118.

Shen, B., Rice, C.K., McDowell, T.P., Baxter, V.D., 2013. Energy simulation of integrated multiple-zone variable refrigerant flow system, in: 2013 ASHARE Annual Conference. pp. 1–9.

Smith, A., Lott, N., Vose, R., 2011. The integrated surface database: Recent developments and partnerships. Bulletin of the American Meteorological Society 92, 704–708.

Solecki, W.D., Rosenzweig, C., Parshall, L., Pope, G., Clark, M., Cox, J., Wiencke, M., 2005. Mitigation of the heat island effect in urban New Jersey. Global Environmental Change Part B: Environmental Hazards 6, 39–49.

Sonin, A.A., 2001. Dimensional analysis. Technical report, Massachusetts Institute of Technology.

Spatz, M.W., Motta, S.F.Y., 2004. An evaluation of options for replacing HCFC-22 in medium temperature refrigeration systems. International Journal of Refrigeration 27, 475–483.

Standards, 2017. Performance Rating of Unitary Air-conditioning & Air-source Heat Pump Equipment. AHRI 210/240-2017.

Su, W., Zhao, L., Deng, S., 2017. Developing a performance evaluation model of Organic Rankine Cycle for working fluids based on the group contribution method. Energy Conversion and Management 132, 307–315. https://doi.org/10.1016/j.enconman.2016.11.040

Sun, H., Ding, G., Hu, H., Ren, T., Xia, G., Wu, G., 2017. A general simulation model for variable refrigerant flow multi-split air conditioning system based on graph theory. International Journal of Refrigeration 82, 22–35. https://doi.org/10.1016/j.ijrefrig.2017.07.003

Suzuki, Motoyuki, Suzuki, M., 1990. Adsorption engineering. Kodansha Tokyo.

The 6 Challenges of Big Data Integration | FlyData [WWW Document], 2021. FlyData | Real Time MySQL Replication to Amazon Redshift. URL https://flydata.com/the-6-challenges-of-big-data-integration/ (accessed 2.22.21).

The Climate Reality Project, 2020. How Feedback Loops Are Making the Climate Crisis Worse [WWW Document]. Climate Reality. URL https://www.climaterealityproject.org/blog/how-feedback-loops-are-making-climate-crisis-worse (accessed 3.24.21).

Thornton, B., Wagner, A., 2012. Variable Refrigerant Flow Systems 79.

Tian, Z., Gu, B., Yang, L., Lu, Y., 2015. Hybrid ANN–PLS approach to scroll compressor thermodynamic performance prediction. Applied Thermal Engineering 77, 113–120. https://doi.org/10.1016/j.applthermaleng.2014.12.023

Torcellini, P., Long, N., Judkoff, R., 2003. Consumptive water use for US power production. National Renewable Energy Lab., Golden, CO (US).

Transparency, C., 2018. G20 Brown to Green Report 2018. Climate Transparency.

Troch, S.V., 2016. Harmonization of Life Cycle Climate Performance and Its Improvements for Heat Pump Applications.

Tu, Q., Dong, K., Zou, D., Lin, Y., 2011. Experimental study on multi-split air conditioner with digital scroll compressor. Applied Thermal Engineering 31, 2449–2457. https://doi.org/10.1016/j.applthermaleng.2011.04.010

Tu, Q., Zhang, L., Cai, W., Guo, X., Deng, C., Zhang, J., Wang, B., 2017. Effects of sub-cooler on cooling performance of variable refrigerant flow air conditioning system. Applied Thermal Engineering 127, 1152–1163. https://doi.org/10.1016/j.applthermaleng.2017.08.112

US EIA, 2021. Annual Energy Outlook 2021. US Energy Information Administration. Government Printing Office.

US EPA, 2020. Emissions & Generation Resource Integrated Database (eGRID) [WWW Document]. US Environmental Protection Agency. URL https://www.epa.gov/egrid/emissions-generation-resource-integrated-database-egrid (accessed 8.20.20).

Venkatarathnam, G., Murthy, S.S., 2012. Refrigerants for vapour compression refrigeration systems. Resonance 17, 139–162.

Vilches, A., Garcia-Martinez, A., Sanchez-Montanes, B., 2017. Life cycle assessment (LCA) of building refurbishment: A literature review. Energy and Buildings 135, 286–301.

Wan, H., Cao, T., Hwang, Y., Oh, S., 2020. A review of recent advancements of variable refrigerant flow air-conditioning systems. Applied Thermal Engineering 169, 114893. https://doi.org/10.1016/j.applthermaleng.2019.114893

Wan, H., Cao, T., Hwang, Y., Oh, S., 2019. An Electronic Expansion Valve Modeling Framework Development Using Artificial Neural Network: A Case Study on VRF Systems. International Journal of Refrigeration S0140700719303676. https://doi.org/10.1016/j.ijrefrig.2019.08.018

Wan, H., Hwang, Y., Oh, S., 2018. A Review of Electronic Expansion Valve Correlations for Air-conditioning and Heat Pump Systems.

Wang, S., 2014. Energy modeling of ground source heat pump vs. variable refrigerant flow systems in representative US climate zones. Energy and Buildings 72, 222–228. https://doi.org/10.1016/j.enbuild.2013.12.017

Wang, X., Hwang, Y., Radermacher, R., 2009. Two-stage heat pump system with vapor-injected scroll compressor using R410A as a refrigerant. International Journal of Refrigeration 32, 1442–1451.

Wijeysundera, N.E., 2015. Principles of Heating, Ventilation and Air Conditioning with Worked Examples. World Scientific.

Wile, D.D., 1935. The measurement of expansion valve capacity. Refrigeration Engineering 8, 108–112.

Winkler, J., Aute, V., Radermacher, R., 2008. Comprehensive investigation of numerical methods in simulating a steady-state vapor compression system. International Journal of Refrigeration 31, 930–942.

Won, A., Ichikawa, T., Yoshida, S., Sadohara, S., 2009. Study on running performance of a split-type air conditioning system installed in the national university campus in Japan. Journal of Asian Architecture and Building Engineering 8, 579–583.

Woodland, B.J., Braun, J.E., Groll, E.A., Horton, W.T., 2012. Experimental testing of an organic Rankine cycle with scroll-type expander.

Wu, C., Xingxi, Z., Shiming, D., 2005. Development of control method and dynamic model for multi-evaporator air conditioners (MEAC). Energy conversion and management 46, 451–465.

Wu, J., Chen, Y., Zhou, S., 2016. Online detection of steady-state operation using a multiple-change-point model and exact Bayesian inference. IIE Transactions 48, 599–613. https://doi.org/10.1080/0740817X.2015.1110268

WU, J., JIANG, F., 2017. Life cycle climate performance of air conditioner based on dynamic loads. Journal of ZheJiang University (Engineering Science) 51, 2061–2069.

Wu, J., Xu, Z., Jiang, F., 2019. Analysis and development trends of Chinese energy efficiency standards for room air conditioners. Energy policy 125, 368–383.

Wu, J., Zhou, S., Li, X., 2013. Acoustic emission monitoring for ultrasonic cavitation based dispersion process. Journal of Manufacturing Science and Engineering 135, 031015.

Wu, Y., Liang, X., Tu, X., Zhuang, R., 2012. Study of R161 Refrigerant for Residential Air-conditioning Applications 8.

Xiangguo, X., Yan, P., Shiming, D., Liang, X., Mingyin, C., 2013. Experimental study of a novel capacity control algorithm for a multi-evaporator air conditioning system. Applied thermal engineering 50, 975–984.

Xin, D., Huang, S., Yin, S., Deng, Y., Zhang, W., 2017. Experimental investigation on oil-gas separator of air-conditioning systems. Frontiers in Energy. https://doi.org/10.1007/s11708-017-0447-9

Xu, X., Hwang, Y., Radermacher, R., 2013. Performance comparison of R410A and R32 in vapor injection cycles. International Journal of Refrigeration 36, 892–903. https://doi.org/10.1016/j.ijrefrig.2012.12.010

Xu, X., Wei, Z., Ji, Q., Wang, C., Gao, G., 2019. Global renewable energy development: Influencing factors, trend predictions and countermeasures. Resources Policy 63, 101470.

Yan, J., Meng, Y., Lu, L., Li, L., 2017. Industrial Big Data in an Industry 4.0 Environment: Challenges, Schemes, and Applications for Predictive Maintenance. IEEE Access 5, 23484–23491. https://doi.org/10.1109/ACCESS.2017.2765544

Yang, C., Seo, S., Takata, N., Thu, K., Miyazaki, T., 2021. The life cycle climate performance evaluation of low-GWP refrigerants for domestic heat pumps. International Journal of Refrigeration 121, 33–42. https://doi.org/10.1016/j.ijrefrig.2020.09.020

Ye, Q., Chen, J., Chen, Z., 2007. Experimental investigation of R407C and R410A flow through electronic expansion valve. Energy Conversion and Management 48, 1624–1630. https://doi.org/10.1016/j.enconman.2006.11.011

Yu, X., Yan, D., Sun, K., Hong, T., Zhu, D., 2016. Comparative study of the cooling energy performance of variable refrigerant flow systems and variable air volume systems in office buildings. Applied Energy 183, 725–736. https://doi.org/10.1016/j.apenergy.2016.09.033

Yun, G.Y., Lee, J.H., Kim, H.J., 2016. Development and application of the load responsive control of the evaporating temperature in a VRF system for cooling energy savings. Energy and Buildings 116, 638–645. https://doi.org/10.1016/j.enbuild.2016.02.012

Yun, G.Y., Lee, J.H., Kim, I., 2017. Dynamic target high pressure control of a VRF system for heating energy savings. Applied Thermal Engineering 113, 1386–1395. https://doi.org/10.1016/j.applthermaleng.2016.11.148

Zhang, C., Ma, S., Chen, J., Chen, Z., 2006. Experimental analysis of R22 and R407c flow through electronic expansion valve. Energy Conversion and Management 47, 529–544. https://doi.org/10.1016/j.enconman.2005.05.005

Zhang, D., Cai, N., Gao, D., Xia, X., Huang, X., Zhang, X., 2017. Experimental investigation on operating performance of digital variable multiple air conditioning system. Applied Thermal Engineering 123, 1134–1139. https://doi.org/10.1016/j.applthermaleng.2017.05.196

Zhang, G., Liu, W., Xiao, H., Shi, W., Wang, B., Li, X., Cao, Y., 2019. New method for measuring field performance of variable refrigerant flow systems based on compressor set energy conservation. Applied Thermal Engineering 154, 530–539. https://doi.org/10.1016/j.applthermaleng.2019.03.122

Zhang, M., Muehlbauer, J., Aute, V., Radermacher, R., 2011. Life Cycle Climate Performance Model for Residential Heat Pump System, Air-Conditioning, Heating and Refrigeration Technology Institute. Inc.(AHRTI).

Zhao, H., Magoulès, F., 2012. A review on the prediction of building energy consumption. Renewable and Sustainable Energy Reviews 16, 3586–3592. https://doi.org/10.1016/j.rser.2012.02.049

Zhao, L.-X., Zhang, C.-L., Gu, B., 2009. Neural-network-based polynomial correlation of single-and variable-speed compressor performance. HVAC&R Research 15, 255–268.

Zhifang, X., Lin, S., Hongfei, O., 2008. Refrigerant flow characteristics of electronic expansion valve based on thermodynamic analysis and experiment. Applied

Thermal Engineering 28, 238–243.

https://doi.org/10.1016/j.applthermaleng.2007.03.023